Universidade Federal do Rio Grande do Sul
Programa de pós-graduação em física

Doctoral Thesis

Multicritical points in a model for $5f$-electron systems under pressure and magnetic field

Author:
Julián Faúndez

Supervisor:
Dr. Sérgio G. Magalhães

A thesis submitted in fulfillment of the requirements for the degree of Doctor of Natural Sciences

in the

Condensed Matter Physics Group
Institute of Physics

July 25, 2022

Pesquisadores da Universidade Federal do Rio Grande do Sul (UFRGS) desenvolvem um estudo de pontos multicriticos em transições de fases presentes em compostos de urânio.

Porto Alegre, 2 de junio 2022: O grupo teórico de eléctrons correlacionados (CEG: Correlated electrons group) da UFRGS, liderado pelo Prof. Sérgio G. Magalhães, tem desenvolvidos um novo enfoque no estudo de pontos multicríticos presentes em compostos de Urânio. A idéia geral se concentra no fato de que os pontos multicríticos podem fornecer informações cruciais sobre a natureza das fases convencionais e não convencionais encontradas neste tipo de compostos. O Prof. Sergio G. Magalhães, do Instituto de Física da UFRGS juntamente com o Prof. Peter Riseborough da Temple University, EUA, propuseram desde 2012 um modelo teórico, chamado *Underscreneed Anderson Lattice Model* -em inglês- para descrever a física presente nos compostos de urânio, especificamente no URu_2Si_2. Ao longo dos anos, eles encontraram resultados muito interessantes, tais como fases magnéticas bem definidas e um tipo de fase exótica, que é um forte candidato à descrição da Hidden Order presente no URu_2Si_2, um problema ainda em discussão desde os anos 80. Atualmente, o modelo proposto tem servido como fonte de inspiração para o estudo do surgimento de pontos multicríticos entre diferentes fases encontradas nos átomos de urânio, sob os efeitos da pressão externa e/ou campos magnéticos, e foi proposto que o tipo de ponto crítico pode fornecer informações relevantes sobre a natureza física de cada uma das fases envolvidas, como o comportamento da estrutura eletrônica, até as simetrias presentes nesses compostos. Este tipo de abordagem de pontos multicríticos poderia dar uma imagem mais clara das características de cada fase, sem a necessidade de um estudo individual de cada uma delas e, desta forma, incentivar o papel que certos pontos críticos desempenham nas características físicas de cada uma das fases presentes. Estes novos resultados podem ser encontrados nas revistas: Physica Review B, Journal of Physics: Condenser Matter e Journal of Magnetism and Magnetic Materials.

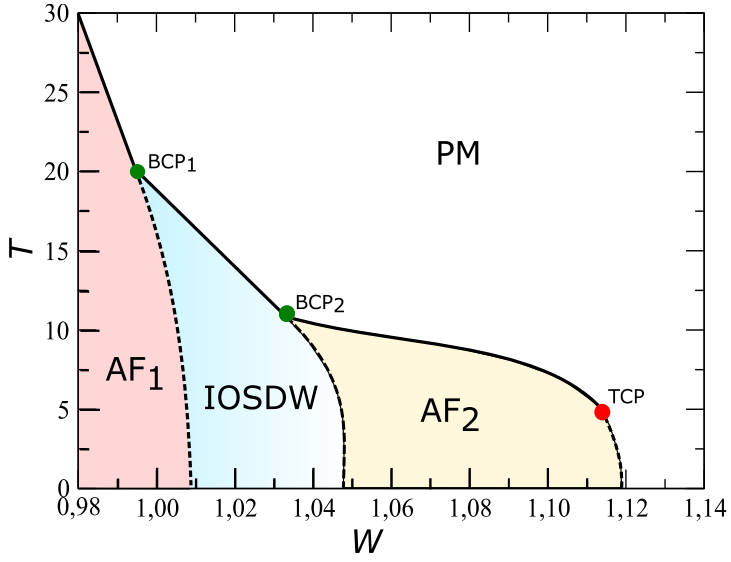

Fig. 1: Diagrama de fase de T (temperatura) versus W (pressão). AF_1 e AF_2 correspondem a duas fases antiferromagnéticas, PM é uma fase paramagnética e IOSDW é uma fase exótica não magnética. BCP_1 e BCP_2 são dois pontos bicríticos, TCP é um ponto tricrítico. Fonte: J. Phys.: Condensed Matter, **33** 295801 (2021).

Autor: Julián Faúndez, Doutorando em Física na Universidade Federal do Rio Grande do Sul (UFRGS).

Acknowledgments

- En primer lugar, quiero agradecer a mi familia: a mi papa Rubén (Chempo), a mis hermanas Carolina (Carola), Maritza (Icha), mi hermano Hernan (Nan) y a mi polola Vânia. También agradezco a mis amigos de la época del colegio/universidad, especialmente a Pablo Oyarzún, Cristian Porma, Sebastián Muñoz y al recién doctor, Tomás Cassanelli.

- Me gustaría agradecer a los Profs. Sérgio G. Magalhães, Eleonir Calegari y Peter Riseborough por toda su ayuda y paciencia durante la realización de este trabajo.

- Un agradecimiento especial al profesor Luis Oyarzún, que ya no está entre nosotros, pero que fue quien me motivó a seguir la carrera científica.

- También quiero agradecer a mis amigos brasileños y mozambicanos, por haber hecho más agradable mi estancia en Porto Alegre.

- A la CNPq (Conselho Nacional de Desenvolvimento Científico e Tecnológico) por el apoyo financiero durante la ejecución de este proyecto.

Abstract

Universidade Federal do Rio Grande do Sul
Instituto de Física
Doctor of Natural Sciences

Multicritical points in a model for $5f$-electron systems under pressure and magnetic field

by Julián FAÚNDEZ

We investigate the evolution of multicritical points under pressure and magnetic field in a model described by two $5f$-bands (labeled as α and β) that hybridize with a single itinerant conduction band. This model is called *Underscreened Anderson Lattice Model* (UALM). The interaction is given by Coulomb and the Hund's rule exchange terms, U and J, respectively. We have three cases of study: *i*) two conventional *Spin Density Waves* (SDWs) where the magnetic field is applied longitudinally to x-axis for cubic lattice, *ii*) two conventional SDWs for both cubic and tetragonal lattices when the magnetic field is applied in z-axis and *iii*) two conventional SDWs and one exotic SDW for cubic lattice when the magnetic field is applied in z-axis. The conventional SDWs, are characterized by AF_1 ($m_f^\beta > m_f^\alpha > 0$) and AF_2 ($m_f^\alpha > m_f^\beta > 0$). The exotic SDW or *Inter-Orbital Spin Density Wave* (IOSDW) is related to a band mixing given by the spin-flip part of the Hund's rule exchange interaction. As result, without magnetic field, in the cases *i*) and *ii*) the phase diagrams of temperature (T) versus pressure (given by the variation of the bandwidth (W)) shows a first-order phase transition between AF_1 and AF_2 and for the case *iii*) show a sequence of first-order phase transitions involving the three phases, AF_1, IOSDW and AF_2. The application of Γ_f (magnetic field in x-axis) in the case *i*) produce the separation of phases AF_1 and AF_2, acquiring a dome shape that is eventually suppressed for large values of the applied field. For the case *ii*) we found that H_z (magnetic field in z-axis) favours the phase AF_2 while the phase AF_1 is suppressed and specifically in the tetragonal lattice, the phase AF_2 is even more favored when H_z and c/a increases continuously. For the case *iii*) the presence of h_z (magnetic field in z-axis) has drastic effects on part of the phase diagram and the location of the multicritical points. We propose that the study of multicritical points can provide relevant information on the conventional and

unconventional phases present in uranium compounds.

Keywork: Multicritical points, $5f$-electron systems, conventional SDWs and exotic SDW.

Resumo

Universidade Federal do Rio Grande do Sul
Instituto de Física
Doutorado em Ciências Naturais

Pontos multicríticos em um modelo para sistemas de elétrons $5f$ sob pressão e campo magnético

por Julián FAÚNDEZ

Investigamos a evolução de pontos multicríticos sob pressão e campo magnético em um modelo descrito por duas bandas $5f$ (chamadas α e β) que se hibridizam com uma única banda de condução itinerante. Este modelo chama-se *Underscreened Anderson Lattice Model* (UALM). A interacção é dada pelos termos de Coulomb e pelo termo de troca da regra de hund, U e J, respectivamente. Temos três casos de estudo: i) duas *Spin Denisty Wave* (SDWs) convencionais onde o campo magnético é aplicado longitudinalmente ao eixo x em uma rede cúbica, ii) duas SDWs convencionais para as redes cúbica e tetragonal, quando o campo magnético é aplicado no eixo z e iii) duas SDWs convencionais e um SDW exótico em uma rede cúbica quando o campo magnético é aplicado ao longo do eixo z. As fases convencionais SDWs, são caracterizadas por AF_1 ($m_f^\beta > m_f^\alpha > 0$) e AF_2 ($m_f^\alpha > m_f^\beta > 0$). O exótico SDW ou *Inter-Orbital Spin Density Wave* (IOSDW) está relacionada com uma mistura de bandas dada pela parte spin-flip da interacção de troca de regras do Hund. Como resultado, sem campo magnético, nos casos i) e ii) os diagramas de fase de temperatura (T) versus pressão (variação da largura de banda (W)) mostram uma transição de fase de primeira ordem entre AF_1 e AF_2 e para o caso iii) mostram uma sequência de transições de fase de primeira ordem envolvendo as três fases, AF_1, IOSDW e AF_2. A aplicação de Γ_f (campo magnético no eixo x) no caso i) produz a separação das fases AF_1 e AF_2, adquirindo uma forma de cúpula que é eventualmente suprimida para grandes valores do Γ_f. Para o caso ii) descobrimos que H_z (campo magnético no eixo z) favorece a fase AF_2 enquanto a fase AF_1 é suprimida e especificamente na rede tetragonal, a fase AF_2 é ainda mais favorecida quando H_z e c/a aumenta continuamente. Para o

caso *iii*) a presença de h_z (campo magnético no eixo z) tem efeitos drásticos sobre parte do diagrama de fase e a localização dos pontos multicríticos. Propomos que o estudo de pontos multicríticos possa fornecer informações relevantes sobre as fases convencionais e não-convencionais presentes nos compostos de urânio.

Palavras claves: Pontos multicríticos, sistemas de elétrons $5f$, convencional SDWs e exótica SDW.

List of Abbreviations

Abbreviate	**Meaning**
HO	Hidden Order
TCP	Tricritical point
BCP	Bicritical point
UALM	Underscreened Anderson Latiice Model
UKLM	Underscreened Kondo Latiice Model
TRS	Time-reversal symmetry
SRS	Spatial-reversal symmetry
U	Coulomb interaction term
J	Hund's rule exchange interaction term
SDW	Spin density wave
BCT	Body-centered-tetragonal
W	Bandwidth (pressure variation)
OP	Order parameter
AF	Antiferromagnetic order
PM	Paramagnetic order
FS	Fermi Surface
TTC	Tetracritical point
IOSWD	Inter-orbital spin density wave
CEP	Critical end point
C_v	Specific heat
T	Temperature
T_c	Critical temperature
T_{HO}	Critical temperature of HO
DOS	Density of states
SC	Superconducting state
P	Pressure
B	Magnetic field
μ_B	$5.7883818066(38)\times10^{-5}$ [eV/T] (Bohr magneton)
$\Gamma_{f(d)}$	Magnetic field in x-axis for $f(d)$-electrons

$H_z^{f(d)}$	Magnetic field in z-axis for $f(d)$-electrons in tetragonal lattice
h_z	Magnetic field in z-axis for cubic lattice
QTP	Quantum triple point
$V_{\alpha(\beta)}$	Hybridization term for $\alpha(\beta)$-band
k_B	8.617333262×10^{-5} [eV·K] (Boltzmann constant)
T_N	Néel temperature
$m_f^{\alpha(\beta)}$	Magnetization of $\alpha(\beta)$-band
$\Delta_{\alpha(\beta)}$	Gaps of $\alpha(\beta)$-band with Γ_f
$\phi_\sigma^{\alpha(\beta)}$	Spin gaps of $\alpha(\beta)$-band for H_z
$\phi_{-\mathbf{Q},\sigma}^{\alpha\alpha(\beta\beta)}$	OPs of $\alpha(\beta)$-band with h_z
$z_{-\mathbf{Q},\sigma}^{\beta\alpha}$	Complex OP that describe the exotic SDW

List of Figures

Contents

Chapter 1

Introduction

The physics present in the $5f$-electrons is quite intriguing, since a multiplicity of quantum states of matter are found, from magnetism (localized and itinerant) [1, 2], superconductivity [3, 4], to exotic and enigmatic states such as the Hidden Order (HO), not yet understood, found in the URu_2Si_2 compound [5, 6, 7, 8, 9, 10, 11]. These multiplicities of quantum states can be tuned by pressure variation (hydrostatic or chemical) in addition to the application of external magnetic fields. This means that any microscopic model oriented to the study of $5f$-electrons must be able to track these external perturbations, which could determine the emergence and evolution of conventional, non-conventional or even exotic collective quantum states. Thus the different types of ordering that uranium compounds host makes these systems a natural ground for the emergence of classical and quantum multicritical points.

Recently, there have been several observations in these electron systems indicating classical tricritical points (TCP) as, for example, in the compounds USb_2 [12], UN [13], UAu_2Si_2 [14] and URu_2Si_2 [15] when a magnetic field is applied. Another example is the presence of a classical bicritical point (BCP) that appears in URu_2Si_2 when the hydrostatic pressure is varied and this point is entirely related to the competition between the puzzling state HO and an AF phase [16], see section (1.1). Thus, the presence of classical multicritical points allows an alternative development to the study of $5f$-electron systems.

These classical critical points may eventually evolve, by varying some intensive parameter, e.g., by increasing the pressure, applying a magnetic field or driven by thermal fluctuations, to become quantum critical points [17] and thus possibly exhibit a behavior that deviates from the standard Fermi Liquid [18, 19]. Also, the presence of a specific type of multicritical point could be useful to elucidate an unconventional symmetry breaking that may exist in uranium compounds. Still, the

subject of classical multicritical points in the physics of $5f$-electron systems has not yet received due attention.

In general, at high temperatures, the $5f$-electrons behave as localized magnetic moments decoupled from the d-electrons. As the temperature decreases, the coupling between the $5f$-electrons and the d-electrons increases due to increased hybridization, causing the $5f$-electrons to lose their localized character and begin to be itinerant. In other words, the formation of narrow bands appears with electrons of higher effective mass. The presence of these narrow bands gives rise to strong electronic correlation effects. Thus, depending on the itinerant or localized character of the $5f$-electrons, several theories have been proposed to explain, for example, the nature of HO in URu_2Si_2. Among them, there is one, proposed by Profs. Peter Riseborough, Bernard Coqblin and Sergio G. Magalhães [7], which is directly related to the present PhD thesis. This theory utilizes the *Underscreened Anderson*[1] *Lattice Model* (UALM).

The UALM has been introduced as a generalization of the *Underscreened Kondo Lattice Model* (UKLM) that has successfully described the coexistence of the Kondo[2] effect and magnetism found in uranium monochalcogenides [20, 21]. Furthermore, the UALM can describe, not only the AF ordering observed in the uranium-pnictides, [22, 23] and $UIrSi_3$ [24], but has also been proposed to describe the HO phase of the URu_2Si_2 [7]. Since the UALM can be considered a generalization of the UKLM, it might also be considered appropriate to describe some aspects of the $5f$-electron systems.

The UALM has a direct hopping between distinct orbitals ($\chi = \alpha$ and β) which gives rise to two quite narrow f-bands. These, by their turn, are hybridized with a wide conduction band. Lastly, there are f-electron intra- and inter-orbitals interactions. Remarkably, this model can host itinerant spins orderings where the time-reversal symmetry (TRS) is broken or not [8, 25, 26]. This model consists of two degenerate narrow $5f$-bands (denoted by $\chi = \alpha, \beta$), which acquire itinerant character by direct hopping between neighboring $5f-$bands. The resulting two narrow bands are also hybridized with a single itinerant conduction band. The interaction is composed of the Coulomb interaction (U) between electrons in the same $5f$-band and the Hund's rule exchange interaction (J) between electrons in distinct $5f$-orbitals. To know more about the UALM, see the chapter (2).

The UALM is also suited for the investigation of TRS breaking as source of unfolding of phases and multicritical points. The Hund's rule exchange interaction

[1] Philip Warren Anderson: Winner of Nobel Prize in Physics in 1977. Born on December 13, 1923, United states. Deceased on March 29, 2020, United Sates.

[2] Jun Kondo: Born on February 6, 1930, Japan. Deceased on March 11, 2022, Japan.

term is essential to make the model spin-rotationally invariant [27] and opens distinct routes to long-range ordering. As an example, a phase transition can be driven by the spin-flip part of Hund's rule exchange interaction, breaking spin-rotational and space-translational symmetries but preserving the TRS. As a result, a novel ordered state can be stabilized in which there is spontaneous $5f$ inter-orbital band mixing, that does not involve magnetic order. This ordering exists due to a mixture of electrons in different bands, with very special properties. It is an exotic type of *Spin Density Wave* (SDW) with rotational and translational symmetry breaking, but preserving the TRS and in other words, a non-magnetic SDW. This novel type of long-ranged order has been proposed as describing the HO phase in URu_2Si_2 [7]. The interaction terms can also produce conventional SDW long-range order in the UALM. This convencional SDWs appears below a magnetic phase transition at which spin-rotational, space-translational and TRS are broken. This transition gives rise to not one but two distinct competing conventional SDWs which have spin gaps at the same ordering wave-vector. Therefore, in the transition between the two conventional SDW phases, no further symmetries are broken. In this PhD thesis, we have three different case studies.

As the first case, we consider two conventional SDW phases their respective order parameters (OPs) as found in some uranium compounds [28, 29, 30]. The magnetic field is applied longitudinally in x-axis. In this case, we investigate the temperature - pressure - magnetic field phase diagram of the SDW phases within a mean-field approximation. We assume that the bandwidth W can be varied by the application of pressure while the hybridization, the Coulomb and the Hund's rule interactions remain constant. We also make the following assumptions: (a) The hybridization matrix elements are $\mathbf{k}$-independent. As a consequence, one may transform the basis of the $5f$-states into a new basis in which a linear combination of f-orbitals hybridize and the remaining orthogonal states do not. This has been confirmed by the recent observation of orbital selectivity of the Kondo effect in the uranium-dichalcogenide USb_2, [31] in which the Kondo interaction is caused by the hybridization which only involves a subset of the f-orbitals and orbital Kondo effect in UTe_2 [32]. The asymmetric hybridization breaks the symmetry between the $5f$-bands, so intra-band nesting may occur simultaneously for both bands but, when W increases, one band may become depart from the perfect nesting condition and, hence have a reduced momentum. Ultimately, above some value W, both bands might not satisfy the nesting condition and the material might become non-magnetic. (b) the convencional SDWs has a OP which is fixed by an Ising-like anisotropy. This assumption introduces a magnetic anisotropy which, in fact, is observed in some uranium com-

pounds [28, 29, 30]. As a consequence, there are two types of field effects in the conventional SDW bands [8, 33]. For a field aligned with the easy axis, the Zeeman splitting between the spin-up and spin-down SDW sub-bands increases as the field increases. On the other hand, for a field along a perpendicular direction, there is a spin-dependent momentum-shift of the conventional SDW bands. However, the choice for a transverse field brings the possibility that classical multicritical points can evolve into quantum multicritical points due to spin-flipping effects. In the specific case of two different conventional SDWs (denoted as AF_1 and AF_2), each of the magnetic phases are related to each $5f$-band (no band mixing). Therefore, the phase transition $AF_1 \rightarrow AF_2$ would necessarily imply that the two spins gaps abruptly interchange their sizes. Eventually, as pointed out above, a further variation of W can cause the complete suppression of the conventional SDW ordering. The sequence of transitions $AF_1 \rightarrow AF_2 \rightarrow$ PM should involve changes in the structure of the AF bands and, therefore, should be accompanied by Fermi Surface (FS) reconstruction. One may also expect that other sequences of phase transition involving conventional SDW caused by increasing the magnetic fields in x-axis are also related to changes in the electronic structure.

As second case of study, we have two conventional SDWs in the UALM under simultaneous application of pressure and magnetic fields for both cubic and tetragonal lattices when the magnetic field is applied in z-axis. The SDW is unfolded into two types (with same nesting vectors) AF_1 and AF_2 which have finite distinct staggered magnetization for each orbital label [10, 11]. Thus, the SDWs are characterized by which orbital staggered magnetization is larger. For low pressure, there is the onset of AF_1 at lower temperature and when the pressure is increased, AF_2 starts to compete by the stability with AF_2. As a consequence, of pressure and/or magnetic field, the level of metallicity can be also affected. Therefore, an evolution of the FS can be anticipated with some type of reconstruction as the combined application of this two external parameters. We also highlight the possibility of metamagnetic transitions [2, 34, 35, 36]. Since, the two SDWs are competing by the stability when W is increased, the presence of the magnetic field modifying the band structure can lead to transitions induced by the field [37, 38]. In addition, one can expect that this particular aspect be highly sensitive to the specific lattice structure, cubic or tetragonal. The occurrence of metamagnetic-like-transitions and TCPs have been reported in different uranium compounds, for instance, USB_2 [40] and $U(Pd_{1-x}Ni_x)_2Al_3$ [41]. Moreover, the compound UNiGe showed the presence of an AF phase at low magnetic fields and an uncompensated AF phase at high magnetic fields [42, 43]. In addition, the compound UNiGa exhibits various AF phases

below $T_N = 39$ K. Although the magnetic field along the c-axis induces phase transitions between the different AFM phases, a new AFM phase is induced at high pressures [44, 45].

As as third case study, we highlight the role of the Hund's rule exchange interaction in the UALM which gives a particular type of mixing of the two $5f$-bands, allowing the model to host a phase that break spin-rotational and space-translational symmetry but invariant TRS. More precisely, this exotic SDW, which does not involve magnetic moment formation, is specifically related to the spin-flip part of Hund's rule exchange interaction. Again we remark that this non-magnetic SDW has been proposed to describe the HO in URu_2Si_2 [7]. From now on, we refer to this phase as an Inter-Orbital Spin Density Wave (IOSDW) or exotic SDW with a single imaginary OP. In addition, we have within the mean field approximation, the competition between the IOSDW and the conventional SDWs in phase diagrams where pressure and magnetic field are applied simultaneously. For this purpose, we explore a scenario where the instability of the paramagnetic phase towards to conventional and non-conventional SDWs occurs at the same nesting vector. In this case, we assume that the applied pressure changes the inter-atomic distances and, thereby, changes W. Within UALM, these SDWs - in the three cases of interest- are characterized by a staggered magnetization for each band (here called α or β) given by m_f^α and m_f^β. The first SDW, called AF_1, occurs when $m_f^\beta > m_f^\alpha$, while in the other one, called AF_2, when $m_f^\alpha > m_f^\beta$. Indeed, the prediction of the existence of a critical end point (CEP) has been confirmed in the UALM [46]. In the case where IOSDW is also stabilized, the coupling among OPs is more complicated since they have distinct parity properties under TRS [25]. Therefore, in terms of a Landau free energy expansion, the competition among AF_1, AF_2 and IOSDW can lead to a bicritical point (BCP) or a tetracritical point (TTC) [39]. For further variation of pressure or field, the nesting condition may no longer be satisfied leading to the suppression of the ordered phases. This last phase transition line can present a TCP [46]. Lastly, because of the asymmetry between the bands, we remark that the simultaneous effects of pressure the magnetic field on the phases AF_1, AF_2, IOSDW and, consequently on the multicritical points, are closely connected with changes in the electronic structure of the problem. Particularly, the effects of the magnetic field on each of the phases can be traced directly from changes in the quasiparticle dispersion relations [8].

Our goal in this work is to show how classical multicritical points can emerge from the competition between conventional and non-conventional SDWs hosted in the UALM. We also show that by means of type of critical point it is possible to

know the physical nature of the multiple phases present, e.g., as electronic properties or broken symmetries, without the need for an individual study of each of them. In addition, we try to make an analogy between the exotic SDW phase and HO.

1.1 Motivation of study of URu_2Si_2

In 1984 an unprecedented discovery was made with the observation of a superconducting state at a critical temperature of 1.5 K in a heavy fermion magnetic compound based on uranium, specifically URu_2Si_2. It is now known that that superconducting state is unconventional with d-wave function type, in addition to a TRS breaking. However, the antiferromagnetic state, initially thought in this compound, was not of magnetic nature but of a new and unknown type of non-magnetic order to which the term hidden order was dominated. The Hidden Order (HO) has been a problem still under discussion and the true nature of the HO may reveal new mechanisms capable of generating a state with peculiar electronic and magnetic properties [47].

The heavy fermion compound URu_2Si_2 has a body-centered-tetragonal (BCT) crystal structure at high temperatures, with lattice constants $a = 0.4124\ nm$, $b = 0.4126$ and $c = 0.9582\ nm$ [48], see Fig. (1.1)(a). In Fig. (1.1)(b) on the right side is the crystalline representation of only U atoms. These atoms have an alignment on the c axis of symmetry which through experimental evidence present small localized antimagnetic moments of the order ($\approx 0.03\mu_B$), but the magnitude of these localized antiferromagnet moments cannot give a crystal lattice stability, therefore, the crystalline lattice cannot be defined with a definite magnetic order [18, 19]. From developed experiments it is thought that the emergence of the HO is due to the transformation of the URu_2Si_2 crystal lattice as it lowers the temperature, from a BCT lattice to a tetragonal lattice [20, 21, 23]. But it is also thought that the emergence of the HO has nothing to do with the lattice (distortions, impurities) but with a purely electronic effect.

In the URu_2Si_2 a specific heat peak was observed at $T_{HO} \approx 17.5$ K and below this temperature a new transition to this superconducting phase appears at $T_S \approx 1.5$ K given by a new peak at C_v. The initial interpretation for the state formed in the temperature range between the two C_v peaks is that this would be a conventional antiferromagnetic manifestation that, at lower temperatures, would compete with the superconducting phase. In the specific heat curve of the lower part there are two peaks presented and between the temperature range [2 K - 17 K] the specific

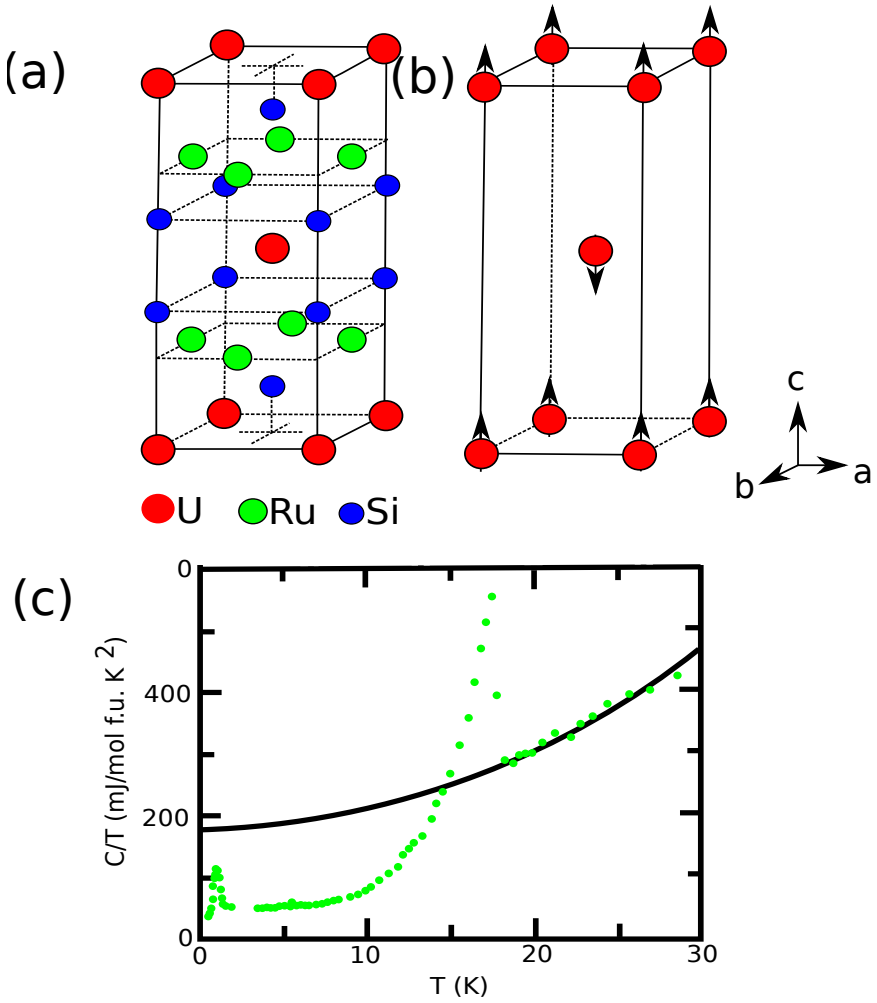

Figure 1.1: (a) Crystal structure of body-centered-tetragonal lattice for URu_2Si_2 and the corresponding space group is the *I4/mmm*. (b) Magnetic structure with only magnetic atoms and (c) specific heat as a function of temperature. We have two specific heat peaks, the first at 2 K and the second at 17.5 K. The region between these two peaks has no magnetic order and corresponds to the HO state region [22].

heat curve is given by the following:

$$C(T) = \gamma T + AT^3 + b\epsilon^{-\Delta/T}, \tag{1.1}$$

where the values of γ and A are given by the material characteristics, Δ corresponds to an energy gap. The first two terms describe to free electrons as well as lattice vibrations, and the third part represents electrons present in the HO phase [8, 33]. Above temperature T= 17.5 K the C_v curve is characterized only by the first two terms of Eq. (1.1). Thus it can be said that these specific heat peaks clearly show the presence of phase transitions: SC and HO, but the nature of the emergence of the HO in URu_2Si_2 is not shown.

1.2 Hidden Order: Experimental Evidence

In the Fig. (1.2)(a) is the phase diagram of temperature versus pressure. As the temperature decreases and at low pressures a first-order transition from a normal state to a HO state is shown. As the pressure begins to increase at low temperatures a first-order transition from the HO state to an antiferromagnetic state occurs. For higher values of pressure and as the temperature begins to increase a second-order transition from the antiferromagnetic state to a normal state is again shown. These transitions are reflections of the presence of a BCP. In Fig. (1.2)(b) the formation of magnetic moments as a function of pressure is shown. At low pressures the HO phase exists and the formation of magnetic moments is nonexistent, but as the pressure increases there is a strong change in the formation of magnetic moments, which are constant at high pressures, here the system is in the antiferromagnetic phase. In Fig. (1.2)(c) we have a phase diagram of temperature versus magnetic field, we can see that at low magnitudes of magnetic field and as the temperature begins to decrease a second-order transition occurs from the normal state to HO, but for low temperatures and as the magnetic field is increasing a first-order phase transition occurs from the HO state to a normal state. The presence of a TCP is also shown. In this manner, several experiments in recent years have shown that the nature of the HO state is much more complex than previously thought [18, 20, 23]. Experiments of inelastic neutron scattering measurements confirmed the existence of localized magnetic moments. However, these magnetic moments are very small on the order of magnitude ($\approx 10^{-2}\mu_B$) as to ensure a conventional magnetic order [18]. The strangeness of the situation was confirmed by the measured entropy value which is completely incompatible with the entropy calculated from the measured magnetic moments. In other words, these results clearly indicate that the origin of the gap found for $T<T_{HO} = 17.5$ K cannot be attributed to the presence of a conventional magnetic state. Other experimental results complete the complexity scenario of the problem, for example, finite pressure measurements showed a first-order phase transition from the HO state to an antiferromagnetic phase ($P = 0.75$ GPA) with well-developed magnetic moments ($0.4\mu_B$). Fig (1.2) (b) shows that as the temperature goes down a new state arises but does not have a conventional magnetic order. Also measured using the Haas-van Alphen effect showed that the HO state and the antiferromagnetic phase have the same Fermi surface (FS) and therefore the same nesting vector $\mathbf{Q}$ [20]. Finally, magnetic field measurements, see Fig. (1.2)(c), showed that the HO state remains until a magnetic field value $B = 35$ T. The phase transition to HO state that was second-order in the absence of field becomes first-order [8, 49]. Indications are strong that this anisotropy known as

magnetic nematicity is one of the most important manifestations of the HO state in URu_2Si_2. A crucial aspect of this problem is the role of spin-orbit interaction. It has recently been shown that this coupling describes the giant magnetic anisotropy in the antiferromagnetic phase of URu_2Si_2. This anisotropy is not the result of spontaneous symmetry breaking, but a similar effect is found in both the paramagnetic phase and the HO [50].

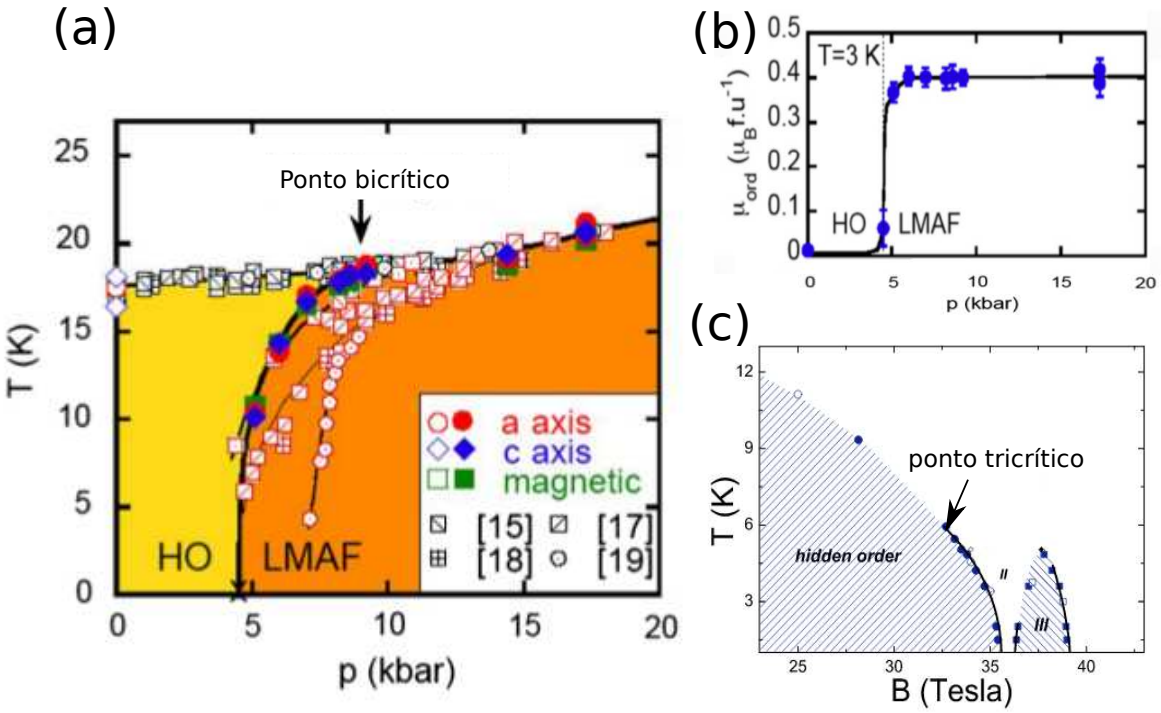

Figure 1.2: (a) Phase diagram for URu_2Si_2 of temperature versus pressure. HO = Hidden Order and AF = Antiferromagnetic. At 17.5 K there is a second-order phase transition from the HO to the paramagnetic state and at 5 kbar there is a first-order transition from HO to paramagnetic phase and for sufficiently high pressures and as the temperature increases, a new second-order transition occurs. We can see that at $T \approx 17.5$ K and $P \approx 7.5$ kbar there is a bicritical point (BCP). (b) Behavior of magnetic moments as a function of pressure, both in the HO and antiferromagnetic phases. (c) Phase diagram of URu_2Si_2 of temperature versus magnetic field. We can see that at low magnitudes of magnetic field and as the temperature begins to decrease a second-order transition occurs from the normal state to HO, but for low temperatures and as the magnetic field is increasing a first-order phase transition occurs from the HO state to a normal state. The presence of a tricritical point is also shown [22].

The difficulty in understanding the nature of the HO state in the URu_2Si_2 compound is strongly associated with the role of the $5f$-electrons. As previously mentioned at high temperature, $5f$-electrons in heavy fermion compounds such as URu_2Si_2 behave as uncoupled localized magnetic moments of conduction electrons. As the temperature decreases, coupling with conduction electrons due to hybridiza-

tion increases, causing the $5f$-electrons to begin to lose their localized character by becoming itinerant, forming narrow bands with increased effective mass electrons. The presence of these narrow bands gives rise to effects of many complex bodies. On the other hand, the discovery of superconductivity and heavy fermion behavior in UBe_{13} [51] and UPt_3 [52] compounds led to the study of other uranium-based compounds in order to find anomalous behaviors. HO is a problem that has been open for over 30 years and with different explanatory theories, but it is not yet possible to find the OP responsible for the transition. Within the theories that have been proposed to explain the nature of the HO phase are the multipolar order [53], the unconventional SDW [11], the modulated spin liquid [54], as examples. These theories are separated into two major groups according to the model used: localized and itinerant $5f$-electrons, due to the dual nature of the $5f$-electrons present in uranium compounds. The central question to be answered can be put in the following terms: what is the OP capable of characterizing the state or state HO in URu_2Si_2 ? what are the symmetries that are broken? Some of these questions can be answered by considering the HO phase as an analogy to the exotic SDW -present in this work-

1.3 Thesis scope

This section is mainly dedicated to a brief introduction to each of the most important points of this thesis.

- To begin with, in Chapter 2, we describe the UALM in two conventional SDWs with their respective OPs, where the magnetic field is applied longitudinally to x-axis for cubic lattice. The following is an extension of the study of two conventional SDWs for both cubic and tetragonal lattices when the magnetic field is applied in z-axis. Finally, we consider a competition between two conventional SDWs and one exotic SDW, in cubic lattice, when the magnetic field is applied in z-axis.

- In Chapter 3, we present the numerical results, for the three cases presented above, when the pressure (variation of bandwidth (W)) and magnetic field are applied. We show the respective phase diagrams, band structure and densities of states.

- In Chapter 4, we present our general conclusions referring to the three case studies carried out in this thesis work.

- In Chapter 5, we present possible future works.

- In Chapter 6, we present the articles published and in preparation during the doctoral stage.

- Finally, in chapter 7, we thank the agencies that have provided financial support for the success of this work.

Chapter 2

Theory and Methodology

2.1 The *Underscreened Anderson Lattice Model* (UALM)

The UALM Hamiltonian consists of three terms

$$\hat{H} \;=\; \hat{H}_f \;+\; \hat{H}_d \;+\; \hat{H}_{fd}. \tag{2.1}$$

The f-electron part of Hamiltonian, $\hat{H}_f$, is given by $\hat{H}_f = \hat{H}_{f,0} + \hat{H}_{f,int}$, where the non-interacting part $H_{f,0}$ describes two degenerate narrow f-bands and is expressed as

$$\hat{H}_{f,0} = \sum_{\mathbf{k},\sigma} \sum_{\chi} \; E_f^{\chi}(\mathbf{k}) \; f_{\mathbf{k},\sigma}^{\dagger\chi} f_{\mathbf{k},\sigma}^{\chi}. \tag{2.2}$$

The χ-bands ($\chi = \alpha$ and β) in Eq. (2.2) obey the intraband and interband nesting condition $E_f^{\chi}(\mathbf{k}+\mathbf{Q}) = -E_f^{\chi'}(\mathbf{k})$ where $\chi = \chi'$ (intraband) or $\chi \neq \chi'$ (interband). The $f_{\mathbf{k},\sigma}^{\dagger}(f_{\mathbf{k},\sigma})$ are the creation (annihilation) f-operators with $\mathbf{k}$-momentum dependence and spin $\sigma = \pm 1$. Fundamentals of second quantization of fermions is found in the Appendix (A). The vector $\mathbf{Q}$ is a commensurate momentum transfer in the Brillouin zone. The interaction between the f-electrons is described by

$$\begin{aligned}
\hat{H}_{f,int} \;=\; & \left(\frac{U-J}{2N}\right) \sum_{\mathbf{k},\mathbf{k}',\mathbf{q},\sigma,\chi\neq\chi'} f_{\mathbf{k}+\mathbf{q},\sigma}^{\dagger,\chi} \; f_{\mathbf{k},\sigma}^{\chi} \; f_{\mathbf{k}'+\mathbf{q},\sigma}^{\dagger,\chi'} f_{\mathbf{k}',\sigma}^{\chi'} \\
& + \left(\frac{U}{2N}\right) \sum_{\mathbf{k},\mathbf{k}',\mathbf{q},\sigma,\chi,\chi'} f_{\mathbf{k}+\mathbf{q},\sigma}^{\dagger,\chi} \; f_{\mathbf{k},\sigma}^{\chi} \; f_{\mathbf{k}',-\sigma}^{\dagger,\chi'} f_{\mathbf{k}',-\sigma}^{\chi'} \\
& + \left(\frac{J}{2N}\right) \sum_{\mathbf{k},\mathbf{k}',\mathbf{q},\sigma,\chi\neq\chi'} f_{\mathbf{k}+\mathbf{q},\sigma}^{\dagger,\chi} \; f_{\mathbf{k},\sigma}^{\chi'} \; f_{\mathbf{k}'+\mathbf{q},-\sigma}^{\dagger,\chi'} \; f_{\mathbf{k}',-\sigma}^{\chi}.
\end{aligned} \tag{2.3}$$

where U is the Coulomb interaction and J is the Hund's rule exchange term. The conduction electron Hamiltonian $\hat{H}_d$ is expressed as

$$\hat{H}_d \;=\; \sum_{\mathbf{k},\sigma} \epsilon_d(\mathbf{k})\; d^{\dagger}_{\mathbf{k},\sigma}\; d_{\mathbf{k},\sigma} \tag{2.4}$$

where $\epsilon(\mathbf{k})$ describes the dispersion relation of conduction electrons labeled by the Bloch wave vector $\mathbf{k}$. The $d^{\dagger}_{\mathbf{k},\sigma}(d_{\mathbf{k},\sigma})$ are the creation (annihilation) d-operators with $\mathbf{k}$-momentum dependence and spin $\sigma = \pm 1$. The last term in Eq. (2.1) describes the on-site hybridization process in the UALM by

$$\hat{H}_{fd} \;=\; \sum_{\mathbf{k},\sigma} \sum_{\chi=\alpha\beta} \left(V_{\chi}(\mathbf{k})\; f^{\dagger,\chi}_{\mathbf{k},\sigma}\; d_{\mathbf{k},\sigma} \;+\; V^{*}_{\chi}(\mathbf{k})\; d^{\dagger}_{k,\sigma}\; f^{\chi}_{\mathbf{k},\sigma} \right). \tag{2.5}$$

We include an applied magnetic field oriented along the x-axis which introduces an additional term into the Hamiltonian $\hat{H}_{ext} = \hat{H}^{f}_{ext} + \hat{H}^{d}_{ext}$ where

$$\hat{H}^{f}_{ext} = -\Gamma_f \sum_{\mathbf{k}} \left(f^{\dagger}_{\mathbf{k},\uparrow}\; f_{\mathbf{k},\downarrow} \;+\; f^{\dagger}_{\mathbf{k},\downarrow}\; f_{\mathbf{k},\uparrow} \right) \tag{2.6}$$

with

$$\Gamma_f = g_f \mu_B h_x. \tag{2.7}$$

The term $\hat{H}^{d}_{ext}$ is the same of Eqs. (2.6) and (2.7), except that the f-operators and the gyromagnetic factor g_f are replaced by d-operators and g_d, respectively. In addition, we can consider the effects of a magnetic field applied parallel to the z-axis. To include this field we must add an extra term in Eq. (2.1) given by

$$\hat{H}^{z}_{ext} = -\sum_{\mathbf{k}} \sum_{\sigma=\pm} \sigma [H^{f}_{z} f^{\dagger}_{\mathbf{k},\sigma} f_{\mathbf{k},\sigma} + H^{d}_{z} d^{\dagger}_{\mathbf{k},\sigma} d_{\mathbf{k},\sigma}] \tag{2.8}$$

with

$$H^{f(d)}_{z} = g_{f(d)} \mu_B h_z. \tag{2.9}$$

The value $\sigma = 1$ and -1 correspond to the up and down spin projections, respectively. The $5f$ band $E^{\chi}_{f}(\mathbf{k}) = \epsilon_f + \epsilon_f(\mathbf{k})$ and the conduction one $\epsilon_d(\mathbf{k})$ refer to a simple tetragonal lattice. Thus

$$\epsilon_A(\mathbf{k}) = -2t_{A,a}\cos(k_x a) - 2t_{A,a}\cos(k_y a) - 2t_{A,c}\cos(k_z c) \tag{2.10}$$

in which $A = f$ or d, and a, b and c are the lattice parameters. If $a = b = c$, we have a cubic lattice and for a tetragonal lattice, we have that the lattice parameter

are $a = b \neq c$.

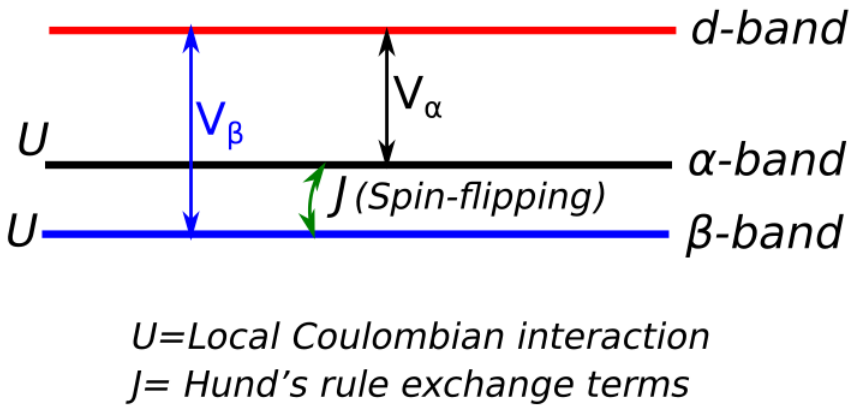

Figure 2.1: *Underscreened Anderson Lattice Model* (UALM): two $5f$-bands (α and β) interacting with a single conduction band (d-band), by means of the hybridization terms, V_α and V_β. Each of the $5f$-bands exhibits local Coulombian interactions and the interaction between the $5f$-bands is given by the spin flipping part of the Hund's rule of the exchange term, U and J, respectively.

2.2 Two conventional SDWs with Γ_f in cubic lattice

From now on, we will focus on the two conventional SDWs with antiferromagentic order (AF_1 and AF_2) and their associated phase transitions using mean field theory (see Appendix C). We shall chose a basis set for the f-orbitals such that $V_\beta(\mathbf{k}) = 0$ in Eqs. (D.9)-(D.10) simply to avoid the transformation to a new basis set. The choice of basis states should not change the main physical results, as is discussed in ref. [7]. The simplest possibility of a conventional SDW ordering with Ising anisotropy in the cubic lattice can be introduced by assuming that the lattice is bipartite. Therefore, we consider that

$$n^{\chi}_{f,\mathbf{q},\sigma} = \frac{n^{\chi}_f}{2}\,\delta_{\mathbf{q},0} + m^{\chi}_f\,\eta(\sigma)\,\delta_{\mathbf{q},\pm\mathbf{Q}} \tag{2.11}$$

where $n^{\chi}_f = n^{\chi}_{f,\uparrow} + n^{\chi}_{f,\downarrow}$ (n^{χ}_f is the f-electron average occupation of the χ-band), $\eta(\uparrow) = +1$ or $\eta(\downarrow) = -1$ and $\mathbf{Q} = (\pi/a, \pi/a, \pi/a)$, is a commensurate nesting vector. Therefore, the modulation of the expectation value of the z-component f-electron spin density operator in real space for each orbital is $\langle \hat{S}^{\chi}_{z,\mathbf{r}_j} \rangle = m^{\chi}_f\, e^{i\mathbf{Q}\,\cdot\,\mathbf{r}_j}$. The conventional SDW OP, i.e., the staggered magnetizations m^{α}_f and m^{β}_f are obtained from

$$m^{\chi}_f = \frac{1}{2}(n^{\chi}_{f,\mathbf{Q},\uparrow} - n^{\chi}_{f,\mathbf{Q},\downarrow}). \tag{2.12}$$

In the Appendix (D) we present the general formulation for find the OPs that describe each antiferromagnetic phase.

2.2.1 Order parameters with $\Gamma_f = 0$

The conventional SDW OPs follow directly from the correlation functions $n^{\chi}_{f,\mathbf{Q},\sigma}$ (see Eq. (2.12)) which can be expressed as

$$n^{\chi}_{f,\mathbf{Q},\sigma} = \frac{1}{N}\sum_{\mathbf{k},\sigma}\oint \frac{d\omega}{2\pi i} f(\omega)\; G^{\chi\chi}_{ff,\sigma}(\mathbf{k},\mathbf{k}+\mathbf{Q},\omega). \tag{2.13}$$

The contour of the path integral encircles the real axis without enclosing any poles of of the Fermi-Dirac distribution. The correlations functions $n^{\chi}_{f,\mathbf{Q},\sigma}$ are found from the Green's function given in Eqs. (D.20)-(D.24). Therefore, from Eq. (2.12), one can obtain:

$$m^{\beta}_f = (U m^{\beta}_f \; + \; J m^{\alpha}_f)\; \chi^{\beta\beta}_f(\mathbf{Q},0) \tag{2.14}$$

where

$$\chi^{\beta\beta}_f(\mathbf{Q},0) = \frac{1}{N}\sum_{\mathbf{k}} \frac{f(E^-(\mathbf{k})) - f(E^+(\mathbf{k}))}{E^+(\mathbf{k}) \; - \; E^-(\mathbf{k})} \tag{2.15}$$

and where $f(\omega)$ is the Fermi function.

The staggered magnetization of the α-bands can be derived in a similar manner to Eq. (2.14). The result is

$$m^{\alpha}_f = (U m^{\alpha}_f \; + \; J m^{\beta}_f)\; \chi^{\alpha\alpha}_f(\mathbf{Q},0) \tag{2.16}$$

where $\chi^{\alpha\alpha}_f(\mathbf{Q},0)$ is now given as

$$\chi^{\alpha\alpha}_f(\mathbf{Q},0) = \\ \frac{1}{2N}\sum_{\mathbf{k},\sigma}\oint \frac{d\omega}{2\pi i} f(\omega)\frac{(\omega-\epsilon_d(\mathbf{k}))(\omega-\epsilon_d(\mathbf{k}+\mathbf{Q}))}{D^{\alpha}(\omega,\mathbf{k})}. \tag{2.17}$$

and where $D^{\alpha}(\mathbf{k},\omega)$ is given in Eq. (D.25). The spin-independent quasiparticles bands are given by the solutions of $D^{\alpha}(\mathbf{k},\omega)=0$. Alternatively, one can formulate the self-consistency equations in terms of the gaps $\Delta_{\alpha(\beta)}$ since

$$\phi^{\alpha(\beta)}_{\uparrow\downarrow} \; = \; \mp\, \Delta_{\alpha(\beta)} \tag{2.18}$$

in which

$$\Delta_{\alpha(\beta)} = U m_f^{\alpha(\beta)} + J m_f^{\beta(\alpha)}. \tag{2.19}$$

The Hund's rule interaction couples the gap of a given band to the staggered magnetization of the other band.

2.2.2 Order parameters with $\Gamma_f \neq 0$

For $\Gamma_f \neq 0$, the pole structure of the Green's functions is much more complex. For finite fields, the Green's functions $G^{\beta\beta}_{ff,\sigma}(\mathbf{k}, \mathbf{k}+\mathbf{Q}, \omega)$ and $G^{\alpha\alpha}_{ff,\sigma}(\mathbf{k}, \mathbf{k}+\mathbf{Q}, \omega)$ shown in Eqs. (D.12)-(D.16), can be used to obtain the OPs m_f^{α}, m_f^{β} and the gaps following the same steps outlined in Appendix (D). We assume that the d-conduction electron band is uncorrelated and wider than the correlated f-bands. We note that the magnetic field on the d-electrons, Γ_d, affects the OPs m_f^{α} and m_f^{β} mainly through the effect of the hybridization $V_{\alpha}(\mathbf{k})$ and is small compared to the α and β bandwidths. Therefore, it is reasonable to disregard the effects of Γ_d on m_f^{α} and m_f^{β}.

2.3 Exotic SDW or IOSDW with h_z in cubic lattice

We apply a mean field approximation to the fluctuations of the f-electrons operators that produces two possible instabilities of the normal-paramagnetic phase in the UALM, i. e., the Exotic SDW phase or IOSDW and the itinerant antiferromagnetic phase. Therefore, we consider the normalized operators below related to each instability:

$$\hat{z}^{\chi'\chi}_{\mathbf{q},\sigma} = \frac{1}{N}\sum_{\mathbf{k}} f^{\dagger,\chi'}_{\mathbf{k}+\mathbf{q},\sigma} f^{\chi}_{\mathbf{k},\sigma} \quad (\chi \neq \chi') \tag{2.20}$$

and

$$\hat{n}^{\chi\chi}_{\mathbf{q},\sigma} = \frac{1}{N}\sum_{\mathbf{k}} f^{\dagger,\chi}_{\mathbf{k}+\mathbf{q},\sigma} f^{\chi}_{\mathbf{k},\sigma} \quad (\chi = \chi'). \tag{2.21}$$

Thus, the interaction term of the Hamiltonian given in the Eq. (2.4) is expanded in powers of

$$\Delta\hat{z}^{\chi\chi'}_{\mathbf{q},\sigma} = \hat{z}^{\chi\chi'}_{\mathbf{q},\sigma} - z^{\chi\chi'}_{\mathbf{q},\sigma} \tag{2.22}$$

and

$$\Delta\hat{n}^{\chi\chi}_{\mathbf{q},\sigma} = \hat{n}^{\chi\chi}_{\mathbf{q},\sigma} - n^{\chi\chi}_{\mathbf{q},\sigma}. \tag{2.23}$$

The general formulation to obtain the OPs is in the Appendix (E).

2.3.1 Order parameters with h_z

The exotic SDW OP is given by the expectation value $z^{\chi'\chi}_{\mathbf{q},\sigma}$. The staggered magnetizations for each f-band, m^{α}_{f} and m^{β}_{f} are obtained from Eq. (2.12). The IOSDW OP is given by the expectation value of the non-hermitian operator given in Eq. (2.20). Thus :

$$z^{\alpha\beta}_{-\mathbf{Q},\sigma} = \frac{1}{N}\sum_{\mathbf{k},\sigma}\int_{C}\frac{d\omega}{2\pi i} f(\omega) G^{\beta\alpha}_{ff,\sigma}(\mathbf{k},\mathbf{k}+\mathbf{Q},\omega), \tag{2.24}$$

where $f(\omega)$ is the Fermi function and $G^{\beta\alpha}_{ff,\sigma}(\mathbf{k},\mathbf{k}+\mathbf{Q},\omega)$ is given in Eq. (E.11). The integration contour closes the real axis and does not include the poles of the Fermi-Dirac distribution. We can re-write Eq. (2.24) as

$$z^{\alpha\beta}_{-\mathbf{Q},\sigma} = \kappa^{\beta\alpha}_{-\mathbf{Q},\sigma} X_{1,\sigma}(\mathbf{Q}) + \phi^{\alpha\alpha}_{-\mathbf{Q},\sigma}\phi^{\beta\beta}_{-\mathbf{Q},\sigma} X_{2,\sigma}(\mathbf{Q}) \tag{2.25}$$

where

$$X_{1,\sigma}(\mathbf{Q}) = \frac{1}{N}\sum_{\mathbf{k}}\int_{C}\frac{d\omega}{2\pi i} f(\omega) \times \frac{g^{\alpha}_{\sigma}(\mathbf{k},\omega) g^{\beta}_{\sigma}(\mathbf{k}+\mathbf{Q},\omega) - |\kappa^{\beta\alpha}_{-\mathbf{Q},\sigma}|^2}{D_{\mathbf{Q},\sigma}(\mathbf{k},\omega)} \tag{2.26}$$

and

$$X_{2\sigma}(\mathbf{Q},\sigma) = \frac{1}{N}\sum_{\mathbf{k}}\int_{C}\frac{d\omega}{2\pi i}\frac{f(\omega)}{D_{\mathbf{Q},\sigma}(\mathbf{k},\omega)} \tag{2.27}$$

with $D_{\mathbf{Q},\sigma}(\mathbf{k},\omega)$ defined in Eq. (E.14). Moreover,

$$g^{\chi}_{\sigma}(\omega,\mathbf{k}) = (\omega - E^{\chi}_{f\sigma}(\mathbf{k}) - \xi^{\chi}(\mathbf{k},\omega)) \tag{2.28}$$

where $\xi(\mathbf{k},\omega)$ is given in Eq. (E.8). From Eqs. (E.9) and (2.25), one can see that $z^{\beta\alpha}_{-\mathbf{Q},\sigma}$ and $z^{\beta\alpha}_{-\mathbf{Q},-\sigma}$ are coupled by the Hund's rule exchange interaction. Actually, the IOSDW solution implies that $z^{\beta\alpha}_{-\mathbf{Q},\sigma} = -z^{\beta\alpha}_{-\mathbf{Q},-\sigma}$. Therefore, for IOSDW to be time reversal invariant, which is the reason for its non-magnetic character, the OP needs to be a purely imaginary quantity [7, 8].

The real staggered magnetizations m^{χ}_{f} ($\chi = \alpha$ and β) (see Eq. (2.12)) are obtained from the Green's function $G^{\chi\chi}_{ff,\sigma}(\mathbf{k},\mathbf{k}+\mathbf{Q},\omega)$ given in Eqs. (E.12) and (E.13). Therefore, the α and β-band staggered magnetizations are expressed as:

$$m^{\chi}_{f} = \sum_{\sigma}\sigma[\phi^{\chi\chi}_{-\mathbf{Q}\sigma}\ X_{3,\sigma}(\mathbf{Q}) + |\kappa^{\beta\alpha}_{-\mathbf{Q},\sigma}|^2\phi^{\chi'\chi'}_{-\mathbf{Q},\sigma}\ X_{2,\sigma}(\mathbf{Q})] \tag{2.29}$$

where $\chi \neq \chi'$, $\sigma = \uparrow, \downarrow$ corresponds to $+-$ and

$$X_{3,\sigma}(\mathbf{Q}) = \frac{1}{N}\sum_{\mathbf{k}}\int_C \frac{d\omega}{2\pi i} f(\omega) \times \frac{(g_\sigma^{\chi'}(\mathbf{k},\omega)g_\sigma^{\chi'}(\mathbf{k}+\mathbf{Q},\omega) - (\phi_{-\mathbf{Q}\sigma}^{\chi'\chi'})^2)}{D_{\mathbf{Q},\sigma}(\mathbf{k},\omega)}. \tag{2.30}$$

The Green function $G_{f,\sigma}^{\chi\chi}(\mathbf{k},\mathbf{k}+\mathbf{Q},\omega)$ is in Eqs. (E.12) and (E.13), so the OP for the β-band is obtained from Eq. (2.12) and expressed as

$$m_f^\beta = (Um_f^\beta + Jm_f^\alpha)\chi_\sigma^{\beta\beta}(\mathbf{Q},\mathbf{k}) \tag{2.31}$$

where

$$\chi_\sigma^{\beta\beta}(\mathbf{Q},\mathbf{k}) = \sum_i^{N^p} f(E_{i,\sigma}(\mathbf{k}))A_{i,\sigma}^{\beta\beta}(\mathbf{k}) \tag{2.32}$$

and similarly for the α-band

$$m_f^\alpha = (Um_f^\alpha + Jm_f^\beta)\chi_\sigma^{\alpha\alpha}(\mathbf{Q},\mathbf{k}) \tag{2.33}$$

with

$$\chi_\sigma^{\alpha\alpha}(\mathbf{Q},\mathbf{k}) = \sum_i^{N^p} f(E_{i,\sigma}(\mathbf{k}))A_{i,\sigma}^{\alpha\alpha}(\mathbf{k}). \tag{2.34}$$

In Eqs. (2.26), (2.32) and (2.34), $E_{i,\sigma}(\mathbf{k})$ are the quasi-particles dispersion relations obtained from $D_\sigma(\mathbf{k},\mathbf{Q},\omega) = 0$ (see Eq. (E.14)), N^p is its number and $A_{i,\sigma}^{\chi\chi'}$ correspond to their respective spectral values which, together with $E_{i,\sigma}(\mathbf{k})$, which are the quasi-particle dispersion relations that depend on the gaps $\phi_{-\mathbf{Q},\sigma}^{\alpha\alpha}$, $\kappa_{-\mathbf{Q},\sigma}^{\beta\alpha}$ and $\phi_{-\mathbf{Q},\sigma}^{\beta\beta}$. are obtained numerically. It should be noticed that the three equations for the order parameters are coupled through of quasi-particle dispersion relations $E_{i,\sigma}(\mathbf{k})$.

2.4 Two conventional SDWs with H_z in tetragonal lattice

The general formalism when we have two conventional SDW with a magnetic field applied on h_z in a tetragonal lattice can be developed as in Appendix (E), but considering that the order parameter describing the exotic SDW phase is null, i.e. $z_{-\mathbf{Q},\sigma}^{\beta\alpha} = 0$. Furthermore, we have to consider that in the dispersion relation equation (Eq. (2.10)) $a = b \neq c$, which corresponds to a tetragonal lattice.

2.4.1 Order parameters with H_z

The Green's function given in Eqs. (E.12) and (E.13) form a closed set of equations, which can be solved exactly. Thus, the spin gap can be calculated directly from in Eq. (E.10). Therefore, we can explore a scenario where the instability of the paramagnetic phase towards to two distinct SDWs occurs at the same nesting vector $\mathbf{Q}$ given by the spin gaps in distinct orbitals. However, it is important to be noted that the spin gaps ϕ_σ^α and ϕ_σ^β are, indeed, coupled. Moreover, the spin gaps are proportional to the magnetic OPs and present exactly same behavior.

Chapter 3

Numerical Results

The numerical results presented in this section have been obtained assuming the following numerical values and conditions. We have that the hybridization term without $\mathbf{k}$ dependence and it exit only for the α-band, $V_\alpha(\mathbf{k}) = V_\alpha = 1/10$ eV, the total occupancy number is $< n_f^\alpha > + < n_f^\beta > + < n_d >= 1.609$, where $< n_d >$ is the average occupation of the conduction electrons, $< n_\alpha >$ and $< n_\beta >$ corresponds to average occupation of $5f$-electrons. This occupation number is chosen to enhance the PM phase instability and does not refer to any specific real $5f$-electron system. The nesting vector is $\mathbf{Q} = (\pi/a, \pi/a, \pi/a)$.

We have also chosen the following parameters: (i) the tight-binding parameters are $t_d = W_d/6$, $t_f = W_d/20$ and $W_f/W_d = 0.3$ where $2W_{d(f)}$ is the width of the conduction band in order to be close to Ref. [46]. From here, we write $W_d = W$ and we also assume that the bandwidth, W, is sensitive to external pressure. Our results are qualitatively robust to the numerical choice of parameters given above. For the construction of OPs, phase diagrams (with and without magnetic field), quasiparticle dispersion relation, density of states and study of multicritical points we consider U=0.165 eV and $J = U/5$. The situation is more complicated when it comes to choosing the J/U ratio and this point will be discussed also in this section. The units of measurement of temperature are given in K (Kelvin), the $\mathrm{k}_B T$ factor and the pressure in eV (electron-volt), since the latter corresponds to the bandwidth variation and the applied magnetic fields are measured in T (Tesla). On another hand, the green functions that help to obtain each of the OPs are described by means of polynomials of different degrees and in which, the sum in the reciprocal space ($\mathbf{k}$-momentum space) is given by means of an integral considering a constant density of states, dependent on the spatial dimension, see Appendix (B).

3.1 Two conventional SDWs when the magnetic field is applied longitudinally to Γ_f for cubic lattice

3.1.1 Hund's rule exchange interaction (J)

Firstly, each of the conventional SDWs are called AF_1 and AF_2, due to the fact that they present a magnetic character. The phase AF_1 is characterized by $m_f^\beta > m_f^\alpha > 0$, while the phase AF_2 occurs when $m_f^\alpha > m_f^\beta > 0$. Phase diagrams are constructed from the self-consistent solutions of Eqs. (2.14) and (2.16) for the OPs m_f^χ ($\chi = \alpha, \beta$) as function of W, T and Γ_f. The effect of Hund's rule exchange interaction (J) on the boundaries of the phases AF_1, AF_2 and PM, as W increases and when $T = 0$, is shown in Fig. (3.1). In this phase diagram we present three phases: two antiferromagnetic phases (AF_1 and AF_2) and a single paramagnetic phase (PM). Note that all the non-continuous lines shown in the phase diagram J/U as a function of W correspond to first-order phase transitions. The first-order line $AF_1 \rightarrow AF_2$ ends at a quantum triple point (QTP) located at $(J/U)_{tri} \approx 0.07$ and $W_{tri} \approx 0.85$ where the AF_1, AF_2 and PM phases coexist. For small values of J/U, the asymmetry of the hybridization between the two bands affects the nesting condition of both bands giving rise to re-entrant behaviour $AF_1 \rightarrow PM \rightarrow AF_2 \rightarrow PM$. For $J/U \geq 0.1$, the phases appear in the sequence $AF_1 \rightarrow AF_2 \rightarrow PM$ as W is increased. This indicates that above a certain threshold of J, the AF phases consist of two magnetic coupled subsystems that describe the α or β bands. We remark the role of the Hund's rule exchange (J) observed in this phase diagram. For $J = 0$, m_f^α and m_f^β are completely independent (see Eqs. (2.14) and (2.16)). In this case, due to the asymmetry of hybridization, the nesting condition is satisfied for both OPs in the region of $W \lesssim 0.8$, whereas for $W \gtrsim 1.1$ only the α band satisfies the nesting condition. In other words, the phase AF_2 has only an α character, i. e., $m_f^\alpha > m_f^\beta$, where $m_f^\beta = 0$. In this case, it is the transition $AF_1 \rightarrow PM$ and $PM \rightarrow AF_2$ as W is increased which corresponds the sequence of phases. For J finite but small, m_f^α and m_f^β become finite in the AF_2 phase. However, the nesting condition for both bands is not satisfied within of an interval of W. As J further increases, the coupling between the two OPs also increases. Above a certain value of J, the nesting condition for both α and β bands is fully recovered. This indicates that there is a threshold of J, where the direct transition $AF_1 \rightarrow AF_2$ starts to occur. This region above the threshold is the focus of the present investigation. Therefore, from now on, we use $J = U/5$ with $U = 0.165$ above mentioned.

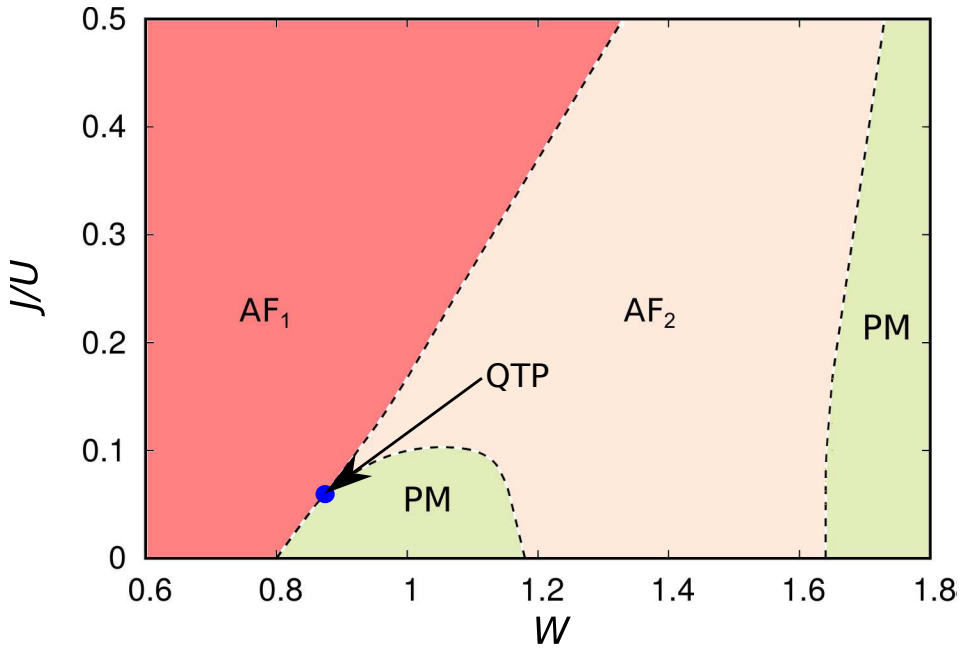

Figure 3.1: The phase diagram for J/U versus W at $T = 0$. the dotted lines are first-order transitions. There are three phases, AF_1, AF−2 and PM. The blue point is a quantum triple point (QTP).

3.1.2 Behaviour of order parameters

The results for the magnetizations m_f^α and m_f^β at finite T are shown in Figs. (3.2)(a) and (3.2)(b), respectively. For $k_BT = 0$, both OPs exhibit two discontinuities, one at $W \approx 1.05$ and another at $W \approx 1.65$. These discontinuities indicate the occurrence of first-order phase transitions. The first transition, occurring at $W \approx 1.05$, is between two types of antiferromagnetic phases. The phase AF_1 is characterized by $m_f^\beta > m_f^\alpha > 0$ while the AF_2 occurs when $m_f^\alpha > m_f^\beta > 0$. As k_BT begins to increase, those first-order transitions begin to decrease in magnitude (green dome) until they disappear completely (c point) when $k_BT = 0.004$ and at the same time it is shown that m_f^α and m_f^β decay more rapidly as W is varied. With the behaviour of the OPs m_f^α and m_f^β is possible to construct the phase diagram shown in Fig. (3.3).

3.1.3 Phase diagram without magnetic field

The phase diagram of k_BT as function of W is in Fig. (3.3). In this phase diagram there are three phases: two antiferromagnetic phases (AF_1 and AF_2) and a paramagnetic phase (PM). Firstly, there is a second-order transition at the Néel temperature T_N which is marked by the opening up of the AF gaps, $AF_1 \rightarrow AF_2$, respectively. Then, for $0.95 < W < 1.05$, there is a direct first-order transition AF_1

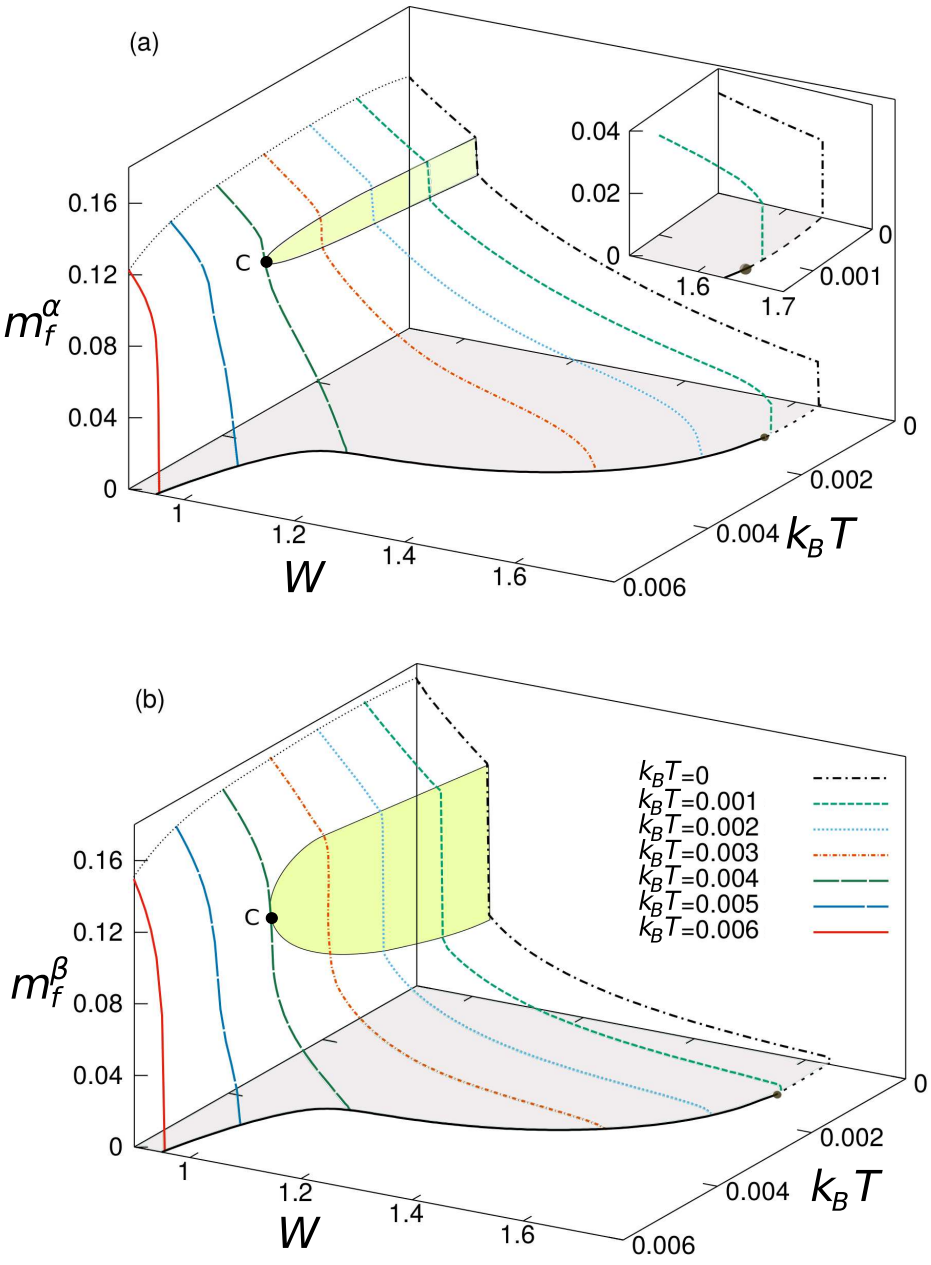

Figure 3.2: (a) The behaviour of the magnetization m_f^α as function of W for different k_BT values. (b) The magnetization m_f^β as function of W for different k_BT values. There in a one C point where the discontinuities disappear.

$\rightarrow$ AF_2 which ends at a CEP located at $k_BT_{CEP} \approx 0.0038$ and $W_{CEP} \approx 0.9826$.

We remark that in the range $T_{CEP} < T < T_N$, the jump in the OPs becomes smooth and the two AF phases can be continuously connected by a path which by passes the CEP. The phase diagram is completed by a new line of transitions AF_2 $\rightarrow$ PM which occurs for $1.6 < W < 1.7$. The line of transitions changes from a second-order to a first-order transition at a TCP located at $k_BT_{TCP} \approx 0.0011$ and $W_{TCP} \approx 1.6410$.

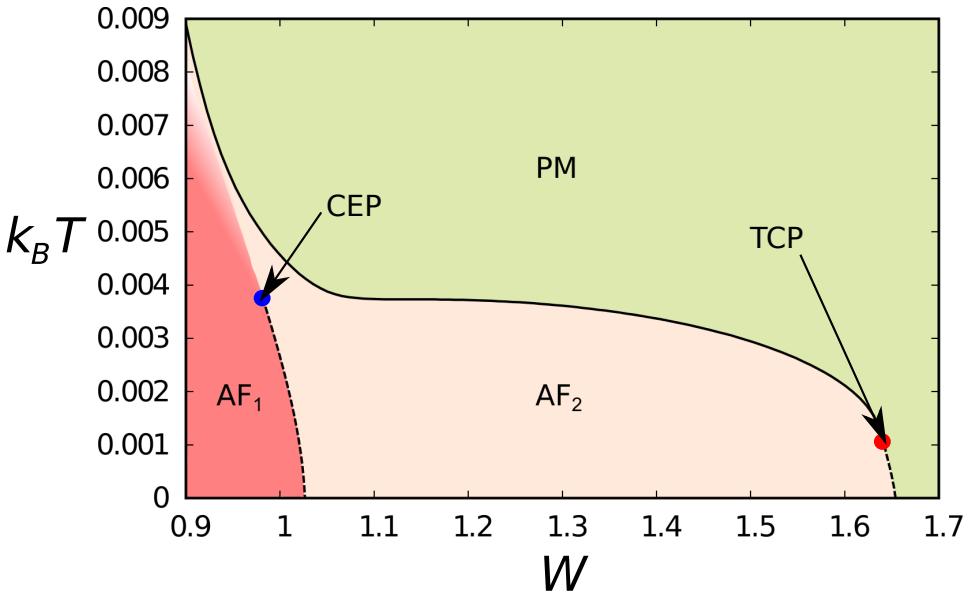

Figure 3.3: The phase diagram for the $k_\beta T$ versus W. The solid and the dashed lines denote second-order and first-order transition, respectively. The blue circle is a critical end point (CEP) and the red circle is a tricritical point (TCP). We have two phases, AF_1 and AF_2, with the variation of K_BT and W.

3.1.4 Partial density of states (p-DOS)

The α and β partial densities of states (p-DOS) are show in Fig. (3.4) for different values of W at $k_BT = 0$ and $k_BT = 0.004$ in close proximity to the dashed line, which separates the phases AF_1 and AF_2. In the AF_1 phase, the β band specifically shows the absence of electronic states at the Fermi energy (E_F) (dotted black vertical line) despite the increase of k_BT (see Figs. (3.4(a)-(3.4)(e)), while the α band in the AF_1 phase shows electronic states crossing the E_F when $k_BT = 0$ and $k_BT = 0.004$ (see Figs. (3.4(c)-(3.4)(g))). In the AF_2 phase, both α and β bands are shown to have electronic states crossing the E_F, see Figs. (3.4)(b)-(3.4)(d)-(3.4)(f) and (3.4)(h). These results, for α and β p-DOS, indicate that in the AF_1 ground state there is a mixed localized-itinerant character while AF_2 only has an itinerant character. The dashed line in the phase diagram of Fig. (3.3) denoted the locus

where FS reconstruction occurs.

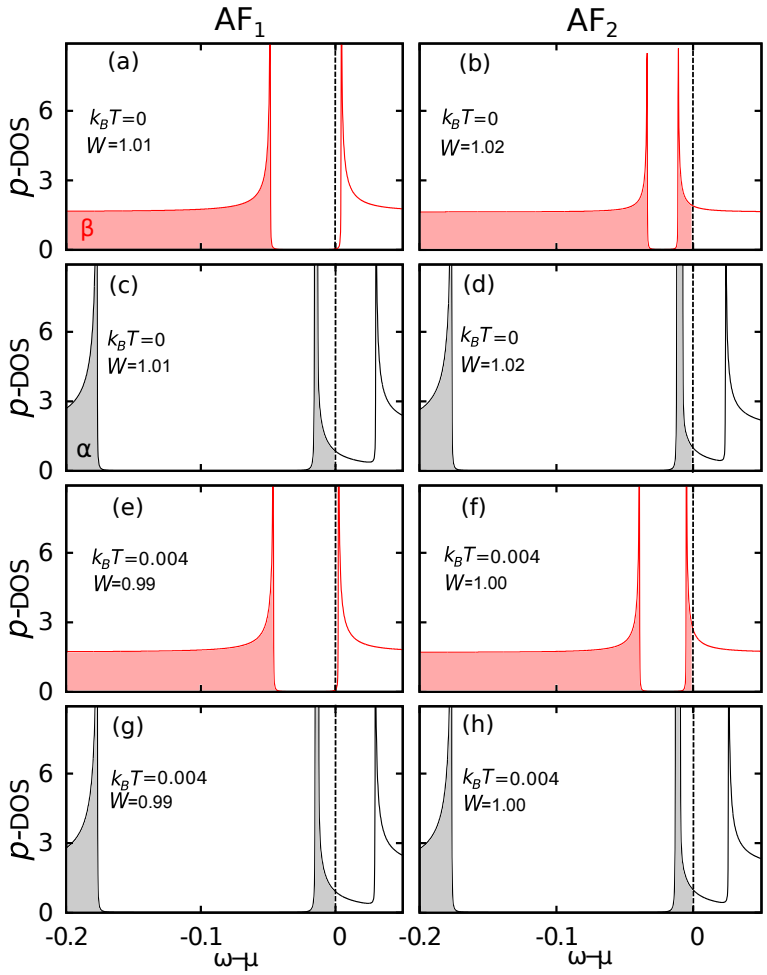

Figure 3.4: The panels show the α (red) and β (gray) p-DOS for values of W close to the dashed line (E_F) of the phase diagram (see Fig. 3.3). The left panel represents the phase AF_1 phase and the right panel to phase AF_2 phase.

3.1.5 Phase diagram with magnetic field

The zero field magnetic phase diagram changes drastically when a transverse field h_x is applied. The resulting k_BT versus W phase diagram is shown in Fig. (3.5) where the values of Γ_f are directly proportional to h_x (see Eq. (2.7)). The main effect of Γ_f is to separate the phases AF_1 and AF_2 creating a dome-shaped region for this phase with two TCPs. As Γ_f increases, the AF_2 domed-shaped region decreases until its complete suppression. We remark that m_f^α is less affected by Γ_f in the region of $W \lesssim 1$ than in the region of $W \gtrsim 1$. For $\Gamma_f = 0.035$, m_f^α is completely suppressed for $W \gtrsim 1$. In fact, the behaviour of the OPs m_f^α and m_f^β are closely related to the nesting condition for the α and β bands. The magnetic field produces a **k**-dependent shift which depends on the spin σ. Also, the E_F is shifted to higher

energies. Therefore, for sufficiently high values of Γ_f, the FS is no longer nested. Nevertheless, the electronic characters of the AF_1 and AF_2 phases, are un-changed. It has been considered $\mu = E_F$ at $T = 0$. The evolution of the phase diagram of Fig. (3.5) can be better understood in terms of the nesting condition between the β and α bands. For $\Gamma_f = 0$, the β sheet of the FS is nested when $E_f^{\beta}(\mathbf{k}) = E_f^{\beta}(\mathbf{k}+\mathbf{Q}) = \mu$. The presence of h_x produces a $\mathbf{k}$-dependent spin splitting of the dispersion relation which and can result in a shift of μ.

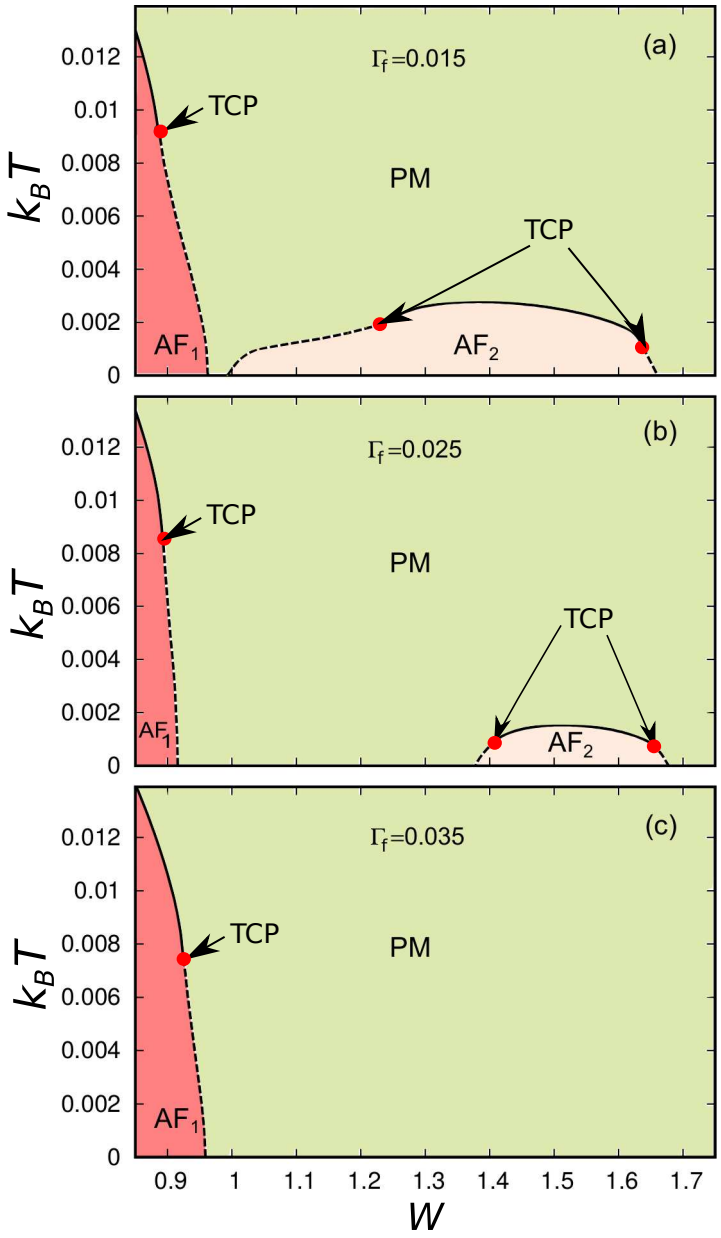

Figure 3.5: The phase diagram of the T versus W for different values of Γ_f. The solid lines denote second-order transitions while the dashed lines denote first-order transitions. The red points are tricritical points (TCPs). There are three phases, AF_1, AF_2 and PM, respectively.

3.1.6 Quasi-particles dispersion relations

The evolution of the gapped regions of β and α bands with increasing Γ_f is shown in Figs. (3.6) and (3.7). The α bands involve the hybridization V_α, which also affects the band's dispersion relation. In Fig. (3.6), the dispersion relation is calculated for a $W = 0.9$, which places the system in the AF_1 phase (see Fig. (3.5)). The E_F (dotted line) is positioned within the gap in the β-band dispersion relation for all values of Γ_f. Meanwhile, at the gapped region, the extent to which the α-band dispersion relation dips below the E_F decreases with increasing Γ_f. Consequently, the nesting of the α band is affected more strongly than the β band. The results show that the AF phases are more stable than the paramagnetic phase, if the E_F (or μ) is inside of both, or either one or other of the α or β gaps. These results indicate that in the AF_1 ground state there is a mixed localized-itinerant character.

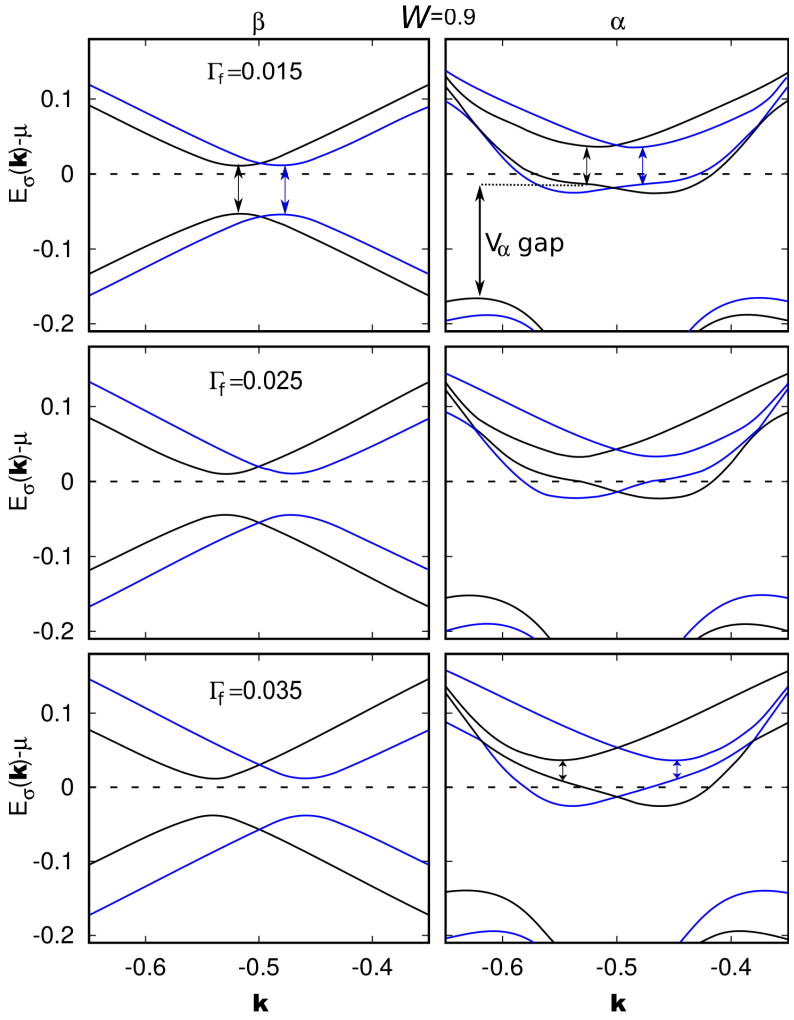

Figure 3.6: The electronic dispersion relations for $W = 0.9$, $T = 0$ and different values of Γ_f in the AF_2 phase. The blue and black colors represent the up and down spin sub-bands, respectively. The dashed black line is the E_F.

For $W = 1.5$ (AF_2 region), we find a different situation, shown in Fig. (3.7). The gap in the β band is always below the E_F, whereas the E_F lies within the gap of the α band. However, as Γ_f increases, the E_F tends to move to the bottom of the α gap, until for $\Gamma_f = 0.035$ (not shown here), the E_F falls below the gap as in the β band case. When both gaps are below E_F the bands are not nested, and the paramagnetic phase is more stable. These results indicate that in the AF_2 ground state has an itinerant character.

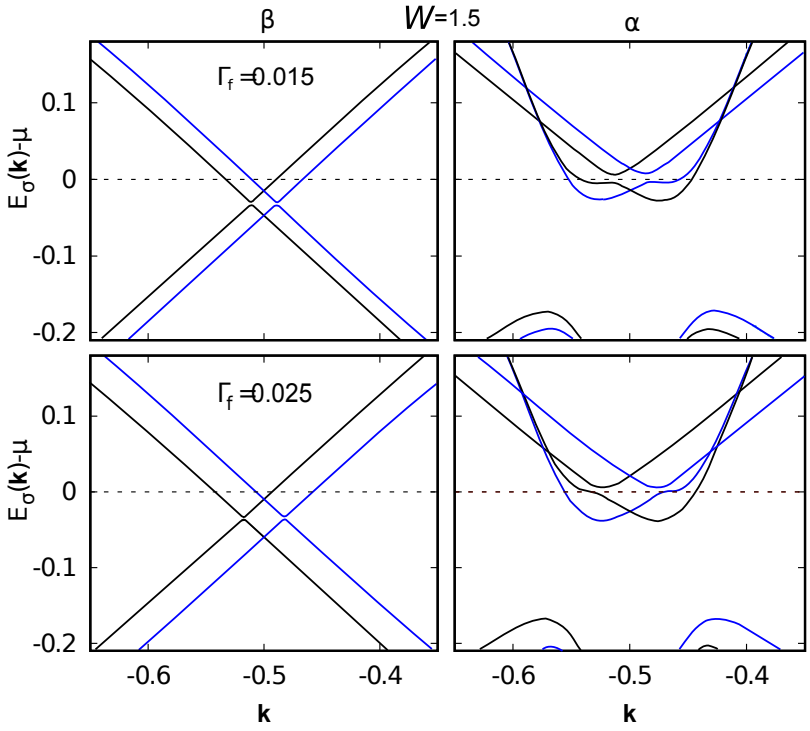

Figure 3.7: The dispersion relations for $W = 1.5$, $T = 0$ and different values of Γ_f in the AF_2 phase. The blue and black colors represent the bands with spin-up and spin-down sub-bands respectively.

3.1.7 Summary on this topic

We have investigated the emergence of multicritical points due to the competition between two conventional SDWs (antiferromagnetic phases) that appear in a multi-orbital model suitable to describe uranium compounds. We use the UALM which describes two narrow $5f$-bands (α and β) hybridize asymmetrically with a single conduction band. Besides the direct Coulomb interaction between electrons in the same f-band, there is a Hund's rule exchange interaction between electrons in the different $5f$-bands. We also consider that there is an asymmetry in the hybridization between the f-bands and the conduction band. As result, we find a competition between two types of antiferromagnetic phases, AF_1 and AF_2. In absence of magnetic field there is a CEP and a TCP, respectively, in the phase transitions $AF_1 \rightarrow AF_2$

and $AF_2 \rightarrow$ PM. The presence of the CEP in our phase diagram is in accordance with the description based on the generic two OPs Landau Free energy described in ref. [57], where the OPs were assumed to present a TRS break.

As W increase, our results show that the β-band goes through an insulator $\rightarrow$ metal transition while the α-band maintain its itinerant character. The scenario for small W resembles the scenario describing half-metallic magnets [55] used in spintronics. Here, the two spin directions are replaced by the two f-bands. Thus, our electronic structure can be described in terms of a transition between half to full metallicity. Below the CEP, this transition exactly coincides with the $AF_1 \rightarrow AF_2$ first-order transition. Therefore, our results indicate that the transitions in the electronic structure are directly coupled with magnetic transitions.

For finite magnetic transverse field Γ_f, the nesting condition has a peculiar behaviour, which is lost and then recovered when the W increases. As a consequence, the direct transition between the AF phases is replaced by a re-entrant sequence of transitions $AF_1 \rightarrow PM \rightarrow AF_2 \rightarrow PM$. The AF_2 phase acquires a dome shape. While the AF_1 line transition has one TCP, the dome shaped AF_2 line transition has two TCPs. All TCPs are effected relatively weakly by further increases of Γ_f. In fact, the dome is gradually suppressed by the field until its complete disappearance. In contrast to the drastic changes in the magnetic phase diagram, the electronic characters of the AF_1 and AF_2 phases are unaffected. They, respectively, remain of mixed insulator-itinerant and itinerant characters. The data and analysis discussed here were published in Phys. Rev. B **101**, 064407 (2020).

3.2 Two conventional SDWs phases for both cubic and tetragonal lattices when the magnetic field is applied in z-axis

Firstly, we present results for a simple cubic lattice, for which $a = c$ and $t_{A,c} = t_{A,a}$, in the dispersion equation relation given in Eq. (2.10).

3.2.1 Behavior of order parameters of cubic lattice

The behavior of gaps ϕ^α and ϕ^β as a function of H_z at T= 0, under different values of W are shown in Fig. (3.8). This gaps are proportional to OPs. Both gaps exhibit discontinuities which indicate the occurrence of first-order phase transitions. The discontinuities denoted by the dotted lines mark first-order transitions between

two competing antiferromagnetic phases, AF_1 and AF_2, or, at higher magnetic fields, between a antiferromagnetic and a paramagnetic phase (PM).

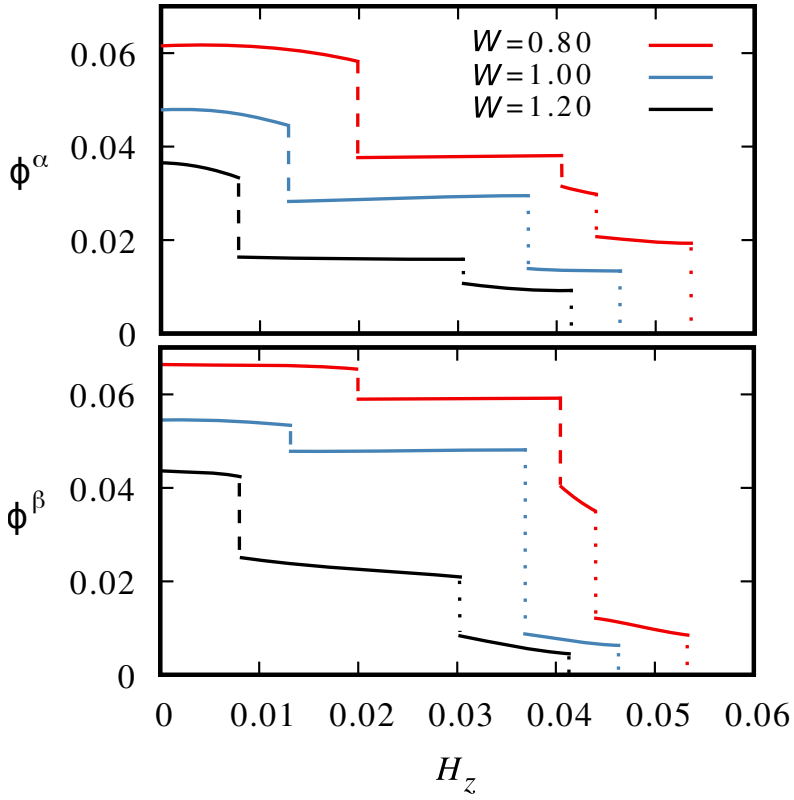

Figure 3.8: Behavior of gaps ϕ^α and ϕ^β for the simple cubic lattice as a function of H_z for $T = 0$ under different values of W. The dotted lines denote the AF_1-AF_2 and AF_2-PM first-order transitions while the dashed lines are associated with metamagnetic-like transitions.

The phase AF_1 is characterized by $\phi^\beta > \phi^\alpha > 0$, while AF_2 denotes the phase where $\phi^\alpha > \phi^\beta > 0$ and when the system evolves to the PM phase we have $\phi^\alpha = \phi^\beta = 0$. The discontinuities marked by the dashed lines, at lower magnetic field, suggests metamagnetic-like transitions which resemble transitions reported in antiferromagnetic systems [34].

Now, in the Fig. (3.9) displays the gaps as a function of the magnetic field H_z, for a fixed $W = 1.00$ under different values of temperatures. These results show that the effect of increasing of the T is to suppress the discontinues found at low magnetic fields. For $k_BT = 0.004$, the transition between the phases AF_2 and PM change its nature from first-order to second-order transition. On the other hand, the nature of the transition AF_1-AF_2, is unaffected. Nevertheless, at higher temperature, for $k_BT = 0.008$, the $AF_{1(2)} \rightarrow$ PM phase transition becomes a first-order transition again. This behavior suggest the existence of TCPs.

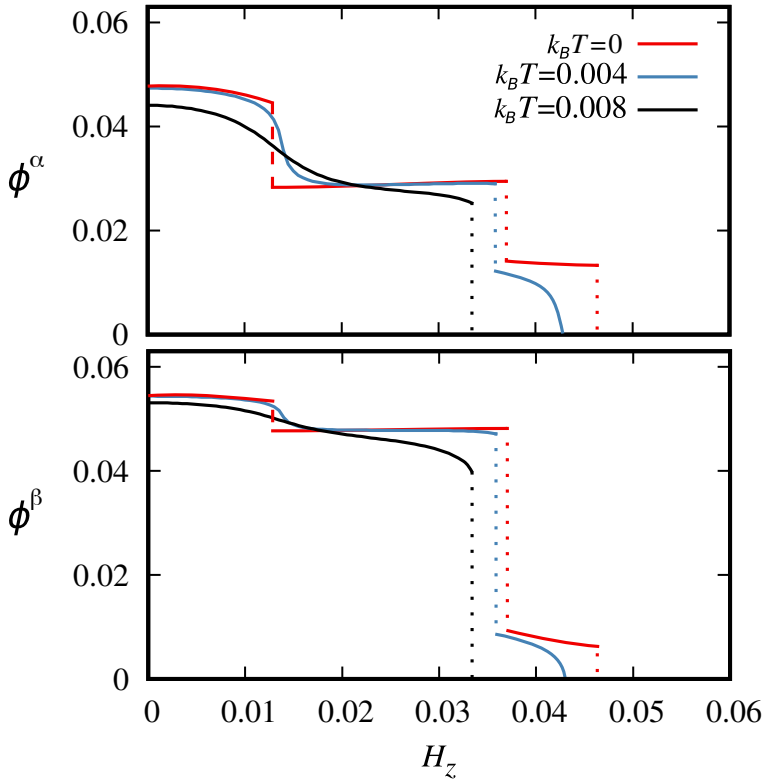

Figure 3.9: Behavior of the gaps ϕ^α and ϕ^β for the simple cubic lattice as a function of H_z for $W = 1.00$ and different values of T. The dotted and the dashed lines play the same role as in Fig. (3.8).

3.2.2 Phase diagram with H_z of cubic lattice

The effect of the temperature on the boundary of the phases AF_1, AF_2, and PM, is summarized in the phase diagrams shown in Fig. (3.10). The dotted lines indicate first-order transitions while the solid lines represent second-order transitions. In the panel (3.10)(a), it can be seen that the phase AF_1 occurs mainly for low values of W while the AF_2 phase is predominant found at higher values of H_z. However, the combination of high values of W and H_z, favors the AF_2 phase. For $T = 0$, we observe two lines representing transitions between the phases AF_1 and AF_2 which end at two CPs localized at the region of $W \approx 1.6$, between $H_z = 0.03$ and $H_z = 0.04$. The CPs are denoted by black solid circles. For finite temperatures, the AF_2 phase is restricted to a small portion of the phase diagram at high magnetic fields and low W, as shown in Figs. (3.10)(b) and (3.10)(c). On the other hand, the AF_1 phase is much more robust to the effect of T. With increasing T, there are regions where the first-order $AF_{1(2)} \rightarrow$ PM phase transitions are replaced by second-order phase transitions, in agreement with the results presented in Fig. (3.9). The red solid circles indicate the positions of the TCP. In addition, the dashed lines denote metamagnetic-like transitions. Such transitions can be observed in both AF phases,

however for $k_BT = 0.004$, the transitions occur only for low values of W. The inset in Fig. (3.10)(b) highlights the region where the metamagnetic-like transitions occurs. For $k_BT = 0.008$ the metamagnetic-like transitions no longer appear in the range of parameters considered.

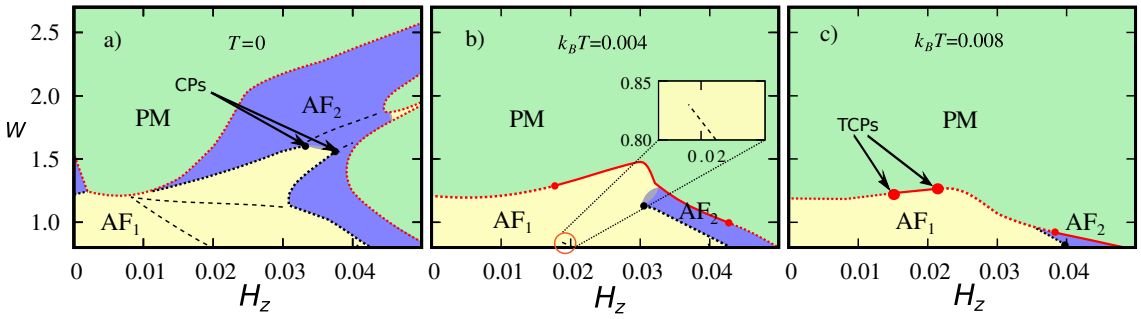

Figure 3.10: The phase diagram for a simple cubic lattice with W versus H_z for several temperatures. The solid and the dotted lines denote second-order and first-order transition, respectively. The dashed lines mark metamagnetic-like transitions. The black points are critical points (CPs) and the red points are tricritical points (TCPs).

3.2.3 Partial density of states (p-DOS) in cubic lattice

In general, the discontinuities in the gaps as a function of H_z (see Fig. (3.8)), are related to the position of the E_F relative to the gaps in the partial densities of states (p-DOS). In Fig. (3.11), the p-DOS associated with the sequence of transitions AF_1 $\rightarrow AF_2$ $\rightarrow$PM, are shown for $T = 0$ and $W = 1.20$. The vertical dashed red lines indicate the position of the E_F, for each case. The first and second columns of the panels shown the p-DOS for the AF_1 and AF_2 phases, respectively. The third column shown the p-DOS in the PM phase of the system. When H_z increases from 0.030 to 0.032, the E_F moves out of the gap of the β-band p-DOS, ρ^{β}_{σ}, resulting in a discontinuity in the gap (see Fig. (3.8)) what gives rise to the AF_1 $\rightarrow AF_2$ phase transition. The positions of E_F in both cases, are shown in Figs. (3.11)(g) and (3.11)(h). In general, every time that E_F moves out of a gap in the p-DOS, due to an increase of either H_z or W, the gaps change discontinuously (see Fig. (3.8)) and are accompanied by a phase transition or a metamagnetic-like transition. We can see that both the character of the phase AF_1 and AF_2 is isolated-itinerant.

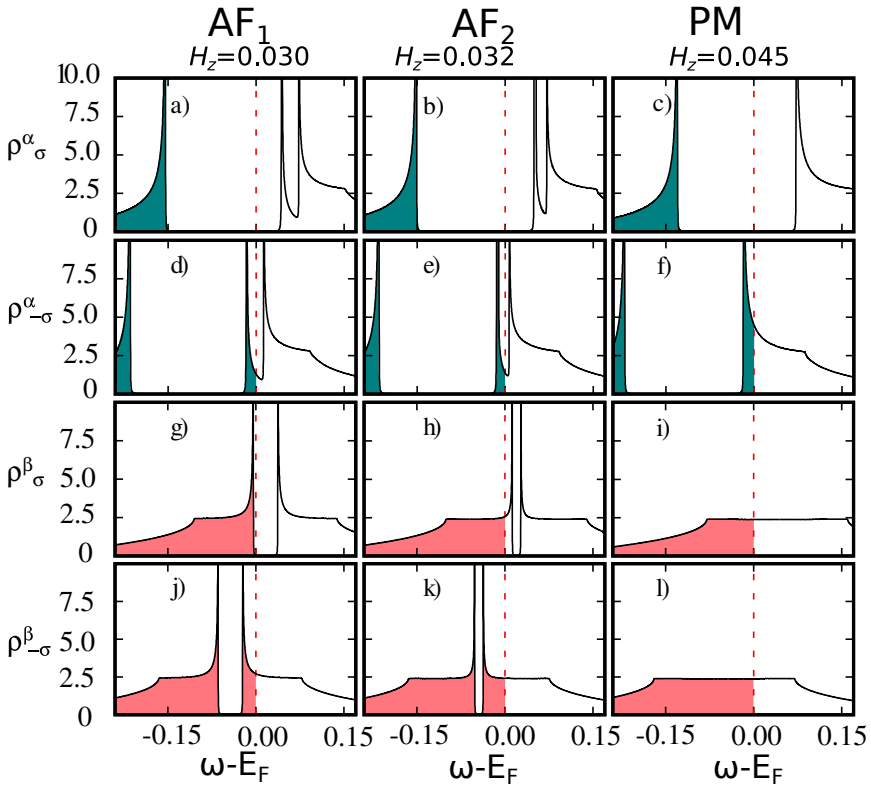

Figure 3.11: The α (green) and β (magenta) p-DOS for $W = 1.20$, $T = 0$, and different values of H_z. The values of H_z have been chosen in order to show the p-DOS behavior inside each phase (AF_1 and AF_2) of the diagram presented in the Fig. (3.10). The red dashed line is the E_F.

Now, we present results for the tetragonal lattice, i.e., $a \neq c$ and $r = t_{A,c}/t_{A,a}$. The crystalline symmetry lifts the degeneracy of the dispersion relations given in Eq. (2.10). In order to stay relatively close to the cubic lattice case, most of the results presented in this section were obtained using the next parameters: $c/a = 1.10$, and $r = 0.90$.

3.2.4 Behavior of order parameters in tetragonal lattice

In Fig. (3.12), it is seen that behavior of the gaps for $W = 0.80$ and $W = 1.00$, is very similar to the behavior observed for the cubic lattice in Fig. (3.8). However, in the tetragonal case, a higher magnetic field is required to close the gaps. For $W = 1.20$, with an increase of H_z, the system leaves the phase AF_1 and enters in the PM phase in which the gaps are zero, for small values of H_z. If the magnetic field and therefore H_z is further increased, the system reaches the AF_1 phase again. When the magnetic field is increased to higher values, the system undergoes a first-order transition to AF_2 phase at $H_z \approx 0.028$ and another first-order transition is found at $H_z \approx 0.05$ where the system enters the PM phase.

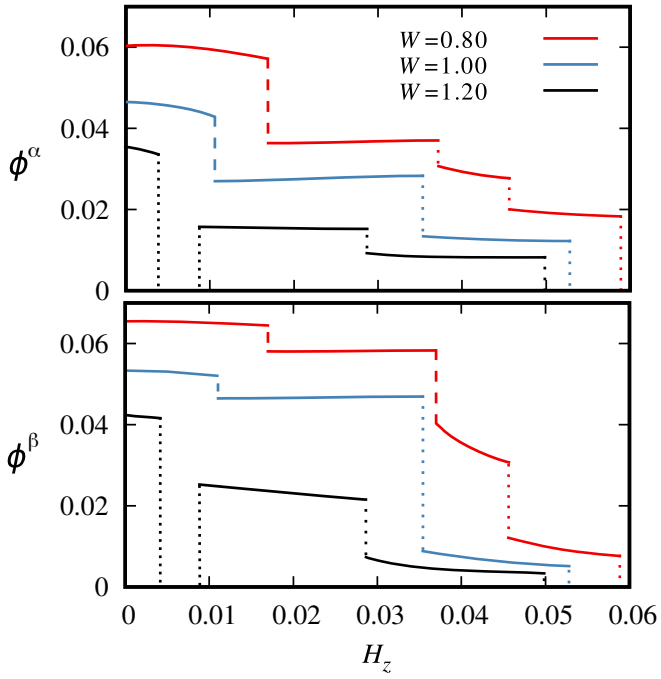

Figure 3.12: Behavior of gaps ϕ^α and ϕ^β for the tetragonal lattice as a function of H_z for $T = 0$ and different values of W. The regions with dashed lines denotes the $AF_1 \rightarrow AF_2$ and $AF_2 \rightarrow PM$ first-order transitions.

3.2.5 Phase diagram in tetragonal lattice

The W versus H_z phase diagrams and their evolution with T are shown in Fig. (3.13). For $T = 0$, the region where the AF_1 phase occurs is similar to that of the cubic lattice. However, the AF_2 phase is concentrated in the region of higher magnetic field while in the cubic lattice the AF_2 phase also occurs for intermediate values of H_z. Indeed, the β-DOS for the tetragonal lattice is asymmetric relative to $\omega = 0$ which results in the phase AF_2 being favored. The asymmetry can be seen, for example, in Fig. (3.14)(l). As in the case of the cubic lattice, two CPs (black solid circles) are present in the $T = 0$ phase diagram. For $k_BT = 0.004$, we observe the presence of four TCPs (red solid circles) while in the cubic lattice the four TCPs first occur at $k_BT = 0.008$. Furthermore, the CP observed for $k_BT = 0.004$ is still present for $k_BT = 0.008$. These facts indicate that the existence of CP and TCPs are favored in the tetragonal lattice. On the other hand, the metamagnetic-like transitions represented by the dashed lines in Fig. (3.13)(a), are less favored than in the cubic lattice.

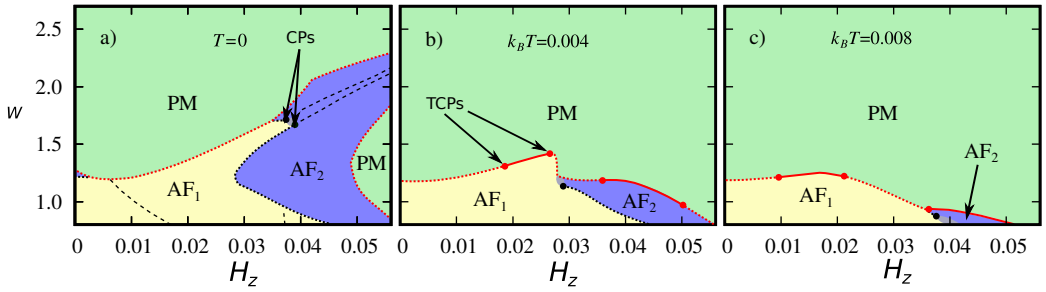

Figure 3.13: The phase diagram for a tetragonal lattice with W versus H_z, for different temperatures. The solid and the dashed lines denote second-order and first-order transition, respectively. The black points are crititcal points (CPs) and the red points are tricritical points (TCPs). The parameters of the dispersion relation are $c/a = 1.10$ and $r = 0.90$.

3.2.6 Partial density of states in tetragonal lattice

The α and β p-DOS, ρ^{α} and ρ^{β}, are shown in Fig. (3.14) for $T = 0$, $W = 1.0$ and different values of H_z. The values of H_z in the AF_1 and AF_2 phases, were chosen in order to be close to the $AF_1 \rightarrow AF_2$ phase transition. The behavior of the gaps for this set of parameters has been shown in Fig. (3.12).

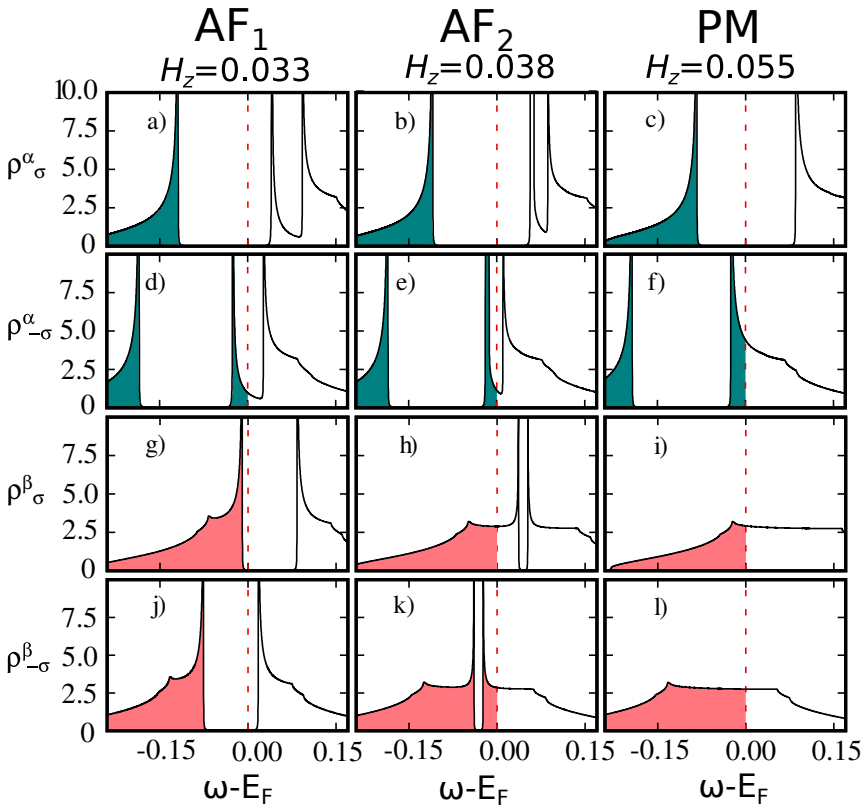

Figure 3.14: The α (green) and β (magenta) p-DOS for W= 1.0, $T = 0$, and different values of H_z. The values of H_z have been chosen in order to show the DOS behavior inside each phase of the diagram presented in Fig. (3.13). The red dashed line is the E_F.

By comparing the results in Fig. (3.14) with those for the cubic lattice shown in Fig. (3.8), it is possible to see that the results are slightly different, mainly for $\rho^{\beta}_{-\sigma}$. For the phase AF_1 with H_z=0.033, the position of the E_F, which is represented by the vertical dashed red line in Fig. (3.14), is found inside the gap for both ρ^{β}_{σ} and $\rho^{\beta}_{-\sigma}$, while for the cubic lattice the E_F is found inside the gap only for ρ^{β}_{σ} (see Figs. (3.11)(g) and (3.11)(j)). This feature is related to the asymmetry of the p-DOS for the tetragonal lattice. For instance, in Fig. (3.14)(j), the area of the $\rho^{\beta}_{-\sigma}$ below the E_F (colored in red) is slightly larger than the area above the E_F. In order to keep the total occupation of the bands constant, the E_F has been moved to lower energies, i.e. into the gap of the $\rho^{\beta}_{-\sigma}$, which results in a phase AF_1 that is less itinerant when compared with the cubic case shown in Fig. (3.11), for which the $\rho^{\beta}_{\pm\sigma}$ is symmetric.

3.2.7 Phase diagram of tetragonal lattice for c/a

The results presented so far in this section have been obtained considering small deviations from the cubic lattice, for the parameters c/a and r. Now, we investigate how the boundaries of the phases AF_1, AF_2 and PM behave when the parameters c/a and r, are changed. Fig. (3.15)(a) exhibit the phase diagram with H_z versus c/a, for fixed W and r, while Fig. (3.15)(c) exhibit the phase diagram with W versus c/a, for H_z=0.0 and r fixed. While the phase AF_1 is robust to the effects of H_z and W when c/a is enhanced, the phase AF_2 is significantly affected by the increasing of H_z or W, in this same situation. Nevertheless, while the phase AF_2 is favored by the increasing of c/a when H_z is enhanced, the same phase is suppressed by the increasing of c/a, when W is enhanced. Such feature is related to the way that H_z and W affect the p-DOS, maily the $\rho^{\beta}_{\pm\sigma}$. While H_z shifts ρ^{β}_{σ} to lower energies and $\rho^{\beta}_{-\sigma}$ to higher energies, the main effect of W is to increases the width of the bands. Therefore, the effects of H_z combined with the asymmetry of the DOS $\rho^{\beta}_{\pm\sigma}$, relative to the gap (see Fig. (3.14)), are the main reasons for the features present in the phase diagrams of Figs. (3.15)(a) and (3.15)(c). In Figs. (3.15)(b) and (3.15)(d) it can be noted that the effect of increasing r keeping c/a fixed, is similar to tthe effect of keeping r while c/a varies. However, the effects of varying r are much less intense. The dashed lines in Figs. (3.15)(a) and (3.15)(b) indicate the metamagnetic-like transitions.

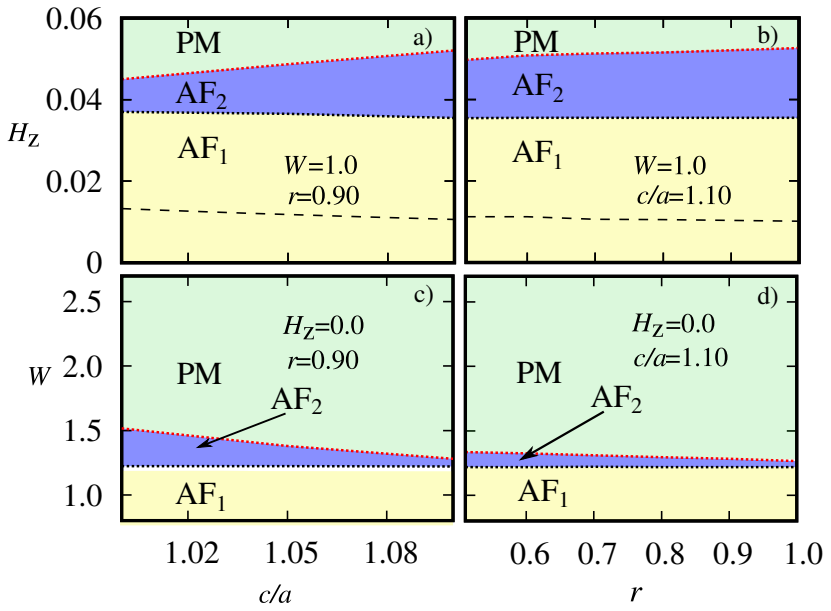

Figure 3.15: Phase diagram for the tetragonal lattice with H_z and W versus c/a in the first column and versus r in the second column. All the transitions shown in the phase diagrams, have first order nature.

3.2.8 Summary on this topic

We have investigated the effects of pressure and magnetic field in z-axes on two distinct itinerant phases using the UALM. We are assuming that pressure is associated with bandwidth variation (W) and the magnetic field is considered parallel to this anisotropy direction. The Hund's rule exchange interaction (J) couples the gaps ϕ^{α} and ϕ^{β} in different bands and gives rise to two competing antiferromagnetic phases AF_1 and AF_2. The nature between such phases has first-order transition at low W. In addition, in this section we analysed the UALM model for two cases, the cubic and the tetragonal lattices.

In order to investigate the effects of H_z for different W, we constructed phase diagrams with W versus H_z at different temperatures. The results show rich phase diagrams for both lattices, mainly at $T = 0$. In a previous section (3.1), we investigated the effects of a magnetic field oriented transverse to the z-axis with the same UALM model. In that case, for a cubic lattice, the results showed that the increasing of the transverse magnetic field suppresses the phase AF_2 while the phase AF_1 persist even at higher magnetic fields. In this section, we note an opposite situation, i. e., the AF_1 phase is replaced by the AF_2 phase at higher magnetic fields H_z, while the phase AF_1 occurs for lower values of W and lower and intermediate values of H_z. This dissemblance is related to the fact that the transverse field produces a spin-dependent momentum shift of the quasi-particles bands. On the other hand,

H_z splits the bands generating a spin-up and a spin-down sub-band [8]. The increasing in H_z shifts the spin-up and the spin-down sub-bands, to opposite sides, in the energy axis. The analysis of $\rho^{\alpha}_{\pm\sigma}$ and $\rho^{\beta}_{\pm\sigma}$ at $T = 0$, helps us better understand how the field H_z favors the phase AF_2. We demonstrated in Fig. (3.11) that in the phase AF_1, the E_F is inside the gaps of $\rho^{\alpha}_{-\sigma}$ and ρ^{β}_{σ}, at least. On the other hand, if the E_F is out of the gaps of $\rho^{\beta}_{\pm\sigma}$, but is still inside the gap of $\rho^{\alpha}_{-\sigma}$, the system is found in the phase AF_2. Considering the fact that H_z shifts the spin-up and the spin-down sub-bands in opposite sides in the energy axis, the configuration in which the E_F is out of the gaps of both $\rho^{\beta}_{-\sigma}$ and ρ^{β}_{σ}, is favored when H_z increases. Moreover, due to the hybridization gap present in $\rho^{\alpha}_{\pm\sigma}$, the gap ϕ^{α} is less affected by the magnetic field (see Fig. (3.8)), allowing the E_F to stay inside the gap of $\rho^{\alpha}_{-\sigma}$, until higher values of H_z. Indeed, these are the main reasons for which the AF_2 phase is favored by the magnetic field H_z. The data and analysis discussed here were published in J. Magn. Magn. Mater. **560**, 169531 (2022).

3.3 Competition between conventional and unconventional SDWs, in cubic lattice, when the magnetic field is applied in z-axis

3.3.1 Effect of Hund's rule exchange interaction (J)

In Fig. (3.16), the phase diagram J/U vs the bandwidth W at $T = 0$ is shown. For $J = 0$, there is a complete decoupling between $z^{\beta\alpha}_{-\mathbf{Q},\sigma}$ and $z^{\beta\alpha}_{-\mathbf{Q},-\sigma}$ as well as m^{α}_{f} and m^{β}_{f} (see Eqs. (2.25) and (2.31)). Although the AF_1 and AF_2 phases appear for certain W ranges, the IOSDW phase does not exist for any W. When J/U is finite but very small, the OPs re-couple weakly. As a consequence, besides phases AF_1 and AF_2 the IOSDW phase begin to appear within a very small range of W. As J/U increases, the width of the PM region within the phase diagram decreases. This behavior is accentuated until for a certain J/U threshold, the PM phase disappears completely. This situation generates a PM dome, where above it there is a direct transition $AF_1 \rightarrow$ IOSDW $\rightarrow AF_2$.

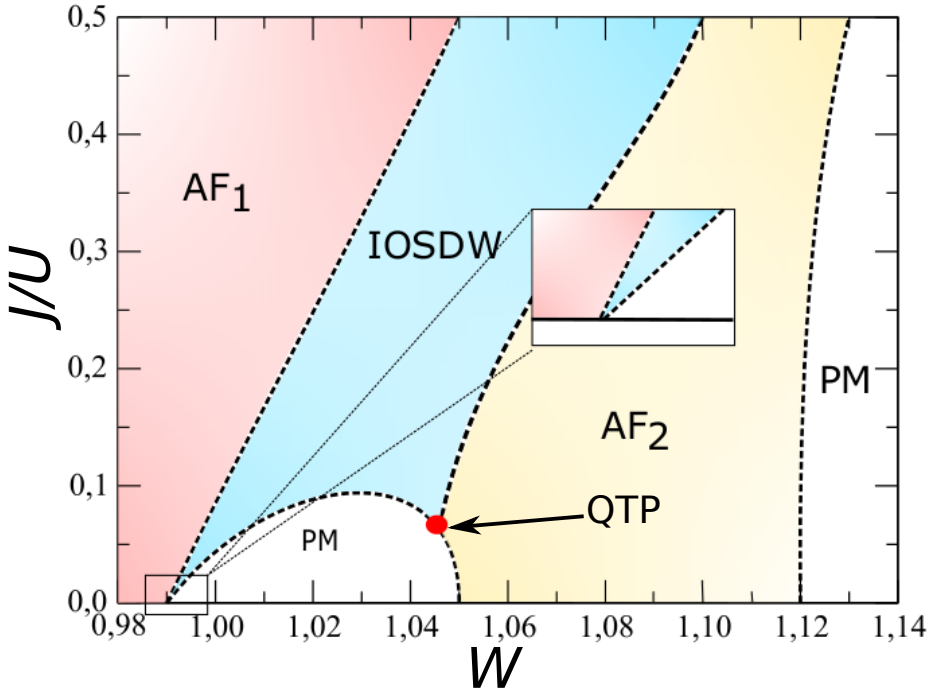

Figure 3.16: The phase diagram for J/U versus W for $T = 0$. The red point represents a quantum triple point (QTP). AF_1 and AF_2 are two antiferromagnetic phases, IOSDW is a exotic inter-orbital spin density wave and PM is a paramagnetic phase.

In Fig. (3.17) is shown the behaviour of the OPs illustrating the evolution of the phase diagram in Fig. (3.16). It should be noted that for $J = 0$ (see Fig. (3.17-a)) the intermediate PM solution is more stable, although, $m_f^\beta > m_f^\alpha = 0$. We remark that the presence of multicritical points in finite T phase diagrams is entirely dependent on direct transitions between phases $AF_1 \rightarrow IOSDW \rightarrow AF_2$ at $T = 0$. Therefore, for finite T diagrams, we will choose values of J/U where the direct transition $AF_1 \rightarrow IOSDW \rightarrow AF_2$ appears at $T = 0$.

3.3.2 Behavior of order parameters

First, the following results are described in the simple three-dimensional cubic lattice, where the lattice parameters are equal in all spatial dimensions. For this case, the dispersion relation is described in Eq. (2.10). The OPs m_f^α, m_f^β and $z^{\beta\alpha}_{-\mathbf{Q},\sigma}$ as a function of W at different values of T and without the presence of h_z are shown in Fig. (3.18).

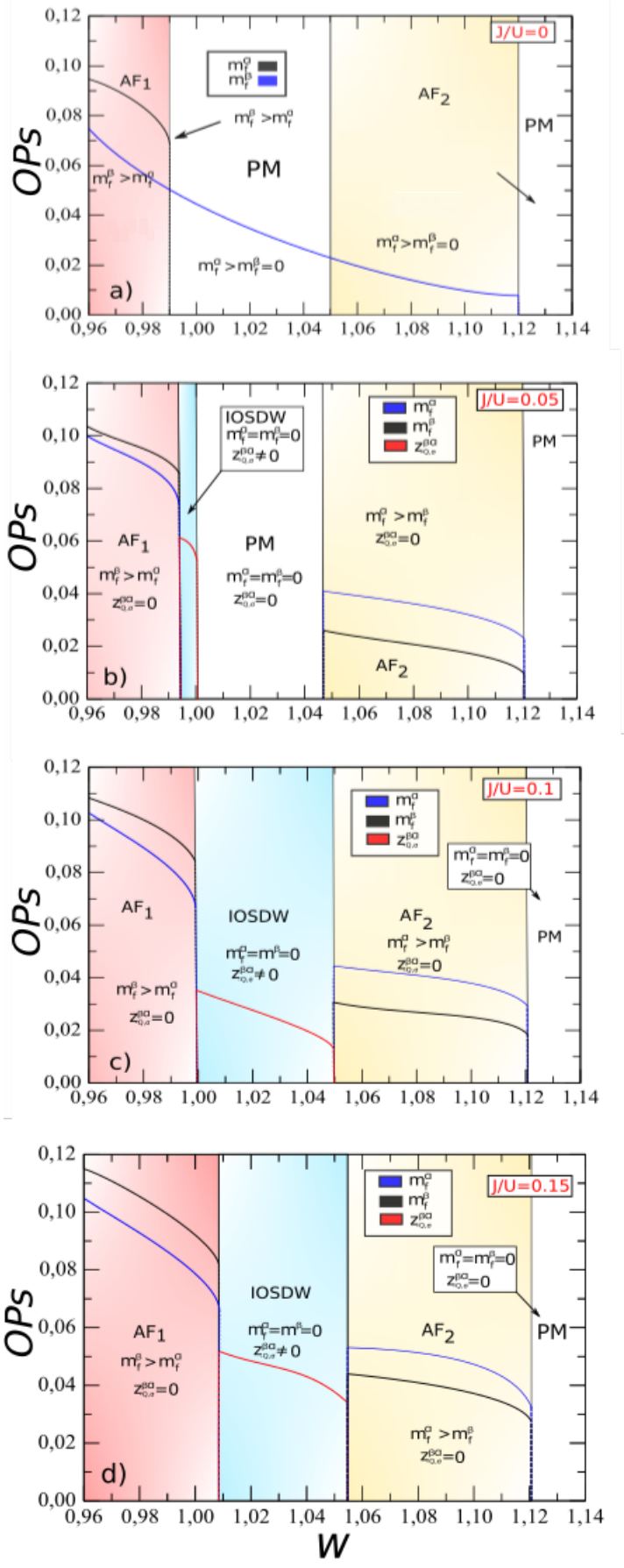

Figure 3.17: Behavior of the OPs as a function of W for different values of J/U at $T = 0$. We can see discontinuities of OPS (m_f^{α}, m_f^{β} and $z^{\beta\alpha}_{-\mathbf{Q},\sigma}$).

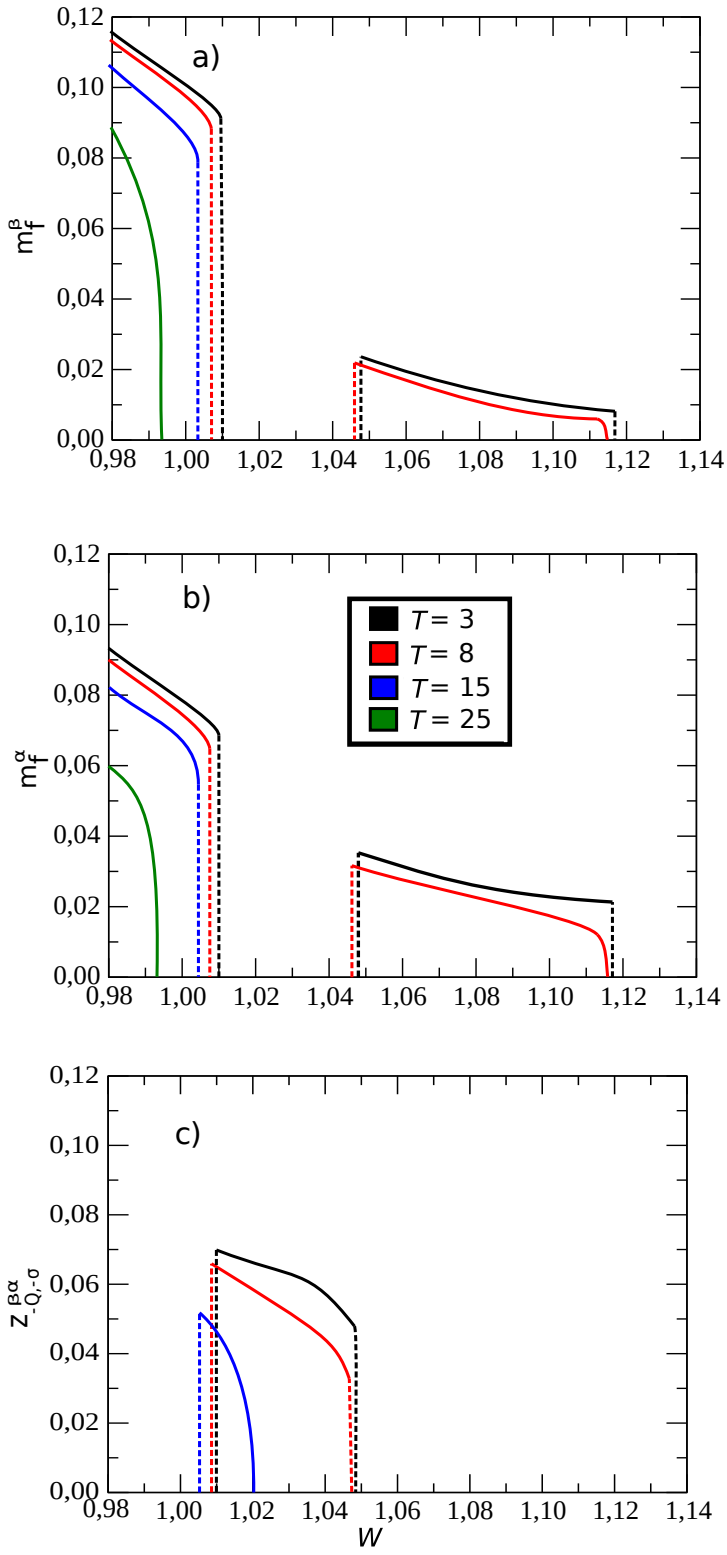

Figure 3.18: Behavior of the OPs as a function of W for different values of T with $h_z = 0$.

We can also see that at $T = 3$ and $T = 8$ the presence of m_f^α, m_f^β and $z_{-\mathbf{Q},\sigma}^{\beta\alpha}$ is shown, and at $T = 15$ the existence of the three OPs, m_f^α, $m_f^{\beta\alpha}$ and $z_{-\mathbf{Q},\sigma}^{\beta\alpha}$ is

observed only for values of $W < 1.02$. For values of $T = 25$ a clear existence of the OPs m_f^α, m_f^β at low values of W is shown. As the temperature starts to increase and at low magnitudes of W, only the presence of the OPs m_f^α and m_f^β is manifested. On the other hand, it is easy to see in Fig. (3.18) that the three gaps are exhibited continuously and discontinuously in certain regions of W, which indicates the occurrence of first-order transitions (dashed lines) and second-order transitions (continuous lines). The behavior of the OPs for low magnitudes of W shows that the existence of only m_f^α, m_f^β while $z^{\beta\alpha}_{-\mathbf{Q},\sigma} = 0$. As the intensity of W begins to increase the OPs $m_f^\alpha = m_f^\beta = 0$ and the OP $z^{\beta\alpha}_{-\mathbf{Q},\sigma^\beta} = 0$. If W continues to increase we show the existence again of m_f^α and m_f^β and again $z^{\beta\alpha}_{-\mathbf{Q},\sigma} = 0$. Thus, for extremely high intensities of W there is no existence of any of the OPs, i.e., $m_f^\alpha = m_f^\beta$ and $z^{\beta\alpha}_{-\mathbf{Q},\sigma} = 0$. These transitions reflect the existence of two conventional phases and a single exotic phase under different magnitudes of W. The two conventional phases are denoted, AF_1 and AF_2 while the exotic phase is called IOSDW. The AF_1 phase is characterized by $m_f^\beta > m_f^\alpha$ and $z^{\beta\alpha}_{-\mathbf{Q},\sigma} = 0$, while the AF_2 phase occurs when $m_f^\alpha > m_f^\beta$ and $z^{\beta\alpha}_{-\mathbf{Q},\sigma} = 0$. The IOSDW phase is presented when $m_f^\beta = m_f^\alpha = 0$ and $z^{\beta\alpha}_{-\mathbf{Q},\sigma} \neq 0$. Finally the PM phase is found when $m_f^\beta = m_f^\alpha = 0$ and $z^{\beta\alpha}_{-\mathbf{Q},\sigma} = 0$.

3.3.3 Phases diagram without magnetic field

In this section we present the phase diagram of T versus W resulting from the compositions of the OPs presented in the previous section. The phases diagrams are constructed from the coupled equations for m_f^α, m_f^β, $z^{\beta\alpha}_{-\mathbf{Q},\sigma}$ and $z^{\beta\alpha}_{-\mathbf{Q},-\sigma}$ (see Eqs. (2.25) and (2.31)) which must be solved self-consistently. In terms of OPs, AF_1 and AF_2 appears when $m_f^\beta > m_f^\alpha$ and $m_f^\alpha > m_f^\beta$, respectively. Both phases have $z^{\beta\alpha}_{-\mathbf{Q},\sigma} = z^{\beta\alpha}_{-\mathbf{Q},-\sigma} = 0$. The IOSDW phase has $z^{\beta\alpha}_{-\mathbf{Q},\sigma} = -z^{\beta\alpha}_{-\mathbf{Q},-\sigma} \neq 0$ with $m_f^\alpha{=}m_f^\beta = 0$ and the PM appears when $z^{\beta\alpha}_{-\mathbf{Q},\sigma} = -z^{\beta\alpha}_{-\mathbf{Q},-\sigma} = m_f^\alpha = m_f^\beta = 0$.

Fig. (3.19) displays the phase diagram T vs W. When the temperature is lowered, there are a second-order phase transitions from PM to any of phases AF_1, AF_2 or IOSDW. Moreover, when W increases at lower T, the two magnetic phases AF_1 and AF_2, i.e., phases with time reversal symmetry breaking, are separated by the non-magnetic IOSDW phases. It appears the phase transitions sequence $AF_1 \rightarrow$ IOSDW $\rightarrow AF_2$, with first order line transitions separating the phases. To complete the sequence of phase transitions, there is a first order transition $AF_2 \rightarrow$ PM. In the transition $AF_1 \rightarrow$ IOSDW both m_f^β and m_f^α (with $m_f^\beta > m_f^\alpha$) collapse and the IOSDW becomes finite. In the transition IOSDW $\rightarrow AF_2$ the opposite happens. The IOSDW OP collapses and m_f^β and m_f^α are abruptly finite. But now with $m_f^\beta < m_f^\alpha$. Note that for $T = 25$, there is only a second order transition $AF_1 \rightarrow$ PM.

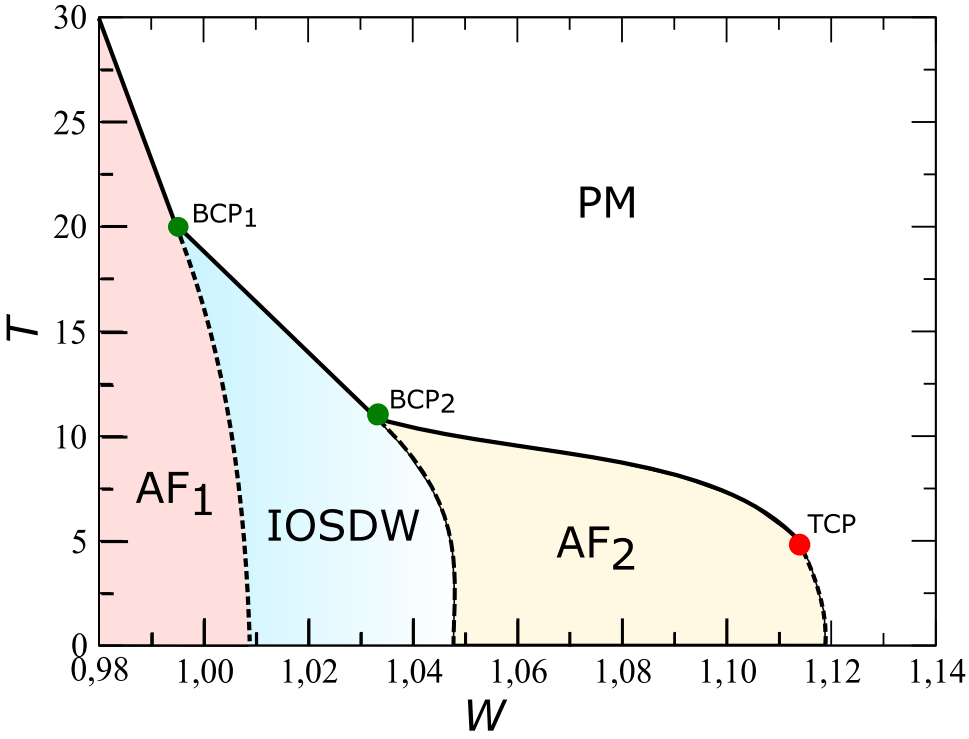

Figure 3.19: Phase diagram of T versus W. The continuous line represents a second-order transition while the dotted line is a first-order transition. There are three phases, AF_1, AF_2 and IOSDW. The two green points are bicritical points (BCPs) and the red point is a tricritical point (TCP).

3.3.4 Phase diagrams with magnetic field

In this section we present the evolution of the phase diagram under the presence of an external magnetic field. In Fig. (3.20), the T vs W phase diagrams are shown with increasing values of h_z. The first significant effect is the lowering the critical temperatures corresponding to the three transitions PM $\rightarrow$ AF_1, PM $\rightarrow$ IOSDW and PM $\rightarrow$ AF_2. This lowering of critical temperatures is more pronounced for the IOSDW and AF_2 phases. Also, the locations of the first-order lines in the phase transitions AF_1 $\rightarrow$ IOSDW $\rightarrow$ AF_2 and AF_2 $\rightarrow$ PM are displaced to larger values of the W. These two effects compose what we will call from now on, flattening of phases. As consequence, there is a slight enlargement in the phase diagram of the AF_1 region at the expense of IOSDW one. The IOSDW and AF_2 regions also enlarge slight at the expense of AF_2 and PM ones, respectively. We emphasize that there is a different size of these effects for each of the phases. Therefore, the AF_2 phases are subjected to greater flattening.

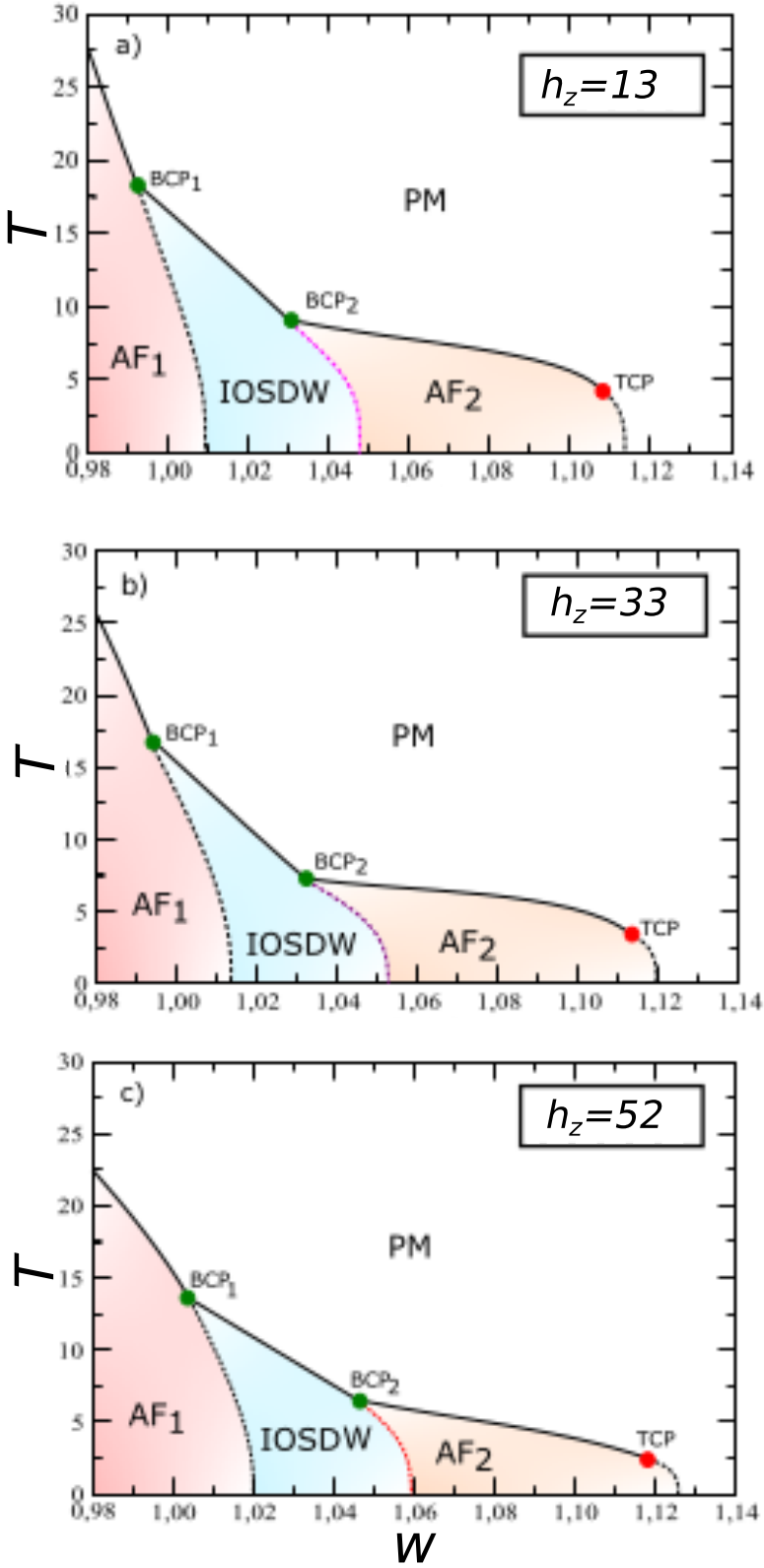

Figure 3.20: Phase diagram T under W for several values of h_z. The continuous line (black color) shows a second-order transition while the discontinuous lines show a first-order transition. There are three phases, AF_1, AF_2 and IOSDW. The green points are bicritical points (BCPs) and the red point is a Tricritical point (TCP).

In Fig. (3.21), we fix the values of W in such way that we can evaluate the evolution of phases AF_1, IOSDW and AF_2 when h_z is varied (proportional to H_z). We find that the three phases are completely suppressed above a certain value of h_z. However, there is a difference in the value of the suppression value of h_z for each phase, i. e., the IOSDW and AF_2 phases have almost the same suppression h_z value while for AF_1, the value is clearly smaller. Interestingly, our results indicate the same process of flattening observed in the T vs W surface occurs in the T vs h_z one. Again, the IOSDW and AF_2 phases are more affected by process than AF_1.

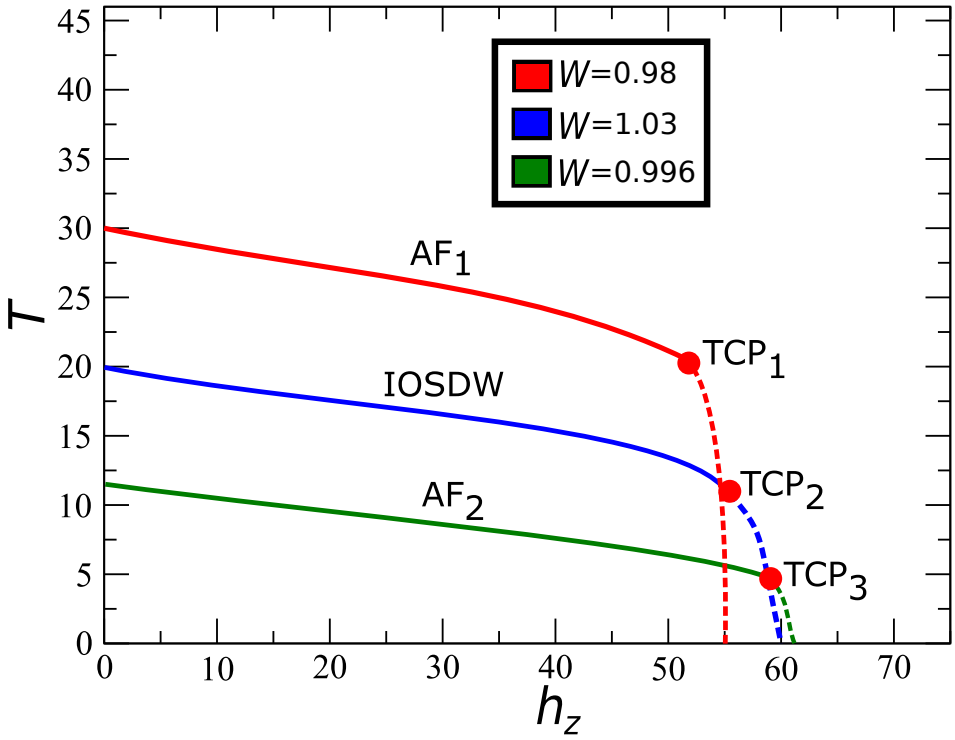

Figure 3.21: Phase diagram T versus h_z for different W values. At $W = 0.98$ only exit the AF_1 phase, for $W = 1.03$ exit the IOSDW phase and at $W = 0.996$ exit only the AF_2 phase.

3.3.5 Quasiparticles dispersion relations

The quasiparticle dispersion relations $E^{\chi}_{i,\sigma}(\mathbf{k})$ for the bands α and β are obtained from $D_\sigma(\mathbf{k},\omega) = 0$ (see (E.14)). In absence of h_z, the evolution of $E^{\chi}_{i,\sigma}(\mathbf{k})$ for different W at $T = 0$ K is shown in Fig. (3.22). The case of the AF_1 phase is shown in Fig. (3.22 a)). Here, the double arrows indicate approximately the locus of the β and α gaps. Notice that the E_F crosses both α and β gaps. However, as an effect of the V_α hybridization, the α band crosses the E_F near the gap, giving a isolated-itinerant character for the AF_1 phase. In other words, the isolated-itinerant refers to the situation where FS is reconstructed in only one of the bands. The same isolated-

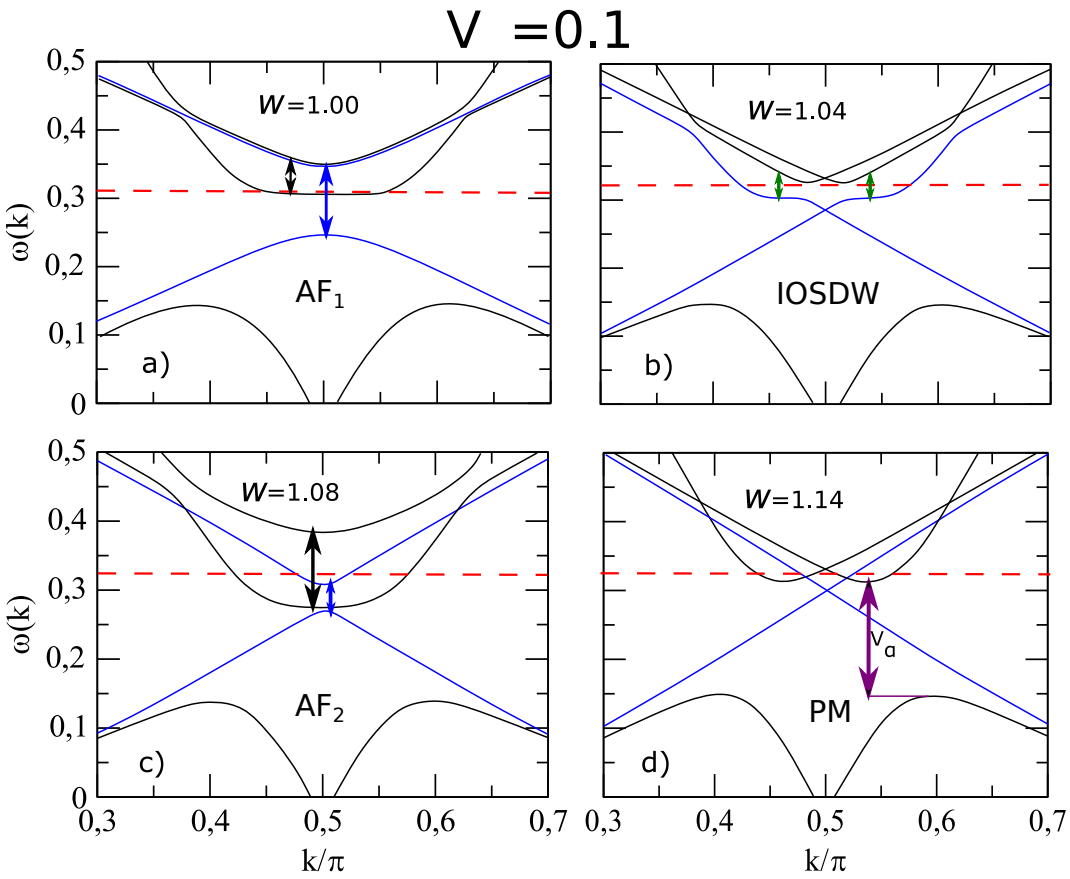

Figure 3.22: Quasi-particle dispersion relations for: a) $W = 1.00$ (AF_1), b) $W = 1.04$ (IOSDW), c) $W = 1.08$ (AF_2), d) $W = 1.14$ (PM) in the absence of the magnetic field $h_z = 0$. The dashed red line indicates the position of the E_F while the black and the blue lines show the α and β bands, respectively.

itinerant character is observed in the band structure of the IOSDW phase shown in Fig. (3.22)) b). In contrast, the band structure for the AF_2 (see Fig. (3.22) c)) phase indicates a itinerant character.

Fig. (3.23) displays $E^{\chi}_{i,\sigma}(\mathbf{k})$ with increasing h_z. Due to the spin dependence, $\sigma = \pm 1$, the number of bands is doubled. The isolated-itinerant nature of the AF_1 phase, Fig. (3.23) a), and the metallic nature of the AF_2 phase, Fig. (3.23) c), are maintained despite the increase in the h_z. On the other hand, in the IOSDW phase, Fig. (3.23) b), the increasing of the h_z leads the system to a purely itinerant state (isolated-itinerant $\rightarrow$ itinerant). In general, as the h_z increases, the system enhances its itinerant electronic character, redistributing the FS, mainly due to the evolution from isolated-itinerant $\rightarrow$ itinerant character of the IOSDW phase.

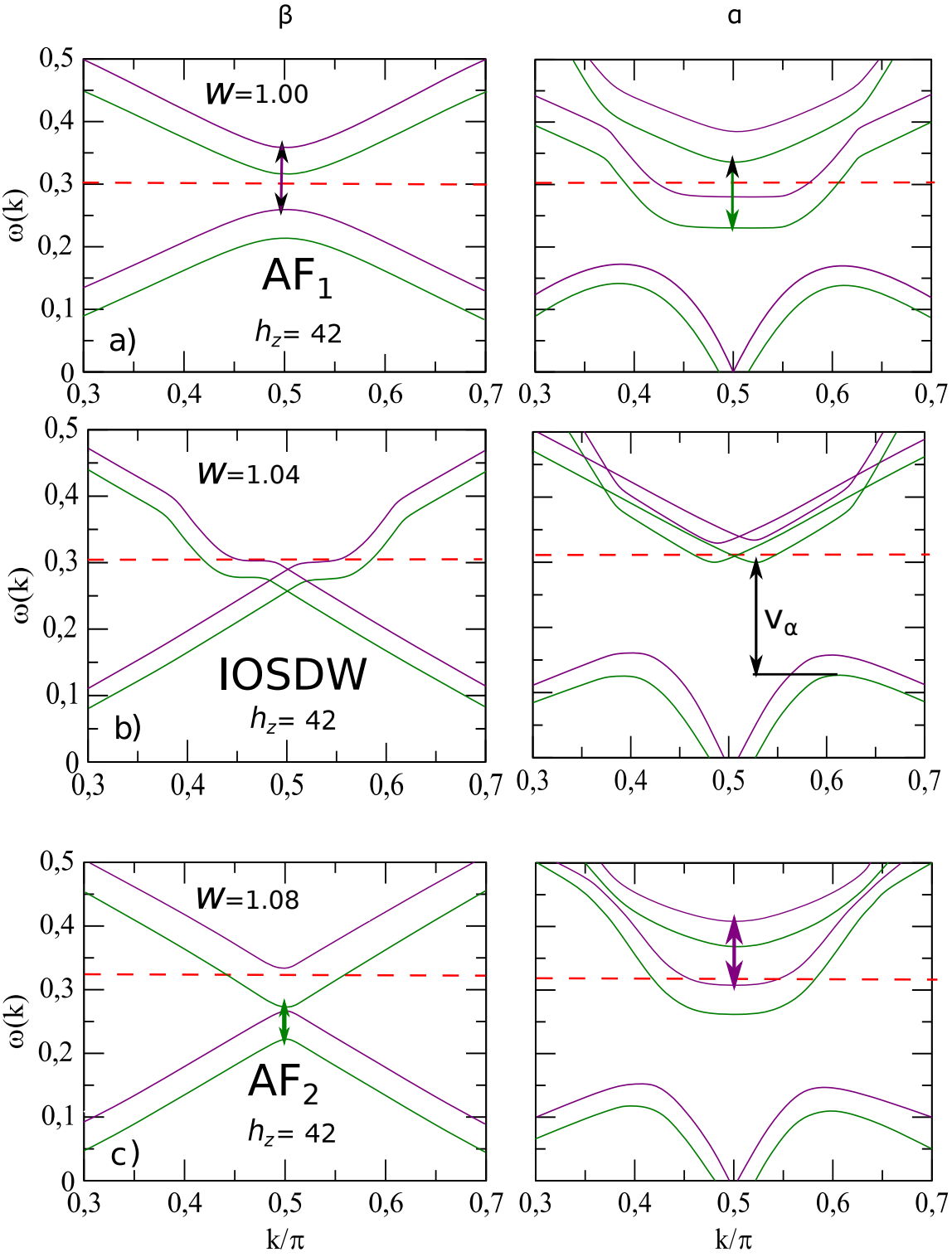

Figure 3.23: Quasi-particles dispersion relations at $T = 0$ for two distinct values of h_z. The purple and green lines represent the spin up ($\sigma = 1$) and spin down ($\sigma = -1$), respectively. Results are shown for the three phases AF_1 a), IOSDW b) and AF_2 c). The dashed red line is the E_F.

3.3.6 Multicritical points

The sequence of first and second order phase transitions, that place the non-magnetic IOSDW phase between the AF_1 and AF_2 phases shown in Fig. (3.19) gives rise to two bicritical points (BCPs). The BCP_1 is the meeting point of the second order transitions PM $\rightarrow$ AF_1 and PM $\rightarrow$ IOSDW with the first order one $AF_1 \rightarrow$ IOSDW. While the second bicritical point BCP_2 involve AF_2 instead of AF_1. Moreover, there is also a TCP in the transition $AF_2 \rightarrow$ PM.

The locations of BCP_1, BCP_2 and TCP in Figs. (3.20)(a)-(c)) when h_z increases, reflects the process of flattening of the phases mentioned above. The effects of such process in the location of these multicritical points can be seen in the details in Fig. (3.24). The mentioned process appears in the shift of the positions of the multicritical points in W as h_z increases. It can be seen that the BCP_1 is less shifted as compared to the BCP_2 and the TCP. On the other hand, the displacement of the TCP is even more pronounced than that of BCP_2.

In Fig. (3.21), the phase transition lines feature three TCPs, TCP_1, TCP_2 and TCP_3 which are related to the transition lines $AF_1 \rightarrow$ PM, IOSDW $\rightarrow$ PM and $AF_2 \rightarrow$ PM, respectively. The process of flattening of the phases AF_1, IOSDW and AF_2 appears clearly in the ordering in T and h_z of each of the TCP's since $T_{TCP_1} > T_{TCP_2} > T_{TCP_3}$ while $h_{z_{TCP_1}} < h_{z_{TCP_2}} < h_{zTCP_3}$.

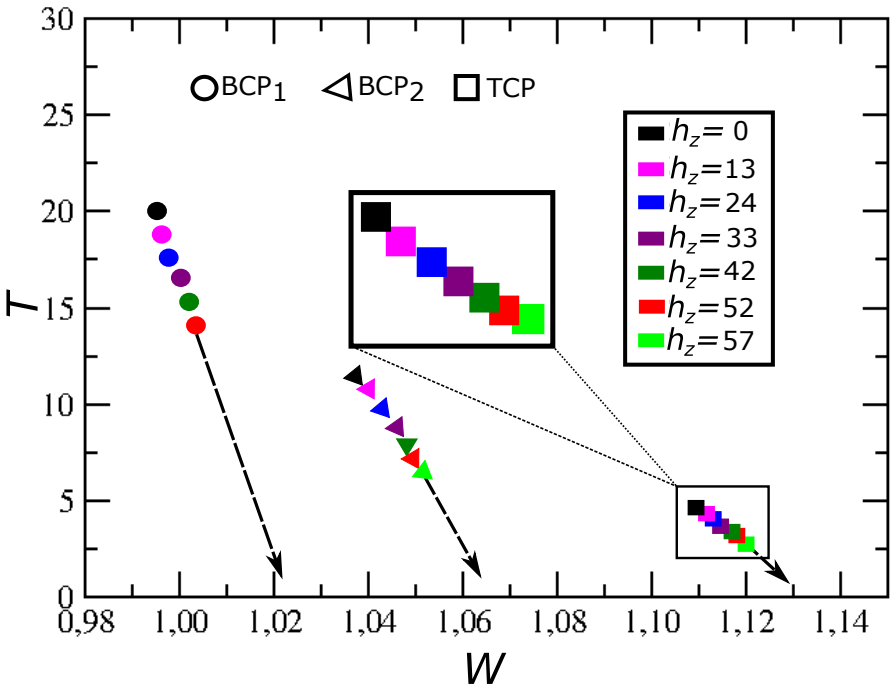

Figure 3.24: Evolution of the bicriticals points (BCPs) and tricritical point (TCPs) when h_z increases.

3.3.7 Summary about this topic

This section has described, within a mean field approximation, the emergence of multicritical points coming from the competition among phases with different OPs, which have distinct parity properties. Again we have used the UALM and we obtain three distinct types of long-range order: (a) two conventional SDWs (AF_1 and AF_2) and, (b) the non-magnetic inter-orbital spin density wave (IOSDW). This exotic SDW is described by a purely imaginary OP that mixes the α and β bands. The conventional SDWs are described by the real magnetization of each band m_f^α and m_f^β, where AF_1 and AF_2 are defined by $m_f^\beta > m_f^\alpha$ and $m_f^\alpha > m_f^\beta$, respectively. It is worth mentioning that the existence of a non-magnetic SDW has been suggested in other context such as iron superconductors [56].

The competition among phases takes place with the variation of the W and h_z. In the absence of h_z, the phase diagram T vs W displays at low T a sequence of first-order phase transitions $AF_1 \rightarrow$ IOSDW $\rightarrow AF_2$. We also found two BCP. The first one, called BCP_1, is the intersection of the second-order line transitions PM $\rightarrow$ AF_1 and PM $\rightarrow$ IOSDW with the first order one $AF_1 \rightarrow$ IOSDW. For the second BCP, called BCP_2, AF_1 is replaced by AF_2. Lastly, there is a TCP in the transition $AF_2 \rightarrow$ PM. The location of the BCPs indicates that their existence is a direct result of the distinct parity property under TRS of the phases AF_1, AF_2 and IOSDW. This is in agreement with general arguments based on a Landau free energy expansion.

When h_z is turned on, there are important changes in the IOSDW phase and more markedly in the AF_2 one. These two phases flatten out which means that they stabilize at lower T but with higher W values as compared to the situation without h_z. This is reflected in the location of BCP_2 and TCP. The evolution of their locations with the field shows the tendency for these multicritical points to disappear because of the flattening process of AF_2 and IOSDW. The different behavior of the phases when applying h_z is related to the very nature of each one. The AF_1 is isolated-itinerant and the AF_2 is totally itinerant. These two phases retain the same nature when the h_z is applied. Nevertheless, the IOSDW phase change its nature when the field is applied. While one of the bands always has the same FS and the other band has a totally constructed. The gradual change from isolated to itinerant is the ultimate cause that leads the IOSDW phase to have the flattening process more accentuated than AF_1 phase, although not as much as the AF_2 one. The data and analysis discussed here were published in J. Phys.: Condens. Matter **33**, 295801 (2021).

Chapter 4

General conclusions

To conclude, we have shown that the *Underscreened Anderson Lattice Model* (UALM) has a varied number of phase diagrams, which exhibit multiple critical points. The model shows that, although the $5f$-bands hybridize asymmetrically with the conduction band, the Hund's rule interaction directly couples the two independent 5f-bands. We have shown that the UALM is a microscopic realization of the situation envisaged in Ref. [57] that considers a Landau-Ginzburg free energy containing a linear coupling between two AF order parameters, in the case *i*) with two conventional SDWs (AF_1 and AF_2) when the magnetic field is applied in x-axis.

As a result, for the case *ii*) we observed that for a tetragonal lattice, there is the presence of metamagnetic-like transitions which occurs in both AF phases under the application of a magnetic field H_z. We highlight that such phenomelogy, the metamagnetic-like transitions inside the antferromagnetic phases have been reported in some antiferromagnetic heavy fermions [34] which also present a competition between two distinct antiferromagnetic phases.

For the case *iii*) we believe that our results with two conventional SDWs and one exotic SDW, the evolution of multicritical points with W and h_z as described here may be more general. For instance, motivated by the concept of adiabatic continuity [58], one may suggest the possibility that the present problem with three OPs (two of them real and one purely imaginary) can be described in a unified way in a single OP. That would be similar to the interesting proposal made by Haule and Kotliar that a complex OP accounts for the behavior of URu_2Si_2 under W and h_z [49]. In such scenario, it would be necessary to re-interpret the multicritical points. We are currently investigating this possibility, in another work in progress. We propose the IOSDW phase, which mixes bands, as an alternative in the study of the HO problem present in URu_2Si_2, due to the fact that it does not exhibit magnetic momentum formation. Finally, we highlight that our results show a detailed evolution of multi-

critical points when pressure and magnetic field are applied simultaneously. As far as we know, there are few theoretical results in the literature showing this particular evolution. Although our results refer to a specific model of two $5f$ degenerate narrow bands, they can shed light on the growing field of the multicritical (classical and quantum) points in the physics of uranium compounds. In general terms, we emphasize that the identification of multicritical can provide relevant information on the conventional and unconventional phases present in uranium compounds.

Chapter 5

Future works

- To study the possibility of describing the two conventional SDWs and the non-conventional SDW phase by means of a single real-complex OP.
- Verify the possible solutions with conventional SDW and unconventional SDW when spin-orbit coupling is included in the UALM.
- Specifically testing the UALM with spin-orbit coupling is able to describe the superconducting phase present in URu_2Si_2 through fluctuations of the unconventional SDW phase.
- Specifically testing the UALM with spin-orbit coupling is able to describe the multiple superconducting phases in UTe_2 via magnetic fluctuations.
- Investigate the effects of hybridization, Coulomb interactions, Hund's rule, and spin-orbit coupling using the tetragonal lattice (URu_2Si_2) and a symmetric orthorbombic central structure (UTe_2).
- Verify the effects of varying pressure and/or magnetic field on the phases eventually found in the UALM with SOC.

Chapter 6

Articles

6.1 Articles published during doctoral studies (until: May, 24 2022)

- ***Julián Faúndez***, ***S. G . Magalhães***, J. E. Calegari and P. S. Riseborough, J. Phys.: Condens. Matter **33**, 295801 (2021).

- A. C. Lausmann, E. J. Calegari, ***Julián Faúndez***, P. S. Riseborough, and ***S. G. Magalhães***. J. Magn. Magn. Mater. **560**, 169531 (2022).

- ***S. G. Magalhães***, ***Julián Faúndez***, J. E. Calegari, and P. S. Riseborough, ***Real-complex order parameter in a three band model for uranium compounds***, (2022). Status: in Preparation.

- ***S. G. Magalhães***, ***Julián Faúndez***, Christopher Thomas, E. J. Calegari, P. S. Riseborough, C. Lacroix, and B. Coqblin, ***Itinerant-localized duality in a model for 5f-electrons beyond mean field approximation***, (2022). Status: in preparation.

Chapter 7

Ackowledgements

The present work was supported by the Brazilian agencies Conselho Nacional de Desenvolvimento Científico e Tecnológico (CNPq) and Fundação de Amparo à pesquisa do Estado do RS (FAPERGS).

Appendix A

Second quantization formalism

The second quantization formalism was initiated by Paul M. Dirac[1] for bosons, and was extended to fermions by Eugene Wigner[2] and Pascual Jordan[3] with the transformation that bears his name. When working with a fairly large number of particles it is indispensable to introduce the second quantization formalism, which is able to greatly simplify manipulations of multi-particle states. Thus, we begin by defining a convenient way of specifying multi-particle states of identical particles, called the occupation number representation. We define a set of single-particle states, $\{|1\rangle, |2\rangle, |3\rangle, \cdots\}$ that form a complete orthonormal basis for the single-particle Hilbert space $\mathscr{H}^{(1)}$. Next, we construct multi-particle states by defining the number of particles that are present in the $|1\rangle$ state denoted n_1 and so on. In this way,

$$|n_1, n_2, n_3, \dots\rangle \tag{A.1}$$

is defined as the appropriate multi-particle state.

A.1 Fock space

The second quantization formalism allows us to interpret quantum fields in terms of particles. Each quantum state can be interpreted as a vector in Fock space. We can make the representation of the occupation number more convenient to work with by defining an "extended" Hilbert space, called Fock space, which is the space of bosonic/fermionic states for an arbitrary number of particles. In the formal language

[1] Paul Adrien Maurice Dirac: Born on August 8, 1902, England. Deceased on October 20, 1984, U.S.

[2] Eugene Wigner: Born on November 17, 1902, Austria-Hungary. Deceased on January 1, 1995, U.S.

[3] Pascual Jordan: Born on October 18, 1902, German Empire. Deceased on July 1, 1980, West Germany.

of linear algebra, the Fock space can be written as

$$\mathscr{H}^F_{S/A} = \mathscr{H}^{(0)} \oplus \mathscr{H}^{(1)} \oplus \mathscr{H}^{(2)}_{S/A} \oplus \mathscr{H}^{(3)}_{S/A} \oplus \mathscr{H}^{(4)}_{S/A} \oplus \cdots , \tag{A.2}$$

where, $\oplus$ represents the direct sum operation, which combines vector spaces by directly grouping their basis vectors into a larger basis set. The subscript S/A depends on whether we are dealing with bosons (S) or fermions (A). If $\mathscr{H}_1$ has dimension d_1 and $\mathscr{H}_2$ has dimension d_2, then $\mathscr{H}_1 \oplus \mathscr{H}_2$ has dimension $d_1 + d_2$.

As a result any multiparticle state written in the occupancy number representation $|n_1, n_2, n_3, \dots\rangle$ is present in the Fock space, $\mathscr{H}^F_{S/A}$, forming a complete basis for $\mathscr{H}^F_{S/A}$. Also, in the Eq. (A.2) the first term $\mathscr{H}^{(0)}$ is the "0-particle Hilbert space", which contains only one state vector given as

$$|\varnothing\rangle \equiv |0, 0, 0, 0, \dots\rangle. \tag{A.3}$$

The last Eq. (A.3) is the vacuum state, in which has no particles and follows the standard normalization $\langle\varnothing|\varnothing\rangle = 1$.

A.2 Second quantization for fermions

The creation operator for fermions can be defined as:

$$\begin{aligned} \hat{c}^\dagger_u |n_1, n_2, \dots, n_u, \dots\rangle &= \begin{cases} (-1)^{n_1+n_2+\cdots+n_{u-1}} |n_1, n_2, \dots, n_{u-1}, 1, \dots\rangle & \text{if } n_u = 0 \\ 0 & \text{if } n_u = 1 \end{cases} \\ &= (-1)^{n_1+n_2+\cdots+n_{u-1}}\, \delta_0^{n_u}\, |n_1, n_2, \dots, n_{u-1}, 1, \dots\rangle. \end{aligned} \tag{A.4}$$

- If state u is unoccupied, then $\hat{c}^\dagger_u$ increments the occupation number to 1, and multiply the state by a factor of magnitude $(-1)^{n_1+n_2+\dots+n_{u-1}}$ (i.e, $+1$ if there is an even number of occupied states preceding u, and -1 if there is an odd number). Note that this definition requires that the states of a single particle be ordered in order to be able to speak of states "prior" to u.

- If u is occupied, applying $\hat{c}^\dagger_u$ yields a zero vector and according to the Pauli exclusion principle, there can be no occupancy greater than 1,

The annihilation operator for fermions is the conjugate operator, $\hat{c}_u$. We proceed to take the Hermitian conjugate of the creation operator:

$$\langle n_1, n_2, \cdots, n_u, \cdots | \hat{c}_u = (-1)^{n_1+n_2+\cdots+n_{u-1}} \delta_0^{n_u} \langle n_1, n_2, \cdots, n_{u-1}, 1, \cdots |. \tag{A.5}$$

Now, multiplying by $|n_1^{'}, n_2^{'}, ...\rangle$ we have that

$$\langle n_1, n_2, \cdots, n_u, \cdots | \hat{c}_u | n_1^{'}, n_{2,\ldots}^{'} \rangle = (-1)^{n_1+\cdots+n_{u-1}} \delta^{n_1}_{n_1^{'}} \cdots \delta^{n_{u-1}}_{n_{u-1}^{'}} (\delta^{n_u}_0 \delta^1_{n_u^{'}}) \delta^{n_{u+1}}_{n_{u+1}^{'}} \cdots \tag{A.6}$$

deducing finally that

$$\begin{aligned} \hat{c}_u | n_1', \ldots, n_u', \ldots \rangle &= \begin{cases} 0 & \text{if } n_u' = 0 \\ (-1)^{n_1'+\cdots+n_{u-1}'} | n_1', \ldots, n_{u-1}', 0, \ldots \rangle & \text{if } n_u' = 1. \end{cases} \\ &= (-1)^{n_1'+\cdots+n_{u-1}'} \, \delta^1_{n_u'} \, \big| n_1', \ldots, n_{u-1}', 0, \ldots \big\rangle. \end{aligned} \tag{A.7}$$

- if the state u is occupied, applying $\hat{c}_u$ decreases the occupancy number to 0, and multiplies the status by the factor of ± 1.
- If the state u is unoccupied, then applying $\hat{c}_u$ gives the zero vector.

With the definitions of creation/annihilation operators already established, we can demonstrate the following anticommutation relations.

$$\{\hat{c}_u, \hat{c}_v\} = \{\hat{c}_u^\dagger, \hat{c}_v^\dagger\} = 0 \tag{A.8}$$

and

$$\{\hat{c}_u, \hat{c}_v^\dagger\} = \delta_{u,v} \tag{A.9}$$

where, $\{\cdot, \cdot\}$ denotes an anticommutator defined by

$$\left\{\hat{A}, \hat{B}\right\} = \hat{A}\hat{B} + \hat{B}\hat{A}. \tag{A.10}$$

This anticommutation relations can be derived by taking matrix elements with occupation number states. We will demonstrate that $\{\hat{c}_u, \hat{c}_v^\dagger\} = \delta_{u,v}$. Thus, we consider creation/annihilation operators acting on the same single-particle state u

$$\begin{aligned} \big\langle \ldots, n_u, \ldots \big| \hat{c}_u \hat{c}_u^\dagger \big| \ldots, n_u', \ldots \big\rangle &= (-1)^{n_1+\cdots+n_{u-1}} (-1)^{n_1'+\cdots+n_{\mu-1}'} \, \delta_0^{n_u} \delta^0_{n_u'} \\ &\quad \times \big\langle n_1, \ldots, n_{u-1}, 1, \ldots \big| n_1', \ldots, n_{u-1}', 1, \ldots \big\rangle \\ &= \delta^0_{n_u'} \cdot \delta^{n_1}_{n_1'} \delta^{n_2}_{n_2'} \cdots \delta^{n_u}_{n_u'}, \cdots \end{aligned} \tag{A.11}$$

using a similar calculation,

$$\big\langle \ldots, n_u, \ldots \big| \hat{c}_u^\dagger \hat{c}_u \big| \ldots, n_u', \ldots \big\rangle = \delta^1_{n_u'} \cdot \delta^{n_1}_{n_1'} \delta^{n_2}_{n_2'} \cdots \delta^{n_u}_{n_u'} \cdots . \tag{A.12}$$

Now, adding these two previous Eqs. and using that $\delta^0_{n_u'} + \delta^1_{n_u'} = 1$ we have

$$\left\langle \dots, n_u, \dots \right| \left\{ \hat{c}_u, \hat{c}_u^\dagger \right\} \left| \dots, n'_u, \dots \right\rangle = \left\langle \dots, n_u, \dots \right| \left. \dots, n'_u, \dots \right\rangle \tag{A.13}$$

Therefore,

$$\left\{ \hat{c}_u, \hat{c}_u^\dagger \right\} = \hat{I}. \tag{A.14}$$

The next step is to prove that $\left\{ \hat{c}_u, \hat{c}_v^\dagger \right\} = 0$ for $u \neq u$. Thus, by taking elements of the matrix:

$$\begin{aligned}
\left\langle \dots, n_u, \dots, n_v, \dots \right| \hat{c}_u \hat{c}_v^\dagger \left| \dots, n'_u, \dots, n'_v, \dots \right\rangle &= (-1)^{n_1+\dots+n_{u-1}} (-1)^{n'_1+\dots+n'_{v-1}} \delta_0^{n_u} \delta_{n'_v}^0 \\
&\quad \times \left\langle \dots, 1, \dots, n_v, \dots \right| \left. \dots, n'_u, \dots, 1, \dots \right\rangle \\
&= (-1)^{n'_u+\dots+n'_{v-1}} \delta_{n'_1}^{n_1} \delta_{n'_2}^{n_2} \cdots \left(\delta_0^{n_u} \delta_{n'_u}^1 \right) \cdots \left(\delta_1^{n_v} \delta_{n'_v}^0 \right) \cdots \\
&= (-1)^{1+n_{u+1}+\dots+n_{v-1}} \delta_{n'_1}^{n_1} \delta_{n'_2}^{n_2} \cdots \left(\delta_{n_u}^0 \delta_{n'_u}^1 \right) \cdots \left(\delta_{n'_v}^0 \delta_{n_v}^1 \right) \cdots \\
\left\langle \dots, n_u, \dots, n_v, \dots \right| \hat{c}_\nu^\dagger \hat{c}_u \left| \dots, n'_u, \dots, n'_v, \dots \right\rangle &= (-1)^{n_1+\dots+n_{v-1}} (-1)^{n'_1+\dots+n'_{u-1}} \delta_1^{n_v} \delta_{n'_u}^1 \\
&\quad \times \left\langle \dots, n_u, \dots, 0, \dots \right| \left. \dots, 0, \dots, n'_v, \dots \right\rangle \\
&= (-1)^{n_u+\dots+n_{v-1}} \delta_{n'_1}^{n_1} \delta_{n'_2}^{n_2} \cdots \left(\delta_0^{n_u} \delta_{n'_u}^1 \right) \cdots \left(\delta_1^{n_v} \delta_{n'_v}^0 \right) \cdots \\
&= (-1)^{0+n_{u+1}+\dots+n_{v-1}} \delta_{n'_1}^{n_1} \delta_{n'_2}^{n_2} \cdots \left(\delta_0^{n_u} \delta_{n'_u}^1 \right) \cdots \left(\delta_1^{n_v} \delta_{n'_v}^0 \right) \cdots
\end{aligned} \tag{A.15}$$

.

The two equations differ by a factor of -1, so adding them gives zero, checking $\left\{ c_u, c_v^\dagger \right\} = \delta_{uv}$ as stated in (A.9). We emphasize that due to the definitions of the creation and annihilation operators, the derivation of the fermionic anti-commutation relations is rather tedious because of the $(-1)^{(\cdots)}$ factors. Finally, we note that in our work, the creation/annihilation operators can exhibit $\mathbf{k}$-momentum, i site and spin $\sigma = \pm 1$ dependence. This appendix can be viewed at Ref. [65] as a free access textbook and in the Refs. [66, 67].

Appendix B

Density of states (DOS)

Before making a study for high spatial dimensions, we will investigate the behavior of the $\epsilon_\sigma(\mathbf{k})$ dispersion relation and its effects, depending on the spatial dimension. The dispersion relation $\epsilon_\sigma(\mathbf{k})$ for a d-dimensional simple cubic lattice is formally presented as:

$$\epsilon_\sigma(\mathbf{k}) = 2t_\sigma \sum_{n=1}^{d} \cos(k_n a), \tag{B.1}$$

where a is the distance between the sites of lattice. If k_n is independent of each other, it implies that $\epsilon_{\mathbf{k}\sigma}$ corresponds to an independent sum of $2t_\sigma \cos(k_n)$. This independent behavior can be seen in Fig. (B.1), where we show different DOS from a 1-dimensional to 5-dimensional simple cubic lattice. In these dimensions the dispersion relation is given by Eq. (B.1). In the case of $d \leq 3$, we can see that the DOS is governed by van Hove's singularities and its configuration is very different from the Gaussian distribution obtained in $d \to \infty$. Now if we look at the case of lattice with spatial dimensions higher than three ($d > 3$) we can see that the DOS is closer to a well-defined Gaussian dispersion. The fact that in a spatial dimension lattice five ($d = 5$) has a Gaussian type DOS allows us to approximate all other remaining dimensions greater than five ($d > 5$) , such as infinite spatial dimension lattice ($d \to \infty$).

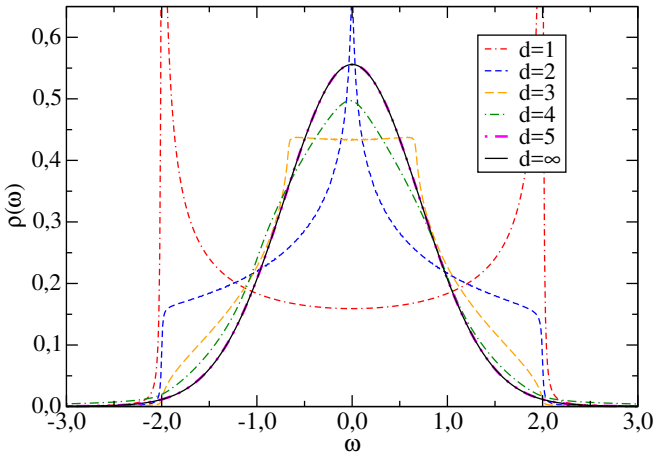

Figure B.1: DOS as function of ω of free electrons in a simple lattice from one dimension to $d \to \infty$.

The limit of infinite spatial dimension ($d \to \infty$), that is, the limit where the coordination number Z tends to infinity, allows the construction of a dynamic mean field theory, where the propagator $G(\omega)$, the $\sum(\omega)$ self-energy and partition function are the most important quantities to obtain. Since the self-energies are dynamic, the results in $d \to \infty$ are also, thus allowing to write the effects of correlations such as metal-insulator transitions, effect of temperatures on transport properties, dynamic excitations particle-hole in optical conductivity, and others interesting physic problems [59, 60, 61, 62, 63].

When we are in a high spatial dimension ($d \to \infty$) we can transform the sum of momentum into an integral, where the DOS becomes a constant of integration. This DOS is given as

$$\rho = \frac{1}{2D}, \tag{B.2}$$

where D correspond to the spatial dimension and the $f(d)$-bands become integration variables so we can define the following.

- The conduction band is given by

$$\epsilon_d(\mathbf{k}) = \epsilon. \tag{B.3}$$

- When include the nesting term $\mathbf{Q}$, the conduction band is

$$\epsilon_d(\mathbf{k} + \mathbf{Q}) = -\epsilon. \tag{B.4}$$

- We also have to find the relations between the f-bands (α and β). First there is a band-centering term called $\epsilon_f = 0.3$. So each of the bands can be

written as,

$$E_f^{\chi}(\mathbf{k}) = \epsilon_f + \epsilon_f(\mathbf{k}) \tag{B.5}$$

where $e_f = -0.3\epsilon$. Therefore, the α and β bands are given by

$$E_f^{\alpha}(\mathbf{k}) = 0.3 - 0.3\epsilon \tag{B.6}$$

and

$$E_f^{\beta}(\mathbf{k}) = 0.3 - 0.3\epsilon. \tag{B.7}$$

- When we include the nesting term the dispersion relations are

$$E_f^{\alpha}(\mathbf{k} + \mathbf{Q}) = 0,3 + 0,3\epsilon \tag{B.8}$$

and

$$E_f^{\beta}(\mathbf{k} + \mathbf{Q}) = 0,3 + 0,3\epsilon. \tag{B.9}$$

Finality, the bands are represented by terms that do not have **k**-momentum dependence, lowering the complexity of system.

Appendix C

Mean Field Approximation

A study of particle interactions can often be very complicated, because the individual motion of a particle depends on the spatial positions of the surrounding particles, which form a system, for example, in charged particle systems that have interaction between them through the Coulombian forces. However, being a very complicated problem, today we have solutions to problems that do not include correlation between electrons, which allows us to develop good approximations to various physical systems of interest. In certain case studies, we can consider average correlations between electrons, thus allowing the effects of one particle on another to be described by an average density or medium field, thus creating a problem of a particle embedded in a effective mean field. The Fig. (C.1) shows the general idea of a particle immersed in an effective mean field. However, there are a wide variety of examples using this mean field method and its applications allow us to show various physical phenomena.

Motivated by the nesting effects found on the Fermi surface (FS) in the HO state in the composite URu_2Si_2 and by the type of symmetry that can be broken in the proposed model to describe this system, the suggested OP to characterize the HO state is given by the correlation function as,

$$z^{\chi\chi'}_{\mathbf{q},\sigma} = \frac{1}{N}\sum_{\mathbf{k}} \langle f^{\dagger\chi}_{\mathbf{k}+\mathbf{q},\sigma} f^{\chi'}_{\mathbf{k},\sigma} \rangle \,. \tag{C.1}$$

In order to describe the exotic SDW state in $5f$ electron systems, we can consider explicitly the nesting effect of the FS found experimentally, so

$$z^{\chi\chi^{'}}_{\mathbf{q},\sigma} = z^{\chi\chi^{'}}_{\mathbf{q},\sigma}\delta_{\mathbf{Q},\mathbf{q}}. \tag{C.2}$$

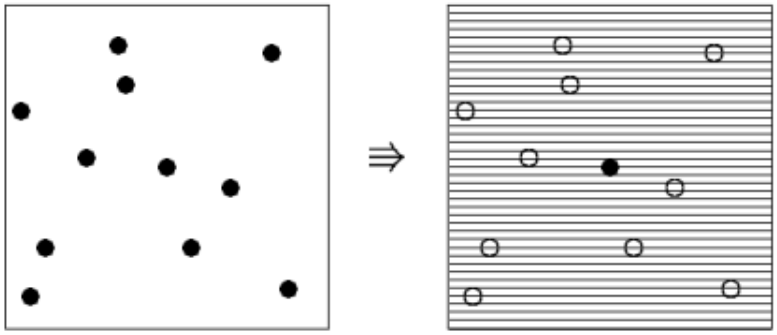

Figure C.1: Representation of the mean field idea. On the left we show a real physical system in which it has correlation between all particles. In the right figure we show a particle (black color) which is in interaction with the rest of the particles (gray color) through an effective field.

If it were nonzero, it would represent a special kind of inter-orbital spin wave density (IOSDW) or exotic SDW. An mean field approximation consists in considering that the deviations of the values assumed by a variable in relation to its mean value are small. This consideration serves to "uncouple" product from operators. Generally given two operators A_i, we can write $A_i = \langle A_i \rangle + \delta A_i$, this allows we to make a problem self-consistent when we have two operators

$$A_1 A_2 = \langle A_1 \rangle A_2 + \langle A_2 \rangle A_1 - \langle A_1 \rangle \langle A_2 \rangle . \tag{C.3}$$

Then, the mean values of the operators appear in the Hamiltonian itself, which must be calculated. The general representation of Green's functions for two bands χ, χ' of itinerant f-electrons with spin σ are given as,

$$\omega G^{\chi\chi'}_{ff,\sigma}(\mathbf{k},\mathbf{k}',\omega) = \delta_{\mathbf{k}\mathbf{k}'}\delta_{\sigma,\sigma'}\delta^{\chi\chi} \langle\langle [f^{\chi}_{\mathbf{k}\sigma}, \hat{H}]; f^{\chi'}_{\mathbf{k}'\sigma} \rangle_{\omega} \rangle , \tag{C.4}$$

or also

$$\omega G^{\chi\chi'}_{ff,\sigma\sigma'}(\mathbf{k},\mathbf{k}',\omega) = \delta_{\mathbf{k},\mathbf{k}'}\delta_{\sigma\sigma'}\delta^{\chi\chi'} + \langle\langle \left[f^{\chi}_{\mathbf{k},\sigma}, \hat{H}_1 \right] \rangle\rangle_{\omega} + \langle\langle \left[f^{\chi}_{\mathbf{k},\sigma}, \hat{H}_2 \right] \rangle\rangle_{\omega} + ... \tag{C.5}$$

With mean field theory we can find the various OP of both the conventional SDW states and the exotic SDW.

Appendix D

General formulation of two conventional SDWs

We include an applied magnetic field oriented to the z-axis, which introduce an additional term into the Hamiltonian $\hat{H}_{ext} = \hat{H}^f_{ext} + \hat{H}^d_{ext}$, where

$$\hat{H}^f_{ext} = -\Gamma_f \sum_{\mathbf{k}} (f^\dagger_{\mathbf{k},\uparrow} f_{\mathbf{k},\downarrow} + f^\dagger_{\mathbf{k},\downarrow} f_{\mathbf{k},\uparrow}) \tag{D.1}$$

with

$$\Gamma_f = g_f \mu_B h_x. \tag{D.2}$$

The term $\hat{H}^d_{ext}$ is the same as Eq. (D.1), except that the f operators and the gyromagnetic factor g_f are replaced by $d$operators and g_d, respectively. The temporal and spatial Fourier transform of the single-electron f-f Green's function, within the Hartree-Fock approximation, satisfy the equations of motion given by:

$$\begin{aligned}[\omega \; - \; \tilde{E}^\alpha_f(\mathbf{k}) \;] \; G^{\alpha,\chi'}_{ff,\sigma}(\mathbf{k},\underline{k}',\omega) = \delta^{\alpha,\chi'} \; \delta_{\mathbf{k},\mathbf{k}'} \; \delta_{\sigma,\sigma'} \\ + \; V_\alpha(\mathbf{k}) \; G^{\chi'}_{df,\sigma\sigma'}(\mathbf{k},\mathbf{k}',\omega) - \; \Gamma_f \; G^{\beta,\chi'}_{ff,-\sigma,\sigma}(\mathbf{k},\mathbf{k}',\omega) \\ + \phi^\alpha_\sigma \; G^{\alpha,\chi'}_{ff,\sigma,\sigma'}(\mathbf{k}+\mathbf{Q},\mathbf{k}',\omega)\end{aligned} \tag{D.3}$$

and

$$\begin{aligned}[\omega \; - \; \tilde{E}^\beta_f(\mathbf{k}) \;] \; G^{\beta,\chi'}_{ff,\sigma,\sigma'}(\mathbf{k},\mathbf{k}',\omega) = \delta^{\beta,\chi'} \; \delta_{\mathbf{k},\mathbf{k}'} \; \delta_{\sigma,\sigma'} \\ + \; V_\beta(\mathbf{k}) \; G^{\chi'}_{df,\sigma,\sigma'}(\mathbf{k},\mathbf{k}',\omega) - \; \Gamma_f \; G^{\alpha,\chi'}_{ff,-\sigma\sigma'}(\mathbf{k},\mathbf{k}',\omega) \\ + \phi^\beta_\sigma \; G^{\beta,\chi'}_{ff,\sigma,\sigma'}(\mathbf{k}+\mathbf{Q},\mathbf{k}',\omega).\end{aligned} \tag{D.4}$$

The spin-independent Hartree-Fock dispersion relation $\tilde{E}_f^{\chi}(\mathbf{k})$ is given by

$$\tilde{E}_f^{\chi}(\mathbf{k}) \;=\; E_f^{\chi}(\mathbf{k}) \;+\; \sum_{\chi'}\left((U-J)\frac{n_f^{\chi'}}{2}(1-\delta^{\chi,\chi'})+U\frac{n_f^{\chi'}}{2}\right) \tag{D.5}$$

where the real function ϕ_σ^{χ} is given by

$$\phi_\sigma^{\chi} \;=\; \sum_{\chi'}\Big(Um^{\chi'}\eta(-\sigma)+(U-J)m^{\chi}(1-\delta^{\chi,\chi'})\eta(\sigma)\Big). \tag{D.6}$$

The mixed f-d Green's function satisfies the equation below

$$\begin{aligned}[\,\omega \;-\; \epsilon(\mathbf{k})\,]\; G^{\chi'}_{df,\sigma,\sigma'}(\mathbf{k},\mathbf{k}',\omega) \;&=\; V_\alpha(\mathbf{k})^*\; G^{\alpha,\chi'}_{ff,\sigma,\sigma'}(\mathbf{k},\mathbf{k}',\omega)\\ +\; V_\beta(\mathbf{k})^*\; G^{\beta,\chi'}_{ff,\sigma,\sigma'}(\mathbf{k},\mathbf{k}',\omega) - \Gamma_d\; G^{\chi'}_{df,-\sigma,\sigma'}(\mathbf{k},\mathbf{k}',\omega).\end{aligned} \tag{D.7}$$

We will choose a basis set for the f orbitals, such that $V_\beta(\mathbf{k}) = 0$ and $V_\alpha(\mathbf{k}) = V_\alpha$ simply to avoid the transformation to a new basis set. The choice of basis states should not change the main physical results, as discussed in ref. [7]. The Green's function equation of motions given in Eqs. (F.44)-(F.46) form a closed set of equations, which can be solved exactly. The equations can be expressed in the matrix form

$$\underline{\underline{\Pi}}^{\chi}(\mathbf{k},\omega)\;\underline{\underline{G}}^{\chi\chi'}(\mathbf{k},\mathbf{k'},\omega) = \underline{\underline{\delta}}^{\chi'}(\mathbf{k},\mathbf{k'}) \tag{D.8}$$

where

$$\underline{\underline{G}}^{\chi\chi'}(\mathbf{k},\mathbf{k'},\omega) = \begin{pmatrix} G^{\chi\chi'}_{ff,\sigma\sigma'}(\mathbf{k},\mathbf{k'},\omega)\\ G^{\chi\chi'}_{ff,\sigma\sigma'}(\mathbf{k}+\mathbf{Q},\mathbf{k'},\omega)\\ G^{\chi\chi'}_{ff,-\sigma\sigma'}(\mathbf{k},\mathbf{k'},\omega)\\ G^{\chi\chi'}_{ff,-\sigma\sigma'}(\mathbf{k}+\mathbf{Q},\mathbf{k'},\omega)\end{pmatrix}$$

$$\underline{\underline{\Pi}}^{\chi}(\mathbf{k},\omega) =$$

$$\begin{pmatrix} \omega-\tilde{E}_f^{\chi}(\mathbf{k})-\xi_\Gamma^{'\chi}(\underline{k}) & -\phi_\sigma^{\chi} & \gamma_\Gamma^{'\chi}(\mathbf{k}) & 0\\ -\phi_\sigma^{\chi} & \omega-\tilde{E}_f^{\chi}(\mathbf{k}+\mathbf{Q})-\xi_\Gamma^{'\chi}(\mathbf{k}+\mathbf{Q}) & 0 & \gamma_\Gamma^{'\chi}(\mathbf{k}+\mathbf{Q})\\ \gamma_\Gamma^{'\chi}(\mathbf{k}) & 0 & \omega-\tilde{E}_f^{\chi}(\mathbf{k})-\xi_\Gamma^{'\chi}(\mathbf{k}) & -\phi_{-\sigma}^{\chi}\\ 0 & \gamma_\Gamma^{'\chi}(\mathbf{k}+\mathbf{Q}) & -\phi_{-\sigma}^{\chi} & \omega-\tilde{E}_f^{\chi}(\mathbf{k}+\mathbf{Q})-\xi_\Gamma^{'\chi}(\mathbf{k}+\mathbf{Q})\end{pmatrix}$$

and

$$\underline{\underline{\delta}}^{\chi'}(\mathbf{k},\mathbf{k'}) = \begin{pmatrix} \delta^{\chi\chi'}\delta_{\mathbf{k},\mathbf{k}},\delta_{\sigma\sigma'}\\ \delta^{\chi\chi'}\delta_{\mathbf{k}+\mathbf{Q},\mathbf{k}},\delta_{\sigma\sigma'}\\ \delta^{\chi\chi'}\delta_{\mathbf{k},\mathbf{k}},\delta_{-\sigma\sigma'}\\ \delta^{\chi\chi'}\delta_{\mathbf{k}+\mathbf{Q},\mathbf{k}},\delta_{-\sigma\sigma'}\end{pmatrix}$$

with $\xi_{\Gamma}^{'\chi}(\mathbf{k}) = \xi_{\Gamma}^{\chi}(\mathbf{k})(\delta_{\chi\alpha} + (1-\delta_{\chi\beta}))$, $\gamma_{\Gamma}^{'\chi}(\mathbf{k}) = \gamma_{\Gamma}^{\chi}(\mathbf{k})(\delta_{\chi\alpha} + (1-\delta_{\chi\beta}))$ where

$$\xi_{\Gamma}^{\chi}(\mathbf{k}) = \frac{(\omega - \epsilon_d(\mathbf{k}))\ |V_\chi|^2}{(\omega - \epsilon_d(\mathbf{k}))^2 - \Gamma_d^2} \tag{D.9}$$

and

$$\gamma_{\Gamma}^{\chi}(\mathbf{k}) = \Gamma_f - \frac{\Gamma_d\ |V_\chi|^2}{(\omega - \epsilon_d(\mathbf{k}))^2 - \Gamma_d^2}. \tag{D.10}$$

Now, when $V_\beta = 0$, by using Eq. (D.8), the Green's function can be explicitly written as

$$G_{ff,\sigma\sigma'}^{\beta\chi'}(\mathbf{k},\mathbf{k'},\omega) = \delta^{\beta\chi'}\delta_{\mathbf{k},\mathbf{k}},\delta_{\sigma\sigma'} \times \frac{[D_{0-\sigma}^{\beta}(\omega,\mathbf{k})(\omega - \tilde{E}_f^{\beta}(\mathbf{k}+\mathbf{Q})) - \Gamma_f^2(\omega - \tilde{E}_f^{\beta}(\mathbf{k}))]}{|A^\beta|}, \tag{D.11}$$

$$G_{ff,\sigma\sigma'}^{\beta\chi'}(\mathbf{k}+\mathbf{Q},\mathbf{k'},\omega) = \delta^{\beta\chi'}\delta_{\mathbf{k}+\mathbf{Q},\mathbf{k}},\delta_{\sigma\sigma'} \times \frac{[\Gamma_f^2\phi_{-\sigma}^{\beta} + \phi_\sigma^\beta D_{0-\sigma}^{\beta}(\omega,\mathbf{k})]}{|A^\beta|} \tag{D.12}$$

where

$$D_{0\sigma}^{\beta}(\omega,\mathbf{k}) = (\omega - \tilde{E}_f^{\beta}(\mathbf{k}+\mathbf{Q}))(\omega - \tilde{E}_f^{\beta}(\mathbf{k})) - (\phi_\sigma^\beta)^2 \tag{D.13}$$

and

$$\begin{aligned} |A^\beta| \ &= \ D_{0\sigma}^{\beta}(\omega,\mathbf{k})D_{0-\sigma}^{\beta}(\omega,\mathbf{k}) + \Gamma_f^2[\Gamma_f^2 - 2\phi_\sigma^\beta\phi_{-\sigma}^\beta] \\ &\quad -\Gamma_f^2[(\omega - \tilde{E}_f^{\beta}(\mathbf{k}))^2 + (\omega - \tilde{E}_f^{\beta}(\mathbf{k}+\mathbf{Q}))^2]. \end{aligned} \tag{D.14}$$

Moreover

$$G_{ff,\sigma\sigma'}^{\alpha\chi'}(\mathbf{k},\mathbf{k'},\omega) = \delta^{\alpha\chi'}\delta_{\mathbf{k},\mathbf{k}},\delta_{\sigma\sigma'}\frac{(\omega - \epsilon(\mathbf{k}))}{|A^\alpha|}A_{1\sigma}^{\alpha}(\omega,\mathbf{k}), \tag{D.15}$$

$$G_{ff,\sigma\sigma'}^{\alpha\chi'}(\mathbf{k}+\mathbf{Q},\mathbf{k'},\omega) = \delta^{\alpha\chi'}\delta_{\mathbf{k}+\mathbf{Q},\mathbf{k}},\delta_{\sigma\sigma'}A_{2\sigma}^{\alpha}(\omega,\mathbf{k}) \times \frac{(\omega - \epsilon(\mathbf{k}))(\omega - \epsilon(\mathbf{k}+\mathbf{Q}))}{|A^\alpha|} \tag{D.16}$$

where

$$\begin{aligned} A_{1\sigma}^{\alpha}(\omega,\mathbf{k}) = D_0^\alpha(\omega,\mathbf{k})(D_0^\alpha(\omega,\mathbf{k}+\mathbf{Q}))^2 - (\gamma_\Gamma^{\alpha\alpha}(\mathbf{k}+\mathbf{Q}))^2 \\ \times D_0^\alpha(\omega,\mathbf{k})(\omega - \epsilon(\mathbf{k}+\mathbf{Q}))^2 - (\phi_{-\sigma}^\alpha)^2 D_0^\alpha(\omega,\mathbf{k}+\mathbf{Q}) \\ \times (\omega - \epsilon(\mathbf{k}+\mathbf{Q}))(\omega - \varepsilon(\mathbf{k})) \end{aligned} \tag{D.17}$$

and

$$A^{\alpha}_{2\sigma}(\omega,\mathbf{k}) = \phi^{\alpha}_{\sigma}[D^{\alpha}_{0}(\omega,\mathbf{k})D^{\alpha}_{0}(\omega,\mathbf{k}+\mathbf{Q}) - (\phi^{\alpha}_{-\sigma})^{2}(\omega-\epsilon(\mathbf{k})) \times (\omega-\varepsilon(\mathbf{k}+\mathbf{Q}))] + \phi^{\alpha}_{-\sigma}\gamma^{\alpha\alpha}_{\Gamma}(\mathbf{k})\gamma^{\alpha\alpha}_{\Gamma}(\mathbf{k}+\mathbf{Q})(\omega-\epsilon(\mathbf{k})) \times (\omega-\epsilon(\mathbf{k}+\mathbf{Q})) \quad \text{(D.18)}$$

with

$$\begin{aligned}|A^{\alpha}| = {} & [D^{\alpha}_{0}(\omega,\mathbf{k})D^{\alpha}_{0}(\omega,\mathbf{k}+\mathbf{Q}) - (\phi^{\alpha}_{-\sigma})^{2}(\omega-\epsilon(\mathbf{k}+\mathbf{Q}))(\omega-\epsilon(\mathbf{k}))] \\ & [D^{\alpha}_{0}(\omega,\mathbf{k})D^{\alpha}_{0}(\omega,\mathbf{k}+\mathbf{Q}) - (\phi^{\alpha}_{\sigma})^{2} \times (\omega-\epsilon(\mathbf{k}+\mathbf{Q}))(\omega-\epsilon(\mathbf{k}))] \\ & + [(\gamma^{\alpha\alpha}_{\Gamma}(\mathbf{k}))^{2}(\gamma^{\alpha\alpha}_{\Gamma}(\mathbf{k}+\mathbf{Q}))^{2} - 2\phi^{\alpha}_{\sigma}\phi^{\alpha}_{-\sigma}\gamma^{\alpha\alpha}_{\Gamma}(\mathbf{k})\gamma^{\alpha\alpha}_{\Gamma}(\mathbf{k}+\mathbf{Q})]\times \\ & (\omega-\epsilon(\mathbf{k}))^{2}(\omega-\epsilon(\mathbf{k}+\mathbf{Q}))^{2} - (\gamma^{\alpha\alpha}_{\Gamma}(\mathbf{k}))^{2}(D^{\alpha}_{0}(\omega,\mathbf{k}+\mathbf{Q}))^{2}(\omega-\epsilon(\mathbf{k}))^{2} \\ & - (\gamma^{\alpha\alpha}_{\Gamma}(\mathbf{k}+\mathbf{Q}))^{2}(D^{\alpha}_{0}(\omega,\mathbf{k}))^{2}(\omega-\epsilon(\mathbf{k}+\mathbf{Q}))^{2} \quad \text{(D.19)}\end{aligned}$$

where ϕ^{χ}_{σ}, $\gamma^{\chi\chi}_{\Gamma}(\mathbf{k})$ and $D^{\alpha}_{0}(\omega,\mathbf{k})$ are defined in Eqs. (E.10), (**??**) and (D.26), respectively. From the equations $|A^{\beta}| = 0$ and $|A^{\alpha}| = 0$, the spin independent quasi-particles energies E^{γ} where γ is the number of solutions. For $\gamma^{\chi}_{\Gamma}(\mathbf{k}) \approx \Gamma_f$ and $\xi^{\chi}_{\Gamma}(\mathbf{k}) \approx \frac{|V_{\chi}|^2}{(\omega-\epsilon_d(\mathbf{k}))}$, the equation $|A^{\beta}| = 0$ has $\gamma = 1...4$ while $|A^{\alpha}| = 0$ has γ =1...8. Thus, the Green's function $G^{\beta\beta}_{ff,\sigma}(\mathbf{k},\mathbf{k}+\mathbf{Q},\omega)$ with $h_x = 0$ acquires a simple form given by:

$$G^{\beta\beta}_{ff,\sigma}(\mathbf{k},\mathbf{k}+\mathbf{Q},\omega) = \phi^{\beta}_{\sigma}\left(\frac{|\widetilde{B}^{+}(\mathbf{k})|^2}{\omega-E_{+}(\mathbf{k})} + \frac{|\widetilde{B}^{-}(\mathbf{k})|^2}{\omega-E_{-}(\mathbf{k})}\right) \quad \text{(D.20)}$$

where the spin-independent quasi-particle bands $E_{\pm}(\mathbf{k})$ are

$$E_{\pm}(\mathbf{k}) = \left(\frac{\tilde{E}^{\beta}_{f}(\mathbf{k}) + \tilde{E}^{\beta}_{f}(\mathbf{k}+\mathbf{Q})}{2}\right) \pm X_{\mathbf{k}} \quad \text{(D.21)}$$

with

$$X_{\mathbf{k}} = \sqrt{\frac{\tilde{E}^{\beta}_{f}(\mathbf{k}) - \tilde{E}^{\beta}_{f}(\mathbf{k}+\mathbf{Q})}{2} + (Um^{\beta}_{f} + Jm^{\alpha}_{f})^2} \quad \text{(D.22)}$$

and the spectral weights $|\widetilde{B}^{\pm}(\mathbf{k})|^2$ in Eq. (D.20) found as

$$|\widetilde{B}^{\pm}(\mathbf{k})|^2 = \pm\frac{1}{2}\frac{1}{\sqrt{\frac{\tilde{E}^{\beta}_{f}(\mathbf{k})-\tilde{E}^{\beta}_{f}(\mathbf{k}+\mathbf{Q})}{2} + (Um^{\beta}_{f} + Jm^{\alpha}_{f})^2}}. \quad \text{(D.23)}$$

Meanwhile, the α-band has no simple form for the Green's function $G^{\alpha\alpha}_{ff,\sigma}(\mathbf{k},\mathbf{k}+$

$\mathbf{Q}, \omega)$,

$$G^{\alpha\alpha}_{ff,\sigma}(\mathbf{k}, \mathbf{k}+\mathbf{Q}, \omega) = \phi^{\alpha}_{\sigma} \frac{(\omega - \epsilon_d(\mathbf{k}))(\omega - \epsilon_d(\mathbf{k}+\mathbf{Q}))}{D^{\alpha}(\omega, \mathbf{k})} \tag{D.24}$$

with

$$\begin{aligned} D^{\alpha}(\mathbf{k}, \omega) &= D^{\alpha}_0(\omega, \mathbf{k})\ D^{\alpha}_0(\omega, \mathbf{k}+\mathbf{Q}) \\ &\quad -(U m^{\alpha}_f + J m^{\beta}_f)^2 (\omega - \epsilon_d(\mathbf{k}))(\omega - \epsilon_d(\mathbf{k}+\mathbf{Q})) \end{aligned} \tag{D.25}$$

and

$$D^{\alpha}_0(\mathbf{k}, \omega) = (\omega - \tilde{E}^{\alpha}_f(\mathbf{k}))\ (\omega - \epsilon_d(\mathbf{k})) - |V_{\alpha}|^2. \tag{D.26}$$

The equation of motion for Green's function are in Appendix (F).

Appendix E

Formulation of two conventional SDWs and one Exotic SDW

We assume the intra-orbital spin density wave (for both χ-orbitals) and the spin-dependent inter-orbital density wave instabilities occur at the same nesting vector $\mathbf{Q}$ of the cubic lattice. Therefore, for the correlations functions give in Eqs. (2.22) and (2.23), we make the ansatz:

$$z^{\chi'\chi}_{\mathbf{q},\sigma} = z^{\chi'\chi}_{\mathbf{Q},\sigma}\delta_{\mathbf{q},\mathbf{Q}} \tag{E.1}$$

and

$$n^{\chi\chi}_{\mathbf{q},\sigma} = n^{\chi\chi}_{\sigma}\delta_{\mathbf{q},0} + n^{\chi\chi}_{\mathbf{Q}\sigma}\delta_{\mathbf{q},\mathbf{Q}}. \tag{E.2}$$

In order to describe the system we must use Green's function theory (see Appendix (F) and Appendix (F.2)). Thus, the complete set is given by the spatial and temporal Fourier transform of the single electron Green function to $\chi = \alpha$ and $\chi = \beta$ by the equation of motion of the form

$$\begin{aligned}[\omega - \widetilde{E}^{\alpha}_{f\sigma}(\mathbf{k})]G^{\alpha,\chi'}_{ff,\sigma}(\mathbf{k},\mathbf{k}',\omega) &= \delta^{\alpha,\chi'}\delta_{\mathbf{k},\mathbf{k}'} \\ +V_{\alpha}(\mathbf{k})G^{\chi'}_{df,\sigma}(\mathbf{k},\mathbf{k}',\omega) + \kappa^{\beta\alpha}_{-\mathbf{Q},\sigma}G^{\beta,\chi'}_{ff,\sigma}(\mathbf{k}+\mathbf{Q},\mathbf{k}',\omega) \\ +\phi^{\alpha\alpha}_{-\mathbf{Q},\sigma}G^{\alpha,\chi'}_{ff,\sigma}(\mathbf{k}+\mathbf{Q},\mathbf{k}',\omega)\end{aligned} \tag{E.3}$$

and

$$\begin{aligned}[\omega - \widetilde{E}^{\beta}_{f\sigma}(\mathbf{k})]G^{\beta,\chi'}_{ff,\sigma}(\mathbf{k},\mathbf{k}',\omega) &= \delta^{\beta,\chi'}\delta_{\mathbf{k},\mathbf{k}'} \\ +V_{\beta}(\mathbf{k})G^{\chi'}_{df,\sigma}(\mathbf{k},\mathbf{k}',\omega) + \kappa^{\beta\alpha}_{\mathbf{Q},\sigma}G^{\alpha,\chi'}_{ff,\sigma}(\mathbf{k}-\mathbf{Q},\mathbf{k}',\omega) \\ +\phi^{\beta\beta}_{\mathbf{Q},\sigma}G^{\beta,\chi'}_{ff,\sigma}(\mathbf{k}-\mathbf{Q},\mathbf{k}',\omega),\end{aligned} \tag{E.4}$$

$$
\begin{aligned}
[\,\omega - \widetilde{\epsilon}(\mathbf{k})]\; G^{\chi'}_{df,\sigma}(\mathbf{k},\mathbf{k}',\omega) \;=\; \\
V_\alpha(\mathbf{k})^* G^{\alpha,\chi'}_{ff,\sigma}(\mathbf{k},\mathbf{k}',\omega) + V_\beta(\mathbf{k})^* G^{\beta,\chi'}_{ff,\sigma}(\mathbf{k},\mathbf{k}',\omega),
\end{aligned}
\tag{E.5}
$$

The temporal and spatial Fourier transform of the single-electron f-f Green's functions is completed with the mixed f-d Green's function equation of motion (see Eq. (**??**)) given a closed set which can be solved within a matricial formalism. Thus, one has

$$
\underline{\mathbf{G}}(\mathbf{k},\mathbf{k}',\omega) = (\underline{\Pi}(\mathbf{k},\omega))^{-1}\underline{\delta}(\mathbf{k},\mathbf{k}') \tag{E.6}
$$

where $\underline{\mathbf{G}}(\mathbf{k},\mathbf{k}',\omega)$ is describe by

$$
\underline{\mathbf{G}}(\mathbf{k},\mathbf{k}',\omega) = \begin{pmatrix} G^{\alpha\chi'}_{ff,\sigma}(\mathbf{k},\mathbf{k}',\omega) \\ G^{\beta\chi'}_{ff,\sigma}(\mathbf{k},\mathbf{k}',\omega) \\ G^{\alpha\chi'}_{ff,\sigma}(\mathbf{k}+\mathbf{Q},\mathbf{k}',\omega) \\ G^{\beta\chi'}_{ff,\sigma}(\mathbf{k}+\mathbf{Q},\mathbf{k}',\omega) \end{pmatrix}
$$

and $\underline{\delta}(\mathbf{k},\mathbf{k}')$ as

$$
\underline{\delta}(\mathbf{k},\mathbf{k}') = \begin{pmatrix} \delta^{\alpha\chi'}\delta_{\mathbf{k},\mathbf{k}'} \\ \delta^{\beta\chi'}\delta_{\mathbf{k},\mathbf{k}'} \\ \delta^{\alpha\chi'}\delta_{\mathbf{k}+\mathbf{Q},\mathbf{k}'} \\ \delta^{\beta\chi'}\delta_{\mathbf{k}+\mathbf{Q},\mathbf{k}'} \end{pmatrix}.
$$

The term $\underline{\Pi}(\mathbf{k},\omega)$ is a matrix given by

$$
\begin{pmatrix}
\omega - \widetilde{E}^{\alpha}_{f\sigma}(\mathbf{k}) - \widetilde{\xi}^{\alpha}(\mathbf{k}) & 0 & -\phi^{\alpha\alpha}_{-\mathbf{Q},\sigma} & -\kappa^{\beta\alpha}_{\mathbf{Q},\sigma} \\
0 & \omega - \widetilde{E}^{\beta}_{f\sigma}(\mathbf{k}) - \widetilde{\xi}^{\beta}(\mathbf{k}) & -\kappa^{\alpha\beta}_{-\mathbf{Q},\sigma} & -\phi^{\beta\beta}_{-\mathbf{Q},\sigma} \\
-\phi^{\alpha\alpha}_{-\mathbf{Q},\sigma} & -(\kappa^{\alpha\beta}_{-\mathbf{Q},\sigma})^* & \omega - \widetilde{E}^{\alpha}_{f\sigma,}(\mathbf{k}+\mathbf{Q}) - \widetilde{\xi}^{\alpha}(\mathbf{k}+\mathbf{Q}) & 0 \\
-(\kappa^{\beta\alpha}_{\mathbf{Q},\sigma})^* & -\phi^{\beta\beta}_{-\mathbf{Q},\sigma} & 0 & \omega - \widetilde{E}^{\beta}_{f\sigma}(\mathbf{k}+\mathbf{Q}) - \widetilde{\xi}^{\beta}(\mathbf{k}+\mathbf{Q})
\end{pmatrix}.
$$

In the matrix $\underline{\Pi}(\mathbf{k},\omega)$ the mean field dispersion relation $\tilde{E}^{\chi}_{f}(\mathbf{k})$ is given by

$$
\begin{aligned}
E^{\chi}_{f\sigma}(\mathbf{k}) \;&=\; E^{\chi}_{f}(\mathbf{k}) - \sigma H^{f}_{z} + \\
&\sum_{\chi'}\Big(U n^{\chi'\chi'}_{-\sigma} + (U-J) n^{\chi'\chi'}_{\sigma}(1-\delta^{\chi,\chi'})\Big).
\end{aligned}
\tag{E.7}
$$

One also has

$$
\xi^{\chi}(\mathbf{k},\omega) = \frac{|V_\chi|^2}{\omega - \epsilon_{d\sigma}(\mathbf{k})}[\delta_{\chi\alpha} + (1-\delta_{\chi\beta})] \tag{E.8}
$$

with $\epsilon_{d\sigma}(\mathbf{k}) = \epsilon(\mathbf{k}) - \sigma H_z^d$. The gaps $\kappa^{\chi'\chi}_{-\mathbf{Q},\sigma}$ and $\phi^{\chi\chi}_{-\mathbf{Q},\sigma}$ in the matrix $\underline{\Pi}(\mathbf{k},\omega)$ are given as

$$\kappa^{\chi'\chi}_{-\mathbf{Q},\sigma} = J\ z^{\chi'\chi}_{\mathbf{Q},-\sigma} - (U-J)\ z^{\chi'\chi}_{\mathbf{Q},\sigma} \tag{E.9}$$

and

$$\phi^{\chi\chi}_{-\mathbf{Q}\sigma} = \sum_{\chi'}(U\ n^{\chi'\chi'}_{\mathbf{Q},-\sigma} + (U-J)\ n^{\chi'\chi'}_{\mathbf{Q},\sigma}(1-\delta^{\chi,\chi'})). \tag{E.10}$$

The Green functions necessary to obtain the IOSDW and AF order parameters can be obtained directly from the Eq. (E.6). Therefore, $G^{\beta\alpha}_{f,\sigma}(\mathbf{k},\mathbf{k}+\mathbf{Q},\omega)$ is given as

$$\begin{aligned} G^{\beta\alpha}_{f,\sigma}(\mathbf{k},\mathbf{k}+\mathbf{Q},\omega) = D^{-1}_{\sigma}(\mathbf{k},\mathbf{Q},\omega) \times [|\kappa^{\beta\alpha}_{-\mathbf{Q},\sigma}|^3 - \\ (\omega - E^{\beta}_{f,\sigma}(\mathbf{k}+\mathbf{Q}))|\kappa^{\beta\alpha}_{-\mathbf{Q},\sigma}|(\omega - E^{\alpha}_{f,\sigma}(\mathbf{k}+\mathbf{Q}) - \xi^{\alpha}(\mathbf{k}+\mathbf{Q})) \\ + |\phi^{\alpha\alpha}_{-\mathbf{Q},\sigma}||\kappa^{\beta\alpha}_{-\mathbf{Q},\sigma}||\phi^{\beta\beta}_{-\mathbf{Q},\sigma}|]. \end{aligned} \tag{E.11}$$

While $G^{\alpha\alpha}_{f,\sigma}(\mathbf{k},\mathbf{k}+\mathbf{Q},\omega)$ and $G^{\beta\beta}_{f,\sigma}(\mathbf{k},\mathbf{k}+\mathbf{Q},\omega)$ are:

$$\begin{aligned} G^{\alpha\alpha}_{f,\sigma}(\mathbf{k},\mathbf{k}+\mathbf{Q}\omega) = D^{-1}_{\sigma}(\mathbf{k},\mathbf{Q},\omega) \times [|\phi^{\beta\beta}_{-\mathbf{Q},\sigma}|^2|\phi^{\alpha\alpha}_{-\mathbf{Q},\sigma}| \\ - (\omega - E^{\beta}_{f,\sigma}(\mathbf{k}+\mathbf{Q}))|\phi^{\alpha\alpha}_{-\mathbf{Q},\sigma}|(\omega - E^{\beta}_{f,\sigma}(\mathbf{k})) \\ - |\kappa^{\beta\alpha}_{-\mathbf{Q},\sigma}|^2|\phi^{\beta\beta}_{-\mathbf{Q},\sigma}|] \end{aligned} \tag{E.12}$$

and

$$\begin{aligned} G^{\beta\beta}_{f,\sigma}(\mathbf{k},\mathbf{k}+\mathbf{Q},\omega) = D^{-1}_{\sigma}(\mathbf{k},\mathbf{Q},\omega) \times [|\phi^{\alpha\alpha}_{-\mathbf{Q},\sigma}|^2|\phi^{\beta\beta}_{-\mathbf{Q},\sigma}| \\ - (\omega - E^{\alpha}_{f,\sigma}(\mathbf{k}) - \xi^{\alpha}(\mathbf{k}))|\phi^{\beta\beta}_{-\mathbf{Q},\sigma}|(\omega - E^{\alpha}_{f,\sigma}(\mathbf{k}+\mathbf{Q}) - \xi^{\alpha}(\mathbf{k}+\mathbf{Q})) \\ - |\kappa^{\beta\alpha}_{-\mathbf{Q},\sigma}|^2|\phi^{\alpha\alpha}_{-\mathbf{Q},\sigma}|]. \end{aligned} \tag{E.13}$$

The term $D_\sigma(\mathbf{k},\mathbf{Q},\omega)$ in Eqs. (E.11)-(E.12) and (E.13) is explicitly given as:

$$\begin{aligned}
D_\sigma(\mathbf{k},\mathbf{Q},\omega) = [&(\omega - E^\alpha_{f\sigma}(\mathbf{k}) - \xi^\alpha(\mathbf{k}))(\omega - E^\beta_{f\sigma}(\mathbf{k}))\times \\
&(\omega - E^\alpha_{f\sigma}(\mathbf{k}+\mathbf{Q}) - \xi^\alpha(\mathbf{k}+\mathbf{Q}))(\omega - E^\beta_{f\sigma}(\mathbf{k}+\mathbf{Q})] \\
&- |\kappa^{\alpha\beta}_{-\mathbf{Q},\sigma}|^2(\omega - E^\alpha_{f\sigma}(\mathbf{k}) - \xi^\alpha(\mathbf{k}))(\omega - E^\beta_{f\sigma}(\mathbf{k}+\mathbf{Q})) \\
&- |\kappa^{\beta\alpha}_{\mathbf{Q},\sigma}|^2(\omega - E^\beta_{f\sigma}(\mathbf{k}))(\omega - E^\alpha_{f\sigma}(\mathbf{k}+\mathbf{Q}) - \xi^\alpha(\mathbf{k}+\mathbf{Q})) - \\
&(\phi^{\beta\beta}_{-\mathbf{Q},\sigma})^2(\omega - E^\alpha_{f\sigma}(\mathbf{k}) - \xi^\alpha(\mathbf{k}))(\omega - E^\alpha_{f\sigma}(\mathbf{k}+\mathbf{Q}) - \xi^\alpha(\mathbf{k}+\mathbf{Q})) \\
&- (\phi^{\alpha\alpha}_{-\mathbf{Q},\sigma})^2(\omega - E^\beta_{f\sigma}(\mathbf{k}))(\omega - E^\beta_{f\sigma}(\mathbf{k}+\mathbf{Q})) + \\
&(\phi^{\alpha\alpha}_{-\mathbf{Q},\sigma})^2(\phi^{\beta\beta}_{-\mathbf{Q},\sigma})^2 - (\phi^{\alpha\alpha}_{-\mathbf{Q},\sigma})(\phi^{\beta\beta}_{-\mathbf{Q},\sigma})(|\kappa^{\beta\alpha}_{\mathbf{Q},\sigma}|^2 + |\kappa^{\alpha\beta}_{-\mathbf{Q},\sigma}|^2) \\
&+ |\kappa^{\beta\alpha}_{\mathbf{Q},\sigma}|^2|\kappa^{\alpha\beta}_{-\mathbf{Q},\sigma}|^2. \quad \text{(E.14)}
\end{aligned}$$

The equation of motion for Green's function are in Appendix (F).

Appendix F

Equations of motion of Green's function

F.1 Coulombian (U) and Exchange (J) interactions

We can describe by the theory of Zubarev's Green equations of motion that the Hamiltonian of Coulombian and Exchange interactions in Hartree-Fock approximation theory can be expressed as

$$\hat{H}_{1,int} - = \left(\frac{U}{2}\right) \sum_{\mathbf{k}\mathbf{k}'} \sum_{\mathbf{q},\sigma} \sum_{\chi=\chi'} [n^{\chi}_{\mathbf{q},\sigma} f^{\dagger\chi'}_{\mathbf{k}'-\mathbf{q},-\sigma} f^{\chi'}_{\mathbf{k}',-\sigma} + f^{\dagger\chi}_{\mathbf{k}+\mathbf{q},\sigma} f^{\chi}_{\mathbf{k},\sigma} n^{\chi'}_{\mathbf{q},-\sigma} - n^{\chi}_{\mathbf{q},\sigma} n^{\chi'}_{\mathbf{q},-\sigma}]. \quad \text{(F.1)}$$

Introducing the property

$$n^{\chi}_{\mathbf{q},\sigma} = n^{\chi}_{\sigma} \delta_{\mathbf{0},\mathbf{q}} \quad \text{(F.2)}$$

in the previous Hamiltonian we have after that

$$\hat{H}_{1,int} = \left(\frac{U}{2}\right) \sum_{\mathbf{k},\sigma} \sum_{\chi=\chi'} n^{\chi}_{\sigma} f^{\dagger\chi'}_{\mathbf{k},-\sigma} f^{\chi'}_{\mathbf{k},-\sigma} + \left(\frac{U}{2}\right) \sum_{\mathbf{k},\sigma} \sum_{\chi=\chi'} f^{\dagger\chi}_{\mathbf{k},\sigma} f^{\chi}_{\mathbf{k},\sigma} n^{\chi'}_{-\sigma} - \left(\frac{U}{2}\right) \sum_{\sigma} n^{\chi}_{\sigma} n^{\chi'}_{-\sigma}, \quad \text{(F.3)}$$

now, by assembling the equations with the $f_{\mathbf{k}}$ operator,

$$\left[f^{\chi}_{\mathbf{k},\sigma}, \hat{H}_{1,int}\right] = \frac{U}{2} \sum_{\mathbf{k}',\sigma'} \sum_{\chi'\chi''} n^{\chi'}_{\sigma'} \left[f^{\chi}_{\mathbf{k},\sigma}, f^{\dagger\chi''}_{\mathbf{k}',-\sigma'} f^{\chi''}_{\mathbf{k}',-\sigma'}\right] + \frac{U}{2} \sum_{\mathbf{k}',\sigma'} \sum_{\chi'\chi''} n^{\chi''}_{-\sigma'} \left[f^{\chi}_{\mathbf{k},\sigma}, f^{\dagger\chi'}_{\mathbf{k}',-\sigma'} f^{\chi'}_{\mathbf{k}',-\sigma'}\right].$$

depreciating the last additive term because it does not affect the system. Like this

$$\left[f^{\chi}_{\mathbf{k},\sigma}, \hat{H}_{1,int}\right] = \frac{U}{2}\sum_{\mathbf{k}',\sigma'}\sum_{\chi'\chi''} n^{\chi'}_{\sigma'}\delta_{\mathbf{k},\mathbf{k}'}\delta_{\sigma,-\sigma'}\delta^{\chi\chi''}f^{\chi''}_{\mathbf{k}',-\sigma'} + \frac{U}{2}\sum_{\mathbf{k}',\sigma'}\sum_{\chi'\chi''} n^{\chi''}_{-\sigma'}\delta_{\mathbf{k},\mathbf{k}'}\delta_{\sigma,\sigma'}\delta^{\chi\chi'}f^{\chi'}_{\mathbf{k}',\sigma'}.$$

therefore

$$\left[f^{\chi}_{\mathbf{k},\sigma}, \hat{H}^{M.F}_{1,int}\right] = \frac{U}{2}\sum_{\chi'=\chi} n^{\chi'}_{-\sigma}f^{\chi}_{\mathbf{k},\sigma} + \frac{U}{2}\sum_{\chi=\chi''} n^{\chi''}_{-\sigma}f^{\chi}_{\mathbf{k},\sigma}$$

$$\left[f^{\chi}_{\mathbf{k},\sigma}, \hat{H}^{M.F}_{1,int}\right] = U\sum_{\chi'=\chi} n^{\chi'}_{-\sigma}f^{\chi}_{\mathbf{k},\sigma}. \tag{F.4}$$

The second term of the interacting Hamiltonian is given by

$$\hat{H}_{2,int} = \left(\frac{U-J}{2}\right)\sum_{\mathbf{k}\mathbf{k}'}\sum_{\mathbf{q},\sigma}\sum_{\chi\neq\chi'}[n^{\chi}_{\mathbf{q},\sigma}f^{\dagger\chi'}_{\mathbf{k}'-\mathbf{q},\sigma}f^{\chi'}_{\mathbf{k}',\sigma} + f^{\dagger\chi}_{\mathbf{k}+\mathbf{q},\sigma}f^{\chi}_{\mathbf{k},\sigma}n^{\chi'}_{-\mathbf{q},\sigma} - n^{\chi}_{\mathbf{q},\sigma}n^{\chi'}_{-\mathbf{q},\sigma}], \tag{F.5}$$

and using the property (F.2) again we can write that

$$\hat{H}_{2,int} = \left(\frac{U-J}{2}\right)\sum_{\mathbf{k},\sigma}\sum_{\chi\neq\chi'} n^{\chi}_{\sigma}f^{\dagger\chi'}_{\mathbf{k}',\sigma}f^{\chi'}_{\mathbf{k}',\sigma} + \left(\frac{U-J}{2}\right)\sum_{\mathbf{k},\sigma}\sum_{\chi\neq\chi'} f^{\dagger\chi}_{\mathbf{k},\sigma}f^{\chi}_{\mathbf{k},\sigma}n^{\chi'}_{\sigma}$$

$$-\left(\frac{U-J}{2}\right)n^{\chi}_{\sigma}n^{\chi'}_{\sigma}. \tag{F.6}$$

Like this,

$$\left[f^{\chi}_{\mathbf{k},\sigma}, \hat{H}_{1,int}\right] = \left(\frac{U-J}{2}\right)\sum_{\mathbf{k}',\sigma'}\sum_{\chi'\neq\chi''} n^{\chi'}_{\sigma'}\left[f^{\chi}_{\mathbf{k},\sigma}, f^{\dagger\chi''}_{\mathbf{k}',\sigma'}f^{\chi''}_{\mathbf{k}',\sigma'}\right] +$$

$$\left(\frac{U-J}{2}\right)\sum_{\mathbf{k}',\sigma'}\sum_{\chi'\neq\chi''} n^{\chi''}_{\sigma'}\left[f^{\chi}_{\mathbf{k},\sigma}, f^{\dagger\chi'}_{\mathbf{k}',\sigma'}f^{\chi'}_{\mathbf{k}',\sigma'}\right], \tag{F.7}$$

what is equal to

$$\left[f^{\chi}_{\mathbf{k},\sigma}, \hat{H}_{1,int}\right] = \left(\frac{U-J}{2}\right)\sum_{\mathbf{k}',\sigma'}\sum_{\chi'\neq\chi''} n^{\chi'}_{\sigma'}\delta_{\mathbf{k},\mathbf{k}'}\delta_{\sigma\sigma'}\delta^{\chi\chi''}f^{\chi''}_{\mathbf{k}',\sigma'} +$$

$$\left(\frac{U-J}{2}\right)\sum_{\mathbf{k}',\sigma'}\sum_{\chi'\neq\chi''} n^{\chi''}_{\sigma'}\delta_{\mathbf{k},\mu'}\delta_{\sigma\sigma'}\delta^{\chi\chi'}f^{\chi'}_{\mathbf{k}',\sigma'} \tag{F.8}$$

then, the bracket is describe as

$$\left[f^{\chi}_{\mathbf{k},\sigma}, \hat{H}_{1,int}\right] = \left(\frac{U-J}{2}\right)\sum_{\chi\neq\chi'} n^{\chi'}_{\sigma'}f^{\chi'}_{\mathbf{k},\sigma} + \left(\frac{U-J}{2}\right)\sum_{\chi'\neq\chi''} n^{\chi''}_{\sigma}f^{\chi}_{\mathbf{k},\sigma}.$$

Finally, we have that

$$\left[f^{\chi}_{\mathbf{k},\sigma}, \hat{H}_{1,int}\right] = (U-J)\sum_{\chi\neq\chi'} n^{\chi'}_{\sigma} f^{\chi}_{\mathbf{k},\sigma}.$$

The third term of the Hamiltonian is written as

$$\hat{H}_{3,int} = \left(\frac{J}{2}\right)\sum_{\mathbf{k}\mathbf{k}'}\sum_{\mathbf{q}\sigma}\sum_{\chi}[n^{\chi}_{\mathbf{q},\sigma} f^{\dagger\chi}_{\mathbf{k}'-\mathbf{q},-\sigma} f^{\chi}_{\mathbf{k}',-\sigma} + f^{\dagger\chi}_{\mathbf{k}+\mathbf{q},\sigma} f^{\chi}_{\mathbf{k},\sigma} n^{\chi}_{-\mathbf{q},-\sigma} - n^{\chi}_{\mathbf{q},\sigma} n^{\chi}_{-\mathbf{q},-\sigma}], \quad \text{(F.9)}$$

and again using the property (F.2) we have to

$$\hat{H}_{3,int} = \left(\frac{J}{2}\right)\sum_{\mathbf{k}\sigma}\sum_{\chi} n^{\chi}_{\sigma} f^{\dagger\chi}_{\mathbf{k},-\sigma} f^{\chi}_{\mathbf{k},-\sigma} + \left(\frac{J}{2}\right)\sum_{\mathbf{k}\sigma}\sum_{\chi} f^{\dagger\chi}_{\mathbf{k},\sigma} f^{\chi}_{\mathbf{k},\sigma} n^{\chi}_{-\sigma} - n^{\chi}_{\sigma} n^{\chi}_{-\sigma}, \quad \text{(F.10)}$$

so,

$$\left[f^{\chi}_{\mathbf{k},\sigma}, \hat{H}_{3,int}\right] = \left(\frac{J}{2}\right)\sum_{\mathbf{k}',\sigma'}\sum_{\chi'} n^{\chi'}_{\sigma'}\left[f^{\chi}_{\mathbf{k},\sigma}, f^{\dagger\chi'}_{\mathbf{k}',-\sigma'} f^{\chi'}_{\mathbf{k}',-\sigma'}\right] + \left(\frac{J}{2}\right)\sum_{\mathbf{k}',\sigma'}\sum_{\chi'} n^{\chi'}_{-\sigma'}\left[f^{\chi}_{\mathbf{k},\sigma}, f^{\dagger\chi'}_{\mathbf{k}',\sigma'} f^{\chi'}_{\mathbf{k}',\sigma'}\right], \quad \text{(F.11)}$$

what is equal to

$$\left[f^{\chi}_{\mathbf{k},\sigma}, \hat{H}_{3,int}\right] = \left(\frac{J}{2}\right)\sum_{\mathbf{k}',\sigma'}\sum_{\chi'} n^{\chi'}_{\sigma'}\delta_{\mathbf{k},\mathbf{k}'}\delta_{\sigma,-\sigma'}\delta^{\chi\chi'} f^{\chi}_{\mathbf{k},\sigma} + \left(\frac{J}{2}\right)\sum_{\mathbf{k}',\sigma'}\sum_{\chi'} n^{\chi'}_{-\sigma'}\delta_{\mathbf{k},\mathbf{k}'}\delta_{\sigma,\sigma'}\delta^{\chi\chi'} f^{\chi}_{\mathbf{k},\sigma}, \quad \text{(F.12)}$$

hence

$$\left[f^{\chi}_{\mathbf{k},\sigma}, \hat{H}_{3,int}\right] = J n^{\chi}_{\sigma} f^{\chi}_{\mathbf{k},\sigma}. \quad \text{(F.13)}$$

For our fourth term we need the following property

$$z^{\chi\chi'}_{\mathbf{q},\sigma} = \frac{1}{N}\sum_{\mathbf{k}}\left\langle f^{\dagger\chi}_{\mathbf{k}+\mathbf{q},\sigma} f^{\chi'}_{\mathbf{k},\sigma}\right\rangle, \quad \text{(F.14)}$$

in which it is realized that

$$z^{\chi\chi'*}_{\mathbf{Q},\sigma} = z^{\chi'\chi}_{-\mathbf{Q},\sigma}. \quad \text{(F.15)}$$

The previous property allow the $\hat{H}_{4,int}$ Hamiltonian to be written as

$$\hat{H}_{4,int} = \left(\frac{U-J}{2}\right) \sum_{\mathbf{k}\mathbf{k}'} \sum_{\mathbf{Q},\sigma} \sum_{\chi \neq \chi'} [Z^{\chi\chi'}_{\mathbf{Q},\sigma} f^{\dagger\chi'}_{\mathbf{k}'-\mathbf{Q},\sigma} f^{\chi}_{\mathbf{k}',\sigma} + f^{\dagger\chi}_{\mathbf{k}+\mathbf{Q},\sigma} f^{\chi'}_{\mathbf{k},\sigma} z^{\chi'\chi}_{-\mathbf{Q},\sigma} - z^{\chi\chi'}_{\mathbf{Q},\sigma} z^{\chi'\chi}_{-\mathbf{Q},\sigma}] \tag{F.16}$$

equal to

$$\hat{H}_{4,int} = \left(\frac{U-J}{2}\right) \sum_{\mathbf{k}} \sum_{\mathbf{Q},\sigma} \sum_{\chi \neq \chi'} z^{\chi\chi'}_{\mathbf{Q},\sigma} f^{\dagger\chi'}_{\mathbf{k}'-\mathbf{Q},\sigma} f^{\chi}_{\mathbf{k}',\sigma} + \left(\frac{U-J}{2}\right) \sum_{\mathbf{k}} \sum_{\mathbf{Q},\sigma} \sum_{\chi \neq \chi'} f^{\dagger\chi}_{\mathbf{k}+\mathbf{Q},\sigma} f^{\chi'}_{\mathbf{k},\sigma} z^{\chi'\chi}_{-\mathbf{Q},\sigma}$$

$$- \left(\frac{U-J}{2}\right) \sum_{\mathbf{Q},\sigma} \sum_{\chi \neq \chi'} z^{\chi\chi'}_{\mathbf{Q},\sigma} z^{\chi'\chi}_{-\mathbf{Q},\sigma}. \tag{F.17}$$

like this,

$$\left[f^{\chi}_{\mathbf{k},\sigma}, \hat{H}_{4,int}\right] = \left(\frac{U-J}{2}\right) \sum_{\mathbf{k}'} \sum_{\mathbf{Q},\sigma'} \sum_{\chi' \neq \chi''} z^{\chi'\chi''}_{\mathbf{Q},\sigma'} \left[f^{\chi}_{\mathbf{k},\sigma}, f^{\dagger\chi''}_{\mathbf{k}'-\mathbf{Q},\sigma'} f^{\chi'}_{\mathbf{k}',\sigma'}\right] \tag{F.18}$$

$$\left(\frac{U-J}{2}\right) \sum_{\mathbf{k}'} \sum_{\mathbf{Q},\sigma'} \sum_{\chi' \neq \chi''} \left[f^{\dagger\chi'}_{\mathbf{k}'+\mathbf{Q},\sigma'} f^{\chi''}_{\mathbf{k}\mathbf{u}',\sigma'} z^{\chi''\chi'}_{-\mathbf{Q},\sigma'}\right],$$

so, we have

$$\left[f^{\chi}_{\mathbf{k},\sigma}, \hat{H}^{M.F}_{4,int}\right] = \left(\frac{U-J}{2}\right) \sum_{\mathbf{k}'} \sum_{\mathbf{Q},\sigma'} \sum_{\chi' \neq \chi''} Z^{\chi'\chi''}_{\mathbf{Q},\sigma'} \delta_{\mathbf{k},\mathbf{k}'-\mathbf{Q}} \delta_{\sigma\sigma'} \delta^{\chi\chi''} f^{\chi'}_{\mathbf{k}',\sigma'} \tag{F.19}$$

$$+ \left(\frac{U-J}{2}\right) \sum_{\mathbf{k}'} \sum_{\mathbf{Q},\sigma'} \sum_{\chi' \neq \chi''} Z^{\chi''\chi'}_{-\mathbf{Q},\sigma'} \delta_{\mathbf{k},\mathbf{k}'+\mathbf{Q}} \delta_{\sigma\sigma'} \delta^{\chi\chi'} f^{\chi''}_{\mathbf{k}',\sigma'}. \tag{F.20}$$

hence

$$\left[f^{\chi}_{\mathbf{k},\sigma}, \hat{H}_{4,int}\right] = \left(\frac{U-J}{2}\right) Z^{\chi'\chi}_{\mathbf{Q},\sigma} f^{\chi'}_{\mathbf{k}+\mathbf{Q},\sigma} + \left(\frac{U-J}{2}\right) Z^{\chi'\chi}_{-\mathbf{Q},\sigma} f^{\chi'}_{\mathbf{k}-\mathbf{Q},\sigma}. \tag{F.21}$$

Finally

$$\left[f^{\chi}_{\mathbf{k},\sigma}, \hat{H}_{4,int}\right] = (U-J) Z^{\chi'\chi}_{\mathbf{Q},\sigma} f^{\chi'}_{\mathbf{k}+\mathbf{Q},\sigma}. \tag{F.22}$$

the end term is given by

$$\hat{H}_{5,int} = \left(\frac{J}{2}\right) \sum_{\mathbf{k}\mathbf{k}'} \sum_{\mathbf{q}\sigma} \sum_{\chi \neq \chi'} [z^{\chi\chi'}_{q,\sigma} f^{\dagger\chi'}_{\mathbf{k}'-\mathbf{q},-\sigma} f^{\chi}_{\mathbf{k}',-\sigma} + f^{\dagger\chi}_{\mathbf{k}+\mathbf{q},\sigma} f^{\chi'}_{\mathbf{k},\sigma} z^{\chi\chi'}_{-\mathbf{q},-\sigma} - z^{\chi'\chi}_{\mathbf{q},\sigma} z^{\chi'\chi}_{-\mathbf{q},\sigma}], \tag{F.23}$$

and using the property (F.2)

$$\hat{H}_{5,int} = \left(\frac{J}{2}\right) \sum_{\mathbf{k}} \sum_{\mathbf{Q}\sigma} \sum_{\chi \neq \chi'} Z^{\chi\chi'}_{Q,\sigma} f^{\dagger\chi'}_{\mathbf{k}-\mathbf{Q},-\sigma} f^{\chi}_{\mathbf{k},-\sigma} + \sum_{\mathbf{k}} \sum_{\mathbf{Q}\sigma} \sum_{\chi \neq \chi'} f^{\dagger\chi}_{\mathbf{k}+\mathbf{Q},\sigma} f^{\chi'}_{\mathbf{k},\sigma} Z^{\chi'\chi}_{-\mathbf{Q},-\sigma}$$

$$- z^{\chi'\chi}_{\mathbf{Q},\sigma} z^{\chi'\chi}_{-\mathbf{Q},\sigma}, \tag{F.24}$$

which can be written as

$$\left[f^{\chi}_{\mathbf{k},\sigma}, \hat{H}_{4,int}\right] = \left(\frac{J}{2}\right) \sum_{\mathbf{k}'} \sum_{\mathbf{Q},\sigma'} \sum_{\chi' \neq \chi''} z^{\chi'\chi''}_{Q,\sigma'} \left[f^{\chi}_{\mathbf{ku},\sigma} f^{\dagger\chi''}_{\mathbf{k}'-\mathbf{Q},-\sigma'} f^{\chi'}_{\mathbf{k}',-\sigma'}\right] +$$

$$\sum_{\mathbf{k}'} \sum_{\mathbf{Q},\sigma'} \sum_{\chi' \neq \chi''} z^{\chi''\chi'}_{-\mathbf{Q},-\sigma'} \left[f^{\chi}_{\mathbf{k},\sigma}, f^{\dagger\chi'}_{\mathbf{k}'+\mathbf{Q},\sigma'} f^{\chi''}_{\mathbf{k}',\sigma'}\right], \tag{F.25}$$

this is equal to

$$\left[f^{\chi}_{\mathbf{k},\sigma}, \hat{H}_{4,int}\right] = \left(\frac{J}{2}\right) \sum_{\mathbf{k}'} \sum_{\mathbf{Q},\sigma'} \sum_{\chi' \neq \chi''} z^{\chi'\chi''}_{Q,\sigma'} \delta_{\mathbf{k},\mathbf{k}'-\mathbf{Q}} \delta_{\sigma,-\sigma} \delta^{\chi\chi''} f^{\chi'}_{\mathbf{k}',-\sigma'}$$

$$\sum_{\mathbf{k}'} \sum_{\mathbf{Q},\sigma'} \sum_{\chi' \neq \chi''} Z^{\chi''\chi'}_{-\mathbf{Q},-\sigma'} \delta_{\mathbf{k},\mathbf{k}'+\mathbf{Q}} \delta_{\sigma,\sigma} \delta^{\chi\chi'} f^{\chi''}_{\mathbf{k}',\sigma'}. \tag{F.26}$$

Once we have done each of the bracket calculations joining only one interaction Hamiltonian we finally have to

$$\left[f^{\chi}_{\mathbf{k},\sigma}, \hat{H}_{4,int}\right] = \frac{J}{2} z^{\chi'\chi}_{Q,-\sigma} f^{\chi'}_{\mathbf{k}+\mathbf{Q},\sigma} + \frac{J}{2} z^{\chi'\chi}_{-\mathbf{Q},-\sigma} f^{\chi'}_{\mathbf{k}-\mathbf{Q},\sigma}. \tag{F.27}$$

With the previous bracket we can write our Green functions for the $\chi = \alpha$ bands,

$$\omega \langle\langle f^{\chi}_{\mathbf{k},\sigma}; f^{\chi'}_{\mathbf{k}',\sigma'} \rangle\rangle = \delta_{\mathbf{k},\mathbf{k}'} \delta_{\sigma\sigma'} \delta^{\alpha\chi'} + (U - J) \sum_{\chi'} n^{\chi'}_{\sigma} \langle\langle f^{\alpha}_{\mathbf{k},\sigma}; f^{\chi'}_{\mathbf{k}',\sigma'} \rangle\rangle_{\omega} +$$

$$U \sum_{\chi'} n^{\chi'}_{-\sigma} \langle\langle f^{\alpha}_{\mathbf{k},\sigma}; f^{\chi'}_{\mathbf{k}',\sigma'} \rangle\rangle_{\omega} + J n^{\alpha}_{-\sigma} \langle\langle f^{\alpha}_{\mathbf{k},\sigma}; f^{\chi'}_{\mathbf{k}',\sigma'} \rangle\rangle_{\omega} +$$

$$(U - J) \sum_{\chi'} z^{\beta\alpha}_{\mathbf{Q},\sigma} \langle\langle f^{\beta}_{\mathbf{k}+\mathbf{Q},\sigma}; f^{\chi'}_{\mathbf{k}',\sigma'} \rangle\rangle_{\omega} + J z^{\beta\alpha}_{\mathbf{Q},-\sigma} \langle\langle f^{\beta}_{\mathbf{k}+\mathbf{Q},\sigma}; f^{\chi'}_{\mathbf{k}',\sigma'} \rangle\rangle_{\omega},$$

so

$$\omega G^{\alpha\chi'}_{ff,\sigma\sigma'}(\mathbf{k},\mathbf{k}',\omega) = \delta_{\mathbf{k},\mathbf{k}'} \delta_{\sigma\sigma'} \delta^{\alpha\chi'} + (U - J) \sum_{\beta} n^{\beta}_{\sigma} G^{\alpha\chi'}_{ff,\sigma\sigma'}(\mathbf{k},\mathbf{k}',\omega) +$$

$$U \sum_{\beta'} n^{\chi'}_{-\sigma} G^{\alpha\chi'}_{ff,\sigma\sigma'}(\mathbf{k},\mathbf{k}',\omega) + J n^{\alpha}_{-\sigma} G^{\alpha\chi'}_{ff,\sigma\sigma'}(\mathbf{k},\mathbf{k}',\omega) -$$

$$(U-J)z^{\beta\alpha}_{\mathbf{Q},\sigma}G^{\beta\chi'}_{ff,\sigma\sigma'}(\mathbf{k}+\mathbf{Q},\mathbf{k}',\omega)+Jz^{\beta\alpha}_{\mathbf{Q},-\sigma}G^{\beta\chi'}_{ff,\sigma\sigma'}(\mathbf{k},\mathbf{k}',\omega),$$

joining terms

$$\left[\omega-(U-J)\sum_{\beta}n^{\beta}_{\sigma}-U\sum_{\beta}n^{\beta}_{-\sigma}+Jn^{\alpha}_{-\beta}\right]G^{\alpha\chi'}_{ff,\sigma\sigma'}(\mathbf{k},\mathbf{k}',\omega)+$$

$$\left[(U-J)Z^{\beta\alpha}_{\mathbf{Q},\sigma}-JZ^{\alpha\beta}_{\mathbf{Q},-\sigma}\right]G^{\beta\chi'}_{ff,\sigma\sigma'}(\mathbf{k}+\mathbf{Q},\mathbf{k}',\omega)=\delta_{\mathbf{k},\mathbf{k}'}\delta_{\sigma\sigma'}\delta^{\alpha\chi'}.$$

Now, introducing

$$\hat{H}_{f,0}=\sum_{\mathbf{k},\sigma}\sum_{\chi}E^{\chi}_{f}(\mu)f^{\dagger\chi}_{\mu,\sigma}f^{\chi}_{\mathbf{k},\sigma},$$

therefore, the Green function is

$$\left[\omega-[E^{\alpha}_{f}(\mathbf{k})+(U-J)\sum_{\beta}n^{\beta}_{\sigma}-U\sum_{\beta}n^{\beta}_{-\sigma}]-Jn^{\alpha}_{-\beta}\right]G^{\alpha\chi'}_{ff,\sigma\sigma'}(\mathbf{k},\mathbf{k}',\omega)+$$

$$\left[(U-J)Z^{\beta\alpha}_{\mathbf{Q},\sigma}-Jz^{\alpha\beta}_{\mathbf{Q},-\sigma}\right]G^{\beta\chi'}_{ff,\sigma\sigma'}(\mathbf{k}+\mathbf{Q},\mathbf{k}',\omega)=\delta_{\mathbf{k},\mathbf{k}'}\delta_{\sigma\sigma'}\delta^{\alpha\chi'}.$$

In the last equation for any χ band, we can define that

$$E^{\chi}_{f,\sigma}(\mathbf{k})=\left[\omega-[E^{\alpha}_{f}(\mathbf{k})+(U-J)\sum_{\beta}n^{\beta}_{\sigma}-U\sum_{\beta}n^{\beta}_{-\sigma}]-2Jn^{\alpha}_{-\beta}\right] \tag{F.28}$$

and

$$\kappa^{\chi'\chi}_{\mathbf{Q},\sigma}=\left[(U-J)z^{\beta\alpha}_{\mathbf{Q},\sigma}-Jz^{\alpha\beta}_{\mathbf{Q},-\sigma}\right]. \tag{F.29}$$

The previous equations allow to write a set of matrix-coupled Green's function, as in Cap. 2.

F.2 External magnetic field H_z

The magnetic field Hamiltonian, $\hat{H}^{z}_{ext}$, for f-electrons is in Eq. (2.8) and this is the given by

$$\hat{H}^{z}_{ext}=\Gamma_z\sum_{\mathbf{k}}\sum_{\chi}f^{\dagger\chi}_{\mathbf{k},\sigma}f^{\chi}_{\mathbf{k},\sigma}, \tag{F.30}$$

where $\Gamma_z=-g_z\mu_B\sigma_z h_z$. We considerate $\chi=\alpha$ and $\chi'=\beta$ and after we have that

$$[f^{\alpha}_{\mathbf{k},\sigma},\hat{H}^{z}_{ext}]=\Gamma_z\sum_{\mathbf{k}'}\sum_{\chi'}[f^{\alpha}_{\mathbf{k},\sigma},f^{\dagger\chi'}_{\mathbf{k}',\sigma'}f^{\chi'}_{\mathbf{k}',\sigma'}] \tag{F.31}$$

$$[f^{\alpha}_{\mathbf{k},\sigma}, \hat{H}_z] = \Gamma_z \sum_{\mathbf{k}'} \sum_{\chi'} \delta^{\alpha\chi} \delta_{\sigma,\sigma'} \delta_{\mathbf{k},\mathbf{k}'} f^{\chi'}_{\mathbf{k}',\sigma'} \tag{F.32}$$

$$[f^{\alpha}_{\mathbf{k},\sigma}, \hat{H}^z_{ext}] = \Gamma_z f^{\alpha}_{\mathbf{k},\sigma} \tag{F.33}$$

after we can to write that

$$\langle\langle [f^{\alpha}_{\mathbf{k},\sigma}, \hat{H}^z_{ext}], f^{\chi'}_{\mathbf{k}',\sigma'} \rangle\rangle_{\omega} = \Gamma_z G^{\alpha\chi'}_{ff,\sigma\sigma'}(\mathbf{k}, \mathbf{k}', \omega) \tag{F.34}$$

thus

$$\langle\langle [f^{\alpha}_{\mathbf{k},\sigma}, \hat{H}^z_{ext}], f^{\chi'}_{\mathbf{k}',\sigma'} \rangle\rangle_{\omega} = \Gamma_z G^{\alpha\chi'}_{ff,\sigma\sigma'}(\mathbf{k}, \mathbf{k}', \omega). \tag{F.35}$$

Therefore, we can describe the dispersion relation for $\chi = \alpha, \beta$ us,

$$\widetilde{E}^{\chi}_{f,\sigma}(\mathbf{k}) = E^{\chi}_{f,\sigma}(\mathbf{k}) - \Gamma_z - \mu. \tag{F.36}$$

F.3 External magnetic field $\mathbf{H}_x$

The magnetic field Hamiltonian, $\hat{H}^f_{ext}$, for f-electrons is in Eq. (2.6) and this is given by

$$\hat{H}_x = \Gamma_x \sum_{\mathbf{k}} \sum_{\chi} f^{\dagger\chi}_{\mathbf{k},\uparrow} f^{\chi}_{\mathbf{k},\downarrow} + \Gamma_x \sum_{\mathbf{k}} \sum_{\chi} f^{\dagger\chi}_{\mathbf{k},\downarrow} f^{\chi}_{\mathbf{k},\uparrow} \tag{F.37}$$

where $\Gamma_x = -g_x \mu_B h_x$, thus

$$\begin{aligned} [f^{\alpha}_{\mathbf{k},\sigma}, \hat{H}^f_{ext}] = \Gamma_x \sum_{\mathbf{k}'} \sum_{\chi'} [f^{\alpha}_{\mathbf{k},\sigma}, f^{\dagger\chi'}_{\mathbf{k}',\uparrow} f^{\chi'}_{\mathbf{k}',\downarrow}] \\ + \Gamma_x \sum_{\mathbf{k}'} \sum_{\chi'} [f^{\alpha}_{\mathbf{k},\sigma}, f^{\dagger\chi'}_{\mathbf{k}',\downarrow} f^{\chi'}_{\mathbf{k}',\uparrow}], \end{aligned} \tag{F.38}$$

$$\begin{aligned} [f^{\alpha}_{\mathbf{k},\sigma}, \hat{H}^f_{ext}] = \Gamma_x \sum_{\mathbf{k}'} \sum_{\chi'} \delta^{\alpha\chi'} \delta_{\sigma,\uparrow} \delta_{\mathbf{k},\mathbf{k}'} f^{\chi'}_{\mathbf{k}',\downarrow} \\ + \Gamma_x \sum_{\mathbf{k}'} \sum_{\chi'} \delta^{\alpha\chi'} \delta_{\sigma,\downarrow} \delta_{\mathbf{k},\mathbf{k}'} f^{\chi'}_{\mathbf{k}',\uparrow}, \end{aligned} \tag{F.39}$$

$$[f^{\alpha}_{\mathbf{k},\sigma}, \hat{H}^f_{ext}] = \Gamma_x \delta_{\sigma,\uparrow} f^{\alpha}_{\mathbf{k},\downarrow} + \Gamma_x \delta_{\sigma,\downarrow} f^{\alpha}_{\mathbf{k},\uparrow} \tag{F.40}$$

$$\begin{aligned} \langle\langle [f^{\alpha}_{\mathbf{k},\sigma}, \hat{H}^f_{ext}], f^{\chi'}_{\mathbf{k}',\sigma'} \rangle\rangle_{\omega} = \Gamma_z \delta_{\sigma,\uparrow} \langle\langle f^{\alpha}_{\mathbf{k},\downarrow}, f^{\chi'}_{\mathbf{k}',\sigma'} \rangle\rangle \\ + \Gamma_z \delta_{\sigma,\downarrow} \langle\langle f^{\alpha}_{\mathbf{k},\uparrow}; f^{\chi'}_{\mathbf{k}',\sigma'} \rangle\rangle . \end{aligned} \tag{F.41}$$

Finally we have that

$$\begin{aligned}\langle\langle[f^{\alpha}_{\mathbf{k},\sigma},\hat{H}^{f}_{ext}],f^{\chi'}_{\mathbf{k}',\sigma'}\rangle\rangle_{\omega}&=\Gamma_z\delta_{\sigma,\uparrow}G^{\alpha\chi'}_{ff,\downarrow\sigma'}(\mathbf{k},\mathbf{k}',\omega)\\&+\Gamma_z\delta_{\sigma,\downarrow}G^{\alpha\chi'}_{ff,\uparrow\sigma'}(\mathbf{k},\mathbf{k}',\omega)\end{aligned}\tag{F.42}$$

or

$$\langle\langle[f^{\alpha}_{\mathbf{k},\sigma},\hat{H}^{f}_{ext}];f^{\chi'}_{\mathbf{k}',\sigma'}\rangle\rangle_{\omega}=\Gamma_z G^{\alpha\chi'}_{ff,-\sigma\sigma'}(\mathbf{k},\mathbf{k}',\omega).\tag{F.43}$$

We assume the intra-orbital SDW instabilities (for both χ-orbitals) and the spin-dependent inter-orbital density wave occur at the same nesting vector $\mathbf{Q}$. As consequence, the temporal and spatial Fourier transform of the single-electron f-f Green's function satisfy the equations of motion given by:

$$\begin{aligned}[\omega-\widetilde{E}^{\alpha}_{\sigma,f}(\mathbf{k})]G^{\alpha,\chi'}_{ff,\sigma\sigma'}(\mathbf{k},\mathbf{k}',\omega)&=\delta^{\alpha,\chi'}\delta_{\mathbf{k},\mathbf{k}'}\delta_{\sigma,\sigma'}\\+V_{\alpha}(\mathbf{k})G^{\chi'}_{df,\sigma\sigma'}(\mathbf{k},\mathbf{k}',\omega)+\kappa^{\beta\alpha}_{-\mathbf{Q},\sigma}G^{\beta,\chi'}_{ff,\sigma\sigma'}(\mathbf{k}+\mathbf{Q},\mathbf{k}',\omega)&\\+\Gamma_x G^{\alpha,\chi'}_{ff,-\sigma\sigma'}(\mathbf{k},\mathbf{k}',\omega)+\phi^{\alpha\alpha}_{-\mathbf{Q},\sigma}G^{\alpha\chi'}_{ff,\sigma\sigma'}(\mathbf{k}+\mathbf{Q},\mathbf{k}',\omega)&\end{aligned}\tag{F.44}$$

and

$$\begin{aligned}[\omega-\widetilde{E}^{\beta}_{\sigma,f}(\mathbf{k})]G^{\beta,\chi'}_{ff,\sigma\sigma'}(\mathbf{k},\mathbf{k}',\omega)&=\delta^{\beta,\chi'}\delta_{\mathbf{k},\mathbf{k}'}\delta_{\sigma,\sigma'}\\+V_{\beta}(\mathbf{k})G^{\chi'}_{df,\sigma\sigma'}(\mathbf{k},\mathbf{k}',\omega)+\ \kappa^{\alpha\beta}_{-\mathbf{Q},\sigma}G^{\alpha,\chi'}_{ff,\sigma\sigma'}(\mathbf{k}+\mathbf{Q},\mathbf{k}',\omega)&\\+\Gamma_x G^{\beta,\chi'}_{ff,-\sigma\sigma}(\mathbf{k},\mathbf{k}',\omega)+\phi^{\beta\beta}_{-\mathbf{Q},\sigma}G^{\beta\chi'}_{ff,\sigma\sigma'}(\mathbf{k}+\mathbf{Q},\mathbf{k}',\omega).&\end{aligned}\tag{F.45}$$

when the Γ_z is increasing. To complete the set of Green's functions, the mixed $f-d$ Green's function is found to satisfy the equation given below

$$\begin{aligned}[\ \omega\ -\ \widetilde{\epsilon}(\mathbf{k})]\ G^{\chi'}_{df,\sigma,\sigma'}(\mathbf{k},\mathbf{k}',\omega)\ &=\\V_{\alpha}(\mathbf{k})^{*}G^{\alpha,\chi'}_{ff,\sigma,\sigma'}(\mathbf{k},\mathbf{k}',\omega)+V_{\beta}(\mathbf{k})^{*}G^{\beta,\chi'}_{ff,\sigma,\sigma'}(\mathbf{k},\mathbf{k}',\omega).&\end{aligned}\tag{F.46}$$

Now we can to write that,

$$\begin{aligned}[\omega-\widetilde{E}^{\alpha}_{\sigma,f}(\mathbf{k})-\widetilde{\xi}^{\alpha\alpha}_{\mathbf{k},\sigma}]G^{\alpha,\chi'}_{ff,\sigma\sigma'}(\mathbf{k},\mathbf{k}',\omega)&=\delta^{\alpha,\chi'}\delta_{\mathbf{k},\mathbf{k}'}\delta_{\sigma,\sigma'}\\+\xi^{\beta\alpha}_{\mathbf{k},\sigma}G^{\beta\chi'}_{ff,\sigma\sigma'}(\mathbf{k},\mathbf{k}',\omega)+\kappa^{\beta\alpha}_{-\mathbf{Q},\sigma}G^{\beta,\chi'}_{ff,\sigma\sigma'}(\mathbf{k}+\mathbf{Q},\mathbf{k}',\omega)&\\+\Gamma_x G^{\alpha,\chi'}_{ff,-\sigma\sigma'}(\mathbf{k},\mathbf{k}',\omega)+\phi^{\alpha\alpha}_{-\mathbf{Q},\sigma}G^{\alpha\chi'}_{ff,\sigma\sigma'}(\mathbf{k}+\mathbf{Q},\mathbf{k}',\omega)&\end{aligned}\tag{F.47}$$

with $\mathbf{k}\to\mathbf{k}+\mathbf{Q}$ in the Eq. (F.47)

$$\begin{aligned}[\omega-\widetilde{E}^{\alpha}_{\sigma,f}(\mathbf{k}+\mathbf{Q})-\widetilde{\xi}^{\alpha\alpha}_{\mathbf{k}+\mathbf{Q},\sigma}]G^{\alpha,\chi'}_{ff,\sigma\sigma'}(\mathbf{k}+\mathbf{Q},\mathbf{k}',\omega)=&\\\delta^{\alpha,\chi'}\delta_{\mathbf{k}+\mathbf{Q},\mathbf{k}'}\delta_{\sigma,\sigma'}+\xi^{\beta\alpha}_{\mathbf{k}+\mathbf{Q},\sigma}G^{\beta\chi'}_{ff,\sigma\sigma'}(\mathbf{k}+\mathbf{Q},\mathbf{k}',\omega)&\\+\kappa^{\beta\alpha}_{-\mathbf{Q},\sigma}G^{\beta,\chi'}_{ff,\sigma\sigma'}(\mathbf{k},\mathbf{k}',\omega)+\Gamma_x G^{\alpha,\chi'}_{ff,-\sigma\sigma'}(\mathbf{k}+\mathbf{Q},\mathbf{k}',\omega)&\\+\phi^{\alpha\alpha}_{-\mathbf{Q},\sigma}G^{\alpha\chi'}_{ff,\sigma\sigma'}(\mathbf{k},\mathbf{k}',\omega),&\end{aligned}\tag{F.48}$$

doing $\sigma \to -\sigma$ in Eq. (F.47),

$$\begin{aligned}[\omega - \widetilde{E}^{\alpha}_{-\sigma,f}(\mathbf{k}) - \xi^{\alpha\alpha}_{\mathbf{k},-\sigma}]G^{\alpha,\chi'}_{ff,-\sigma\sigma'}(\mathbf{k},\mathbf{k}',\omega) = \\ \delta^{\alpha,\chi'}\delta_{\mathbf{k},\mathbf{k}'}\delta_{-\sigma,\sigma'} + \xi^{\beta\alpha}_{\mathbf{k},-\sigma}G^{\beta\chi'}_{ff,-\sigma\sigma'}(\mathbf{k},\mathbf{k}',\omega) \\ +\kappa^{\beta\alpha}_{-\mathbf{Q},-\sigma}G^{\beta,\chi'}_{ff,-\sigma\sigma'}(\mathbf{k}+\mathbf{Q},\mathbf{k}',\omega) \\ +\Gamma_x G^{\alpha,\chi'}_{ff,\sigma\sigma'}(\mathbf{k},\mathbf{k}',\omega) + \phi^{\alpha\alpha}_{-\mathbf{Q},-\sigma}G^{\alpha\chi'}_{ff,-\sigma\sigma'}(\mathbf{k}+\mathbf{Q},\mathbf{k}',\omega)\end{aligned} \tag{F.49}$$

and with $\mathbf{k} \to \mathbf{k}+\mathbf{Q}$ and $\sigma \to -\sigma$ we have that

$$\begin{aligned}[\omega - \widetilde{E}^{\alpha}_{-\sigma,f}(\mathbf{k}+\mathbf{Q}) - \widetilde{\xi}^{\alpha\alpha}_{\mathbf{k},-\sigma}]G^{\alpha,\chi'}_{ff,-\sigma\sigma'}(\mathbf{k}+\mathbf{Q},\mathbf{k}',\omega) = \\ \delta^{\alpha,\chi'}\delta_{\mathbf{k}+\mathbf{Q},\mathbf{k}'}\delta_{-\sigma,\sigma'} + \xi^{\beta\alpha}_{\mathbf{k}+\mathbf{Q},-\sigma}G^{\beta\chi'}_{ff,-\sigma\sigma'}(\mathbf{k}+\mathbf{Q},\mathbf{k}',\omega) \\ +\kappa^{\beta\alpha}_{-\mathbf{Q},-\sigma}G^{\beta,\chi'}_{ff,-\sigma\sigma'}(\mathbf{k},\mathbf{k}',\omega) \\ +\Gamma_z G^{\alpha,\chi'}_{ff,\sigma\sigma'}(\mathbf{k}+\mathbf{Q},\mathbf{k}',\omega) + \phi^{\alpha\alpha}_{-\mathbf{Q},-\sigma}G^{\alpha\chi'}_{ff,-\sigma\sigma'}(\mathbf{k},\mathbf{k}',\omega).\end{aligned} \tag{F.50}$$

For β-band we have the next Green function

$$\begin{aligned}[\omega - \widetilde{E}^{\beta}_{\sigma,f}(\mathbf{k}) - \widetilde{\xi}^{\beta\beta}_{\mathbf{k},\sigma}]G^{\beta,\chi'}_{ff,\sigma\sigma'}(\mathbf{k},\mathbf{k}',\omega) = \delta^{\beta,\chi'}\delta_{\mathbf{k},\mathbf{k}'}\delta_{\sigma,\sigma'} \\ +\widetilde{\xi}^{\alpha\beta}_{\mathbf{k},\sigma}G^{\alpha\chi'}_{ff,\sigma\sigma'}(\mathbf{k},\mathbf{k}',\omega) + \kappa^{\alpha\beta}_{-\mathbf{Q},\sigma}G^{\alpha,\chi'}_{ff,\sigma\sigma'}(\mathbf{k}+\mathbf{Q},\mathbf{k}',\omega) \\ +\Gamma_z G^{\beta,\chi'}_{ff,-\sigma\sigma'}(\mathbf{k},\mathbf{k}',\omega) + \phi^{\beta\beta}_{-\mathbf{Q},\sigma}G^{\beta\chi'}_{ff,\sigma\sigma'}(\mathbf{k}+\mathbf{Q},\mathbf{k}',\omega)\end{aligned} \tag{F.51}$$

also with $\mathbf{k} \to \mathbf{k}+\mathbf{Q}$ in the Eq. (F.50)

$$\begin{aligned}[\omega - \widetilde{E}^{\beta}_{\sigma,f}(\mathbf{k}+\mathbf{Q}) - \xi^{\beta\beta}_{\mathbf{k}+\mathbf{Q},\sigma}]G^{\beta,\chi'}_{ff,\sigma\sigma'}(\mathbf{k}+\mathbf{Q},\mathbf{k}',\omega) = \\ \delta^{\beta,\chi'}\delta_{\mathbf{k}+\mathbf{Q},\mathbf{k}'}\delta_{\sigma,\sigma'} + \xi^{\alpha\beta}_{\mathbf{k}+\mathbf{Q},\sigma}G^{\alpha\chi'}_{ff,\sigma\sigma'}(\mathbf{k}+\mathbf{Q},\mathbf{k}',\omega) \\ +\kappa^{\alpha\beta}_{-\mathbf{Q},\sigma}G^{\alpha,\chi'}_{ff,\sigma\sigma'}(\mathbf{k},\mathbf{k}',\omega) + \Gamma_z G^{\beta,\chi'}_{ff,-\sigma\sigma'}(\mathbf{k}+\mathbf{Q},\mathbf{k}',\omega) \\ +\phi^{\beta\beta}_{-\mathbf{Q},\sigma}G^{\beta\chi'}_{ff,\sigma\sigma'}(\mathbf{k},\mathbf{k}',\omega)\end{aligned} \tag{F.52}$$

we can do that $\sigma \to -\sigma$ in Eq. (F.50),

$$\begin{aligned}[\omega - \widetilde{E}^{\beta}_{-\sigma,f}(\mathbf{k}) - \widetilde{\xi}^{\beta\beta}_{\mathbf{k},-\sigma}]G^{\beta,\chi'}_{ff,-\sigma\sigma'}(\mathbf{k},\mathbf{k}',\omega) = \\ \delta^{\beta,\chi'}\delta_{\mathbf{k},\mathbf{k}'}\delta_{-\sigma,\sigma'} + \widetilde{\xi}^{\alpha\beta}_{\mathbf{k},-\sigma}G^{\alpha\chi'}_{ff,-\sigma\sigma'}(\mathbf{k},\mathbf{k}',\omega) \\ +\kappa^{\alpha\beta}_{-\mathbf{Q},-\sigma}G^{\alpha,\chi'}_{ff,-\sigma\sigma'}(\mathbf{k}+\mathbf{Q},\mathbf{k}',\omega) \\ +\Gamma_z G^{\beta,\chi'}_{ff,\sigma\sigma'}(\mathbf{k},\mathbf{k}',\omega) + \phi^{\beta\beta}_{-\mathbf{Q},-\sigma}G^{\beta\chi'}_{ff,-\sigma\sigma'}(\mathbf{k}+\mathbf{Q},\mathbf{k}1,\omega)\end{aligned} \tag{F.53}$$

with $\mathbf{k} \to \mathbf{k}+\mathbf{Q}$ and $\sigma \to -\sigma$

$$\begin{aligned}[\omega - \widetilde{E}^{\beta}_{\sigma,f}(\mathbf{k}+\mathbf{Q}) - \widetilde{\xi}^{\beta\beta}_{\mathbf{k}+\mathbf{Q},-\sigma}]G^{\beta,\chi'}_{ff,-\sigma\sigma'}(\mathbf{k}+\mathbf{Q},\mathbf{k}',\omega) = \\ \delta^{\beta,\chi'}\delta_{\mathbf{k}+\mathbf{Q},\mathbf{k}'}\delta_{-\sigma,\sigma'} + \xi^{\alpha\beta}_{\mathbf{k}+\mathbf{Q},\sigma}G^{\alpha\chi'}_{ff,-\sigma\sigma'}(\mathbf{k}+\mathbf{Q},\mathbf{k}',\omega) \\ +\kappa^{\alpha\beta}_{-\mathbf{Q},-\sigma}G^{\alpha,\chi'}_{ff,-\sigma\sigma'}(\mathbf{k},\mathbf{k}',\omega) + \Gamma_z G^{\beta,\chi'}_{ff,-\sigma\sigma'}(\mathbf{k}+\mathbf{Q},\mathbf{k}',\omega) \\ +\phi^{\beta\beta}_{-\mathbf{Q},-\sigma}G^{\beta\chi'}_{ff,-\sigma\sigma'}(\mathbf{k},\mathbf{k}',\omega)\end{aligned} \tag{F.54}$$

The Green's function equation of motion given in Eqs. (F.44)-(F.46) form a closed set which can be solved within a matricial formalism.

References

[1] P. Santini, R. Lémanski, and P. Erdos, Adv. Phys. **48**, 537 (1999).

[2] Atsushi Miyake, Yusei Shimizu, Yoshiki J. Sato, Dexin Li, Ai Nakamura, Yoshiya Homma, Fuminori Honda, Jacques Flouquet, Masashi Tokunaga and Dai Aoki, J. Phys. Soc. Jpn. **88**, 063706 (2019).

[3] C. Pfleiderer,Rev. Mod. Phys. **81**, 1551 (2009).

[4] Dai Aoki, Ai Nakamura, Fuminori Honda, DeXin Li, Yoshiya Homma, Yusei Shimizu, Yoshiki J. Sato, Georg Knebel, Jean-Pascal Brison, Alexandre Pourret, Daniel Braithwaite, Gerard Lapertot, Qun Niu, Michal Vališka, Hisatomo Harima, and Jacques Flouquet, J. Phys. Soc. Jpn. **88**, 043702 (2019).

[5] J. A. Mydosh and P. M. Openeer, Rev. Mod. Phys. **83**, 1301 (2011).

[6] J. A. Mydosh, P. M. Oppeneer, Philosophical Magazine **94** (32-33):3642-3662 (2014).

[7] P. S. Riseborough, B. Coqblin, S. G. Magalhaes, Phys. Rev. B **85**, 165116 (2012).

[8] E. J. Calegari, S. G. Magalhaes, P. S. Riseborough, npj Quant. Mat. **48**, 1 (2017).

[9] Wolowiec, Christian T. and Kanchanavatee, Noravee and Huang, Kevin and Ran, Sheng and Breindel, Alexander J. and Pouse, Naveen and Sasmal, Kalyan and Baumbach, Ryan E. and Chappell, Greta and Riseborough, Peter S. and Maple, M. Brian. Proceedings of the National Academy of Sciences **118**, 20 (2021).

[10] S. G. Magalhães, A. C. Lausmann, E. J. Calegari, and P. S. Riseborough, Phys. Rev. B, **101**, 064407 (2020).

[11] J. Faúndez, S.G . Magalhães, J. E. Calegari and P. S. Riseborough, J. Phys.: Condens. Matter **33**, 295801 (2021).

[12] R. L. Stillwell, I-L. Liu, N. Harrison, M. Jaime, J. R. Jeffries, N. P. Butch, Phys. Rev. B **95**, 014414 (2017).

[13] D. Antonio, M. Jaime, N. Harrison, D. S. Mast, D. Safarik, T. Durakiewcz, J. -C. Griveau, K. Gofric, Sci. Rep. **7**, 6642 (2017).

[14] M. Vališka, H. Saito, T. Yanagisawa, C. Tabata, H. Amitsuka, K. Uhlirova, J. Prokleska, P. Proschele, J. Valenta, M. Misek, D. I. Gorbunov, J. Wosnitza, V. Sechovsky, Phys. Rev. B **98**, 174439 (2018).

[15] V. F. Correa, S. Francoual, M. Jaime, N. Harrison, T. P. Murray, E. C. Palm, S. W. Tolzer, A. H. Lacerda, P. A. Sharma. J. A. Mydosh, Phys. Rev. Lett. **109**, 246405 (2012).

[16] P. G. Niklowitz, C. Pfleiderer, T. Keller, M. Vojta, Y. -K. Huang, J. A. Mydosh, Phys. Rev. Lett. **106**, 106406 (2010).

[17] D. Belitz, T. R. Kirkpatrick, Phys. Rev. Lett. **119**, 267202 (2017).

[18] P. Gegenwart, Q. Si, F. Steglich, Nat. Phys. **4**, 186 (2008).

[19] T. Misawa, Y. Yamaji, M. Imada, J. Phys. Soc. Jpn. **77**, 093712-1 (2008).

[20] N. B. Perkins, M.D. Nunez-Regueiro, B. Coqblin and J.R. Iglesias, Phys. Rev. B **76**, 125101 (2007).

[21] C. Thomas, A. S. da Rosa Simoes, J.R. Iglesias, C. Lacroix, N.B. Perkins and B. Coqblin, Phys. Rev. B. **83**, 014415 (2011).

[22] T. Durakiewicz, J.J. Joyce, G.H. Lander, C.G. Olson, M.T. Butterfield, E. Guziewicz, A.J. Arko, L. Morales, J. Rebizant, K. Mattenberger and O. Vogt, Phys Rev. B **70**, 205103 (2004).

[23] P. Wisniewski, A. Gukasov and Z. Henkie, Phys. Rev. B **60**, 6242-6245 (1999).

[24] Valenta, J.; Honda, F.; Valiska, M., Phys Rev B **97**, 144423 (2018).

[25] N. Shah, P. Chandra, P. Coleman, J. A. Mydosh, Phys. Rev. B **61**, 564 (2000).

[26] Xiao Yuan, Peter S Riseborough , E J Calegari and S G Magalhaes, Electronic Structure **3**, 2 (2021).

[27] B. Caroli, C. Caroli and D. R. Fredkin, Phys. Rev. **178**, 599 (1969).

[28] J. Schoenes, Phys. Rep. **66**, 187 (1981).

[29] L. Havela, V. Sechovsky, F. R. de Boer, E. Bruck, H. Nakote, Physica B **177**, 159 (1992).

[30] S. Maskova, A. V. Andreev, Y. Skourski, S. Yasin, D. I. Gorbonov, S. Zherlitsyn, H. Nakotte, H. Kothapalli, F. Nasreen, C. Cupp, H. B. Cao, A. Kolomiets, L. Havela, Phys. Rev. B **99**, 064415 (2019).

[31] Q. Y. Chen, X. B. Luo, D. H. Xie, M. L. Li, X. Y. Ji, R. Zhou, Y. B. Huang, W. Zhang, W. Feng, Y. Zhang, L. Huang, Q. Q. Hao, Q. Liu, X. G. Zhu, Y. Liu, P. Zhang, X. C. Lai, Q. Si, and S. Y. Tan, Phys. Rev. Lett. **123**, 106402 (2019).

[32] B. Kang, S. Choi, H. Kim. arXiv: 2111.08800

[33] P. S. Riseborough, S. G. Magalhaes, E. J. Calegari, Phil. Mag. **94**, 3820 (2014).

[34] Ken Iwakawa, Yusuke Hirose, Kentaro Enoki, Kiyohiro Sugiyama, Tetsuya Takeuchi, Fuminori Honda, Masayuki Hagiwara, Koichi Kindo, Takehito Nakano, Yasuo Nozue, Rikio Settai, and Yoshichika Ōnuki, J. Phys. Soc. Jpn. **81**, (2012).

[35] A. V. Silhanek, N. Harrison, C. D. Batista, M. Jaime, A. Lacerda, H. Amitsuka, and J. A. Mydosh Phys. Rev. Lett. **95**, 026403 (2005).

[36] N. V. Mushnikov, T. Goto, K. Kamishima, H. Yamada, A. V. Andreev, Y. Shiokawa, A. Iwao, and V. Sechovsky, Phys. Rev. B **59**, 6877 (1999).

[37] E. Brück, H. Nakotte, F. R. de Boer, P. F. de Châtel, H. P. van der Meulen, J. J. M. Franse, A. A. Menovsky, N. H. Kim-Ngan, L. Havela, V. Sechovsky, J. A. A. J. Perenboom, N. C. Tuan, and J. Sebek, Phys. Rev. B **49**, 8852 (1994).

[38] Jiří Pospíšil, Yoshinori Haga, Yoshimitsu Kohama, Atsushi Miyake, Shinsaku Kambe, Naoyuki Tateiwa, Michal Vališka, Petr Proschek, Jan Prokleška, Vladimír Sechovský, Masashi Tokunaga, Koichi Kindo, Akira Matsuo, and Etsuji Yamamoto, Phys. Rev. B **98**, 014430 (2018).

[39] P. M. Chaikin, T. C. Lubensky, *Principles of Condensed Matter Physics*, Cambridge Press, Cambridge, UK, (1995).

[40] R. L. Stillwell, I-L. Liu, N. Harrison, M. Jaime, J. R. Jeffries, and N. P. Butch, Phys. Rev. B **95**, 014414 (2017).

[41] K. Mochidzuki, Y. Shimizu, A. Kondo, A. Matsuo, D. Li, D. Aoki, Y. Homma, F. Honda, J. Flouquet, D. Nakamura, S. Takeyama, and K. Kindo, Phys. Rev. B **100**, 165137 (2019).

[42] A. M. Alsmadi, S. Alyones, H. Mielke, R. D. McDonald, V. Zapf, M. M. Altarawneh, A. Lacerda, S. Chang, S. Adak, K. Kothapalli, H. Nakotte, J. Magn. Magn. Mat. **321** 3712–3718 (2009).

[43] H. Nakotte, I. H. Hagmusa, J. C. P. Klaasse, M. S. Torikachvili, A. H. Lacerda, E. Bruck, K. Prokes, F. R. de Boer, Physica B. **246-247**, 441-444 (1998).

[44] F. Honda, K. Prokes, M. Olsovec, F. Bourdarot, P. Burlet, T. Kagayama, G. Oomi, L. Havela, V. Sechovsk y, A. V. Andreev, F. R. de Boer, A. A. Menovsky and M. Mihalik, J. Alloys Compounds **495**, 271–273 (1998).

[45] V. Sechovsky, K. Prokes, F. Honda, B. Ouladdiaf, J. Kulda, Appl. Phys. A **74** S834-S836 (2002).

[46] S. G. Magalhaes, A. C. Lausmann, E. J. Calegari, P. S. Riseborough, Phys. Rev. B **101**, 064407 (2020).

[47] J. A. Mydosh, M. Oppeneer, and P. S. Riseborough, J. Phys.: Condens. Matter **32**, 143002 (2020).

[48] C. Broholm, H. Lin, P. T. Matthews, T. E. Mason, W. J. L. Buyers, M. F. Collins, A. A. Menovsky, J. A. Mydosh, and J. K. Kjems Phys. Rev. B **43**, 12809 (1991).

[49] K. Haule, G. Kotliar, EPL **89**, 57006 (2010).

[50] P. Monachesi and A. Continenza, J. Magn. Magn. Mat. **140**, 1401:1402 (1995).

[51] G. R. Stewart, J Low Temp Phys. **195**, 1–25 (2019).

[52] R. Joynt and L. Taillefer, Rev. Mod. Phys. **74**, 235 (2002).

[53] P. Thalmeier, T. Takimoto and H. Ikeda, Philosophical Magazine, **94**, 3863 (2014).

[54] C. Pépin, M. R. Norman, S. Burdin, and A. Ferraz, Phys. Rev. Lett. **106**, 106601 (2011).

[55] R. A. de Groot, F. M. Mueller, P. G. van Engen and K. H. J Buschow, Phys. Rev. Letter **50**, 2024 (1983).

[56] J. P. Rodriguez, Phys. Rev. B **102**, 024521 (2020).

[57] V. P. Mineev and M. E. Zhitomirsky, Phys. Rev. B **72**, 014432 (2005).

[58] Y. J. Jo, L. Balicas, C. Capan, K. Behnia, P. Lejay, J. Flouquet, J. A. Mydosh, P. Schlottmann , Phys. Rev. Lett., **98**, 166404 (2007).

[59] N. F. Mott, Philosophical Magazine **30**, 398 (1974).

[60] W. E. Eckstein, M. Kollar, K. Byczuk, and D. Vollhardt, Rev. Mod. Phys. **68**, 235119 (2005).

[61] A. Georges, G. Kotliar, W. Krauth, and M. J. Rozenberg, Rev. Mod. Phys. **68**, 13 (1996).

[62] S. Henning and W. Nolting, Phys. Rev. B **85**, 125114 (2012).

[63] M. Balzer and M. Potthoff, Phys. Rev. B **82**, 174441 (2010).

[64] T. Das, Phys. Rev. B **89**, 045135 (2014).

[65] Y. D. Chong, QUANTUM MECHANICS III, Nanyang Technological University

[66] H. Tasaki, arXiv: 1812.10732

[67] F.A. Berazin, Academic Press, 2012